Gas Turbine Laboratory
Department of Aeronautics and Astronautics
Massachusetts Institute of Technology
Cambridge, MA 02139

Final Technical Report on Grant NAG3-770

entitled

ACTIVE STABILIZATION TO PREVENT SURGE IN CENTRIFUGAL COMPRESSION SYSTEMS

submitted to

AVARDCOM
NASA Lewis Research Center
21000 Brookpark Road
Cleveland, OH 44135

ATTN: Larry Schuman
Technical Officer

CO-INVESTIGATORS: Alan H. Epstein
Professor and Associate Director, Gas Turbine Laboratory

Edward M. Greitzer
Professor and Director, Gas Turbine Laboratory

Jon S. Simon
Graduate Research Assistant, Gas Turbine Laboratory

Lena Valavani
Associate Professor, Aeronautics and Astronautics

PERIOD OF INVESTIGATION: December 1, 1986 - February 29, 1992

January 1993

Executive Summary

This report documents an experimental and analytical study of the active stabilization of surge in a centrifugal engine. The aims of the research were both to extend the operating range of a compressor as far as possible and to establish the theoretical framework for the active stabilization of surge from both an aerodynamic stability and a control theoretic perspective. In particular, much attention was paid to understanding the physical limitations to active stabilization and how they are influenced by control system design parameters.

Previously developed linear models of actively stabilized compressors were extended to include such nonlinear phenomena as bounded actuation, bandwidth limits, and robustness criteria. This model was then used to systematically quantify the influence of sensor-actuator selection on system performance. Five different actuation schemes were considered, along with four different sensors. Sensor-actuator choice was shown to have a profound effect on the performance of the stabilized compressor. The optimum choice was not unique but rather shown to be a strong function of some of the non-dimensional parameters which characterize the compression system dynamics. Specifically, the utility of the concepts were shown to depend on the system compliance to inertia ratio ("B" parameter) and the local slope of the compressor speedline. In general, the most effective arrangements are ones in which the actuator is most closely coupled to the compressor, such as a close-coupled bleed valve inlet jet, rather than elsewhere in the flow train, such as a fuel flow modulator.

The analytical model was used to explore the influence of control system bandwidth on control effectiveness. The relevant reference frequency was shown to be the compression system's Helmholtz frequency rather than the surge frequency. The analysis shows that control bandwidths of three to ten times the Helmholtz frequency are required for larger increases in the compressor flow range. This has important implications for implementation in gas turbine engines since the Helmholtz frequencies can be over 100 Hz, making actuator design extremely challenging.

One result of the modelling was to explain the power flow in an actively stabilized

compressor. In particular, it was shown that the power the control system must input (or extract) scales not with the power of the compressor but with the power of the perturbations in the system, which are generally 10^4 to 10^6 smaller. The analysis indicated that the source of the perturbations are important. For example, three times more actuation authority is required if the destabilizing fluctuations come from perturbations in heat release in the combustor than if they come from perturbations in combustor outflow (turbine flow), and 6 times more if the source is unsteady pressure rise in the compressor. The actual structure of the perturbations in gas turbine engines is completely unknown. Since it is only important in the context of active control, it had not been previously studied.

The experimental investigation centered on a small (40 KW) turbocharger configured in a pumping system resembling that of a gas turbine engine, including compressor, plenum (combustor), and throttle (turbine). The actuation consisted of a high speed throttle valve which could be positioned either at the plenum exit or between the compressor and plenum. Sensors included mass flow, total and static pressure at the compressor inlet, and pressure in the plenum.

Open-loop actuation of the valve permitted measurement of the transfer function of the compression system. The flow development process was modelled as a one-dimensional lag. With this addition, a lumped parameter model was then shown to model the measured compressor response.

Closed-loop control of surge was shown to decrease the mass flow at surge inception by 50% compared to the uncontrolled case. The modelling was shown to do quite a good job in predicting the stability boundaries of the stabilized compressor.

Overall, the results of this research are very encouraging. Active control of surge has been shown to give larger gains when applied to centrifugal compressors. The performance of the controlled compressor has been shown to be well predicted by theory, indicating that we now have the tools to extend this concept to new geometries and applications. Work in this area could be very profitably pursued in applying these concepts to small gas turbine engines with centrifugal compressors. Much would be learned from such research.

Contents

1 Introduction 19

1.1 Introduction 19

1.2 Previous Work 21

1.2.1 Modeling of Compression Systems 21

1.2.2 Modeling of Compressors 24

1.2.3 Feedback Stabilization of Compression Systems 25

1.3 Current Research Objectives 29

1.3.1 Modeling and Model Validation 29

1.3.2 Feedback Stabilization 30

1.3.3 Summary 30

1.4 Overview of Thesis 31

2 Experimental Facility 36

2.1 Compression System 37

2.1.1 Flow Path 37

2.1.2 Description of Compressor 38

2.1.3 Flow Path Components 39

3+4

2.2 Actuation System 39
2.3 Measurement system 41
2.3.1 Inlet Duct Instrumentation 42
2.3.2 Compressor Instrumentation 43
2.3.3 Control Valve Instrumentation 45
2.3.4 Plenum Chamber Instrumentation 46
2.3.5 Metering Duct Instrumentation 46
2.4 Digital Data Acquisition and Control System 47
2.4.1 System Operation 47
2.4.2 Loop Timing 48

3 System Modeling **59**

3.1 Description of System 59
3.2 Component Models 61
3.2.1 Ducts 61
3.2.2 Plenum 63
3.2.3 Compressor 64
3.2.4 Throttle 66
3.2.5 Plenum Bleed Valve 67
3.2.6 Close-Coupled Valve 67
3.2.7 Injector 68
3.3 System Model 69
3.3.1 Model Reduction 73

3.4 Simplified System Model 74

3.5 Linearized System Model 75

4 Validation of Compressor Model **77**

4.1 Introduction 77

4.2 Theoretical Compressor Frequency Response 78

4.2.1 Background- Admittance, Impedance, and Phasors 78

4.2.2 Quasi-steady Model 80

4.2.3 Unsteady Loss Model 81

4.2.4 Frequency Normalization 83

4.3 Experimental Methodology 84

4.3.1 Summary 84

4.3.2 Detailed Test Procedure 86

4.4 Signal Processing and Data Analysis 88

4.5 Experimental Results 90

4.5.1 Quasi-steady Model 90

4.5.2 Unsteady Model 94

4.5.3 Relevance of Unsteady Behavior for Control Design 96

4.6 Summary and Conclusions 97

5 Limits to Compression System Stabilization **106**

5.1 Nominal Stabilization 107

5.1.1 Theoretical Background 107

5.1.2 Application of Theory to Compression Systems 108

5.2 Bounded Actuation 112
5.2.1 Theoretical Background 113
5.2.2 Numerical Results for Compression System 116
5.3 Limitations Imposed by Model Uncertainty 119
5.3.1 Theoretical Background 120
5.3.2 Theoretical Stabilization Limitation 124
5.3.3 Numerical Results for a Compression System 126
5.4 Summary 128

6 Evaluation of Alternative Control Strategies **135**

6.1 Introduction 135
6.2 Analytical Comparison 138
6.2.1 Stability Modification Using Proportional Control 139
6.3 Practical Limits To Control 144
6.3.1 Sensor and Actuator Pairs and Fluid Model 145
6.3.2 Results of the Control Scheme Evaluations 148
6.3.3 Effect of Control System Bandwidth 153
6.4 Comparison Based On Actuator Response To Disturbances 154
6.4.1 Background 155
6.4.2 Methodology 156
6.4.3 Effect of Disturbance Type 158
6.5 Summary 159

7 Close-Coupled Control **164**

7.1 Close-coupled Control Theory 165
7.1.1 Introduction 165
7.1.2 Pressure-drop Penalty With and Without Feedback 165
7.1.3 Optimal scheduling 169
7.1.4 An Illustrative Example 172
7.2 Close-coupled Stabilization Experiments 176
7.2.1 Description of Tests 176
7.2.2 Experimental Results 177
7.2.3 Comparison with Theory 178
7.3 Summary 181

8 Summary and Conclusions **193**

8.1 Summary 193
8.2 Conclusions 196
8.3 Suggestions for Future Research 199
8.3.1 Stabilization of Compression Systems 200
8.3.2 Control Theory 201

A Modeling the Injector **203**

A.1 Assumptions 203

B Degree of Controllability **208**

B.1 Recovery Region 208
B.2 Attainable Set 210

B.3 Degree of Controllability 211

C Frequency Domain Limitations **214**

D Minimal RMS Actuator Activity **216**

E Lyapunov Analysis of Close-coupled Control **219**

E.1 Introduction 219

E.2 Dynamic System Model 220

E.2.1 Basic Model 220

E.2.2 Model with Control 222

E.3 Lyapunov Analysis 225

E.3.1 Unsteady Energy and the Lyapunov Formalism 225

E.3.2 Basins of Attraction and Ultimate Boundedness 227

E.3.3 Effect of B parameter 229

E.4 Regions of Positive $\dot{V}(\hat{\phi}, \hat{\psi})$ 231

E.4.1 General Features 231

E.5 Effect of Bounded Disturbances 232

E.5.1 Analytical Formulation 233

References **244**

List of Figures

1-1 Extended range of surge free operation provided by feedback stabilization. (Data of Gysling [20], and Pinsley, [40]) 35

2-1 Overview of experimental facility 52

2-2 Compression system arrangement and flow path 53

2-3 Exploded view of turbocharger used for experiments 54

2-4 Overall Performance Map for Holset H1D Compressor 55

2-5 Control valve used for experiments 56

2-6 Sensor locations for experimental studies 57

2-7 Modified Kiel Probe used to measure compressor exit total pressure . 58

3-1 Compression system equipped with actuators and sensors 76

3-2 Flow stations for for modeling compression system 76

4-1 Schematic representation of compressor for frequency response model 99

4-2 Operating points at which frequency response was measured 99

4-3 Equipment configuration for frequency response measurement 100

4-4 Comparison of experimentally determined compressor admittance with quasi-steady theory without accounting for rotor speed fluctuation . . 101

4-5 Comparison of experimentally determined compressor admittance with quasi-steady theory (accounting for rotor speed fluctuation) 102

4-6 Comparison of experimentally determined compressor impedance with quasi-steady theory 103

4-7 Comparison of experimentally determined compressor impedance with unsteady theory 104

4-8 Comparison of experimentally determined compressor admittance with unsteady theory 105

5-1 Recovery regions for plenum bleed actuator as function of recovery time (illustrative case) 129

5-2 Recovery region for plenum bleed actuator showing circle whose radius determines degree of controllability (illustrative case) 130

5-3 Degree of Controllability as function of system parameters for plenum bleed actuator 131

5-4 Degree of Controllability as function of system parameters for close-coupled actuator 132

5-5 Block Diagram for defining closed loop transfer functions 132

5-6 Typical frequency domain performance specification for the complementary sensitivity transfer function 133

5-7 Geometrical Construction for the weighting function $\theta(\omega_c)$ a)real pole b)complex conjugate pole 133

5-8 Lower Bound on peak complementary sensitivity for close-coupled valve with mass flow measurement 134

6-1 Influence of sensor and actuator selection on maximum stabilized slope for a bandwidth and gain limited system 161

6-2 Influence of normalized control system bandwidth $(\frac{\omega_c}{\omega_h})$ on the feedback gain required and slope at instability onset;close-coupled control valve 162

6-3 Maximum slope at which the RMS actuation will be no greater than 25% of the maximum actuator authority 163

6-4 Influence of compression system disturbance type on actuator motion; close-coupled valve, $B = 2$ 163

7-1 Close-coupled stabilization with fixed valve and with feedback controlled valve (schematic) 183

7-2 Computed optimal scheduled performance with and without feedback for illustrative example 184

7-3 Optimally scheduled valve area as a function of flow for illustrative example 185

7-4 Optimally scheduled proportional gain as a function of flow for illustrative example 186

7-5 Effect of flow rate on optimal scheduled performance similar compressor characteristics 187

7-6 Close-coupled stabilization experimental results 188

7-7 Bode plot of experimentally measured transfer function representing actuator dynamics showing fit to fifth order model 189

7-8 Comparison of close-coupled experimental results with theory 190

7-9 Reduced frequency as a function of flow rate for ducts in experimental apparatus 191

7-10 Open loop compression system pole location as a function of flow coefficient 192

A-1 Injector showing flow stations for analysis 207

E-1 Basic Compression System Configuration 237

E-2 System with Close-Coupled Control Valve 237

E-3 Equivalent Compressor Characteristic 238

E-4 Activity and Passivity with respect to Operating Point 239

E-5 Constant Unsteady Energy - Ellipsoidal Bounds 240

E-6 Effect of B Parameter on Ellipsoidal Bounds 241

E-7 Effect of Bounded Disturbance on Region of Unsteady Power Production 242

E-8 Envelope of Bounded Disturbance on Compressor Characteristic . . . 243

List of Tables

2.1 Compressor Geometry 38

3.1 Reference quantities for non-dimensionalizing the system model . . . 71

3.2 Non-dimensional symbols for the system model 72

6.1 Sensing and Actuation Options 137

6.2 Open Loop Transfer Functions 139

6.3 Limitations on Compressor Flow Range Increase With Proportional Control 143

6.4 Normalization Factors 147

Nomenclature

a - ambient speed of sound
$\bar{a}_p$ - time mean speed of sound in plenum
A - area
A_c - annular inlet area of compressor
$\tilde{A}$ - nondimensional area
$\tilde{A}_{v_o}$ - ratio of wide open cntrl valve area to compressor area
B - Greitzer B-parameter
C_p - specific heat at constant pressure
C_v - specific heat at constant volume
G_w - numerator constant for movable wall $= 2p_p/(p_a {M_T}^2)$
K - proportional gain
L - duct length
$\mathcal{L}$ - equivalent duct length
$L(s)$ - loop transfer function (nominal)
m_p - mass stored in plenum
m_C - slope of compressor pressure rise characteristic
m_{C_e} - slope of nondimensional pressure-rise characteristic of compressor in series with valve
m_T - slope of nondimesional throttle pressure-drop characteristic
m_{T_e} - slope of nondimensional pressure-drop characteristic of throttle in parallel with bleed
m_{V_c} - slope of nondimensional close-coupled valve pressure-drop characteristic
$\tilde{m}_p$ - nondimensional mass in plenum
$\dot{m}$ - mass flow rate
M_i - compressor inlet axial Mach Number
M_T - rotor tip Mach Number
M_w - wall Mach Number
p - absolute static pressure
p_a - absolute ambient static pressure
p_0 - total pressure
Q - heat addition rate
$\tilde{Q}$ - nondimensional heat addition rate
R - resistance
R - gas constant
$\mathcal{R}$ - recovery region
s - Laplace transform argument
$S(s)$ - sensitivity transfer function
t - dimensional time
T - absolute temperature
T_a - absolute ambient temperature
ΔT_{0_c} - compressor total to total temperature rise characteristic
T_s - sampling time
T_0 - absolute total temperature

$T(s)$ - complementary sensitivity transfer function
u - axial velocity in compressor duct
u_T - rotor tip speed
u_w - velocity of movable wall
U_p - energy stored in plenum
$\tilde{U}_p$ - nondimensional plenum energy
v_b - bleed valve sensitivity $\frac{\partial \psi}{\partial \alpha}$
v_c - close-coupled valve sensitivity $\frac{\partial \psi}{\partial \alpha}$
V_c - compressor volume
V_p - plenum volume
$\bar{V}_p$ - time mean plenum volume
$\tilde{V}_p$ - nondimensional plenum volume
$Y(j\omega)$ - admittance
$Z(j\omega)$ - impedance

Greek Symbols

α_b - bleed valve fraction open
α_c - close-coupled valve fraction open
α - throttle fraction open
γ - ratio of specific heats
ε - error
ζ_s - damping ratio of servo
θ - temperature ratio $T_{plenum}/T_{ambient}$
θ_p - plenum temperature ratio $T_{plenum}/T_{ambient}$
Θ_c - compressor total to total temperature ratio characteristic
$\bar{\theta}_p$ - time mean plenum temperature ratio $T_{plenum}/T_{ambient}$
ξ - nondimensional wall displacement rate
π - pressure ratio
π_p - plenum pressure ratio $p_{plenum}/p_{ambient}$
Π_c - compressor total to total pressure ratio characteristic
ρ - gas density
ρ_a - ambient gas density
$\tilde{\rho}$ - compressor density ratio upstream/downstrm
ϱ - degree of controllability
τ - nondimensional time $\omega_h t$
ϕ - nondimensional mass flow rate (flow coefficient)
ϕ_c - nondimensional compressor mass flow rate (flow coefficient
Φ_b - nondimensional plenum bleed valve flow characteristic
Φ_t - nondimensional throttle flow characteristic
ψ - nondimensional pressure difference (pressure coefficient)
ψ_p - nondimensional plenum pressure (pressure coefficient)
Ψ_c - nondimensional compressor pressure rise characteristic
Ψ_{i_u} - nondimensional injector differential pressure characteristic (upstream-supply)

Ψ_{i_d} - nondimensional injector differential pressure characteristic (downstream-supply)
Ψ_t - nondimensional throttle pressure drop characteristic
Ψ_v - nondimensional close-coupled valve pressure drop characteristic
ω_s - servo break frequency
ω_c - robustness cutoff freq
ω_h - Helmholtz freq
ω_c - cutoff frequency

Chapter 1*

Introduction

1.1 Introduction

The useful range of operation of many turbomachine type compressors is limited by the onset of a system instability, known as surge, which occurs when the flow is reduced below some critical value. The unstable operation is characterized by periodic variations in the net through flow and output pressure of the compressor. The severity of the oscillations depends upon the overall dynamics of the system in which the compressor is installed and can be quite energetic, with flow reversal through the system. The forces involved may be great enough to cause structural damage [29] and, in addition, there may be consequences such as loss of power and overheating in an aircraft gas turbine engine.

Traditionally, such undesirable behavior has been avoided by using control systems which prevent the operating point from entering the unstable regime delineated by the surge line ([32, 47]). The approach described here is fundamentally different than

* The remainder of this document is condensed from the Ph.D. thesis of J.S. Simon.

these previous concepts in that it makes use of feedback stabilization to allow stable operation in the naturally unstable regions of the performance map [10]. This idea is illustrated in Figure 1-1 which shows an extended region of stable operation made possible with feedback stabilization.

Such an approach may have significant benefits for particular applications. The peak efficiency region is often quite close to the surge line [48] and feedback stabilization could thus allow stable operation in a more efficient region of the performance map. Other benefits include greater operating range and greater flexibility in designing compressors, if stability is not a primary concern.

Several researchers to date [12, 20, 40] have experimentally demonstrated that significant extensions in mass flow range can be achieved using various feedback stabilization mechanisms. Those studies focused on modeling and demonstrating particular implementations. In contrast, the overall purpose of this thesis is to report the results of a fundamental study of some of the more generic aspects of the compression system feedback stabilization problem.

It should be noted that any such attempt to artificially stabilize a compression system is not without associated risks and costs which must ultimately be considered and weighed against the benefits. In particular, the consequences of a control system failure could be be catastrophic in an aircraft application. The expense of additional hardware, added complexity and a probable resulting reduction in overall reliability are all admitted drawbacks. Before any final judgement can be passed, however, it is necessary to obtain a thorough understanding of the basic physics involved, the fundamental limitations to stabilization, and the available implementation options.

This thesis represents a first step in this direction.

1.2 Previous Work

1.2.1 Modeling of Compression Systems

Low order, lumped element, models for the surge process have been proposed by many researchers. Classic papers in which such models are derived and analyzed include those of Emmons et al [9] and Taylor [48]. Other references in which such models may be found include [2, 17, 22, 30, 49]. A comprehensive treatment is given by Greitzer [19] including an extensive literature review.

The approaches taken by these authors have many similarities and include assumptions of one dimensional, incompressible flow in the ducts, spatially uniform pressure in plenum chambers and quasi-steady pressure/flow relations for the throttling valves. The compressor is treated as an actuator disk which either follows its steady state performance characteristic (the quasi-steady assumption) or, in some cases (see for example Greitzer [17]), a first order lag is used to model the flow development process.

The system model is obtained by performing momentum balances for the ducts, and mass balances for the plenum chambers with the ideal gas law and some form of polytropic process used to relate the plenum density to plenum pressure. The models proposed by these authors vary primarily in the number of elements which are used, with some including additional plenum chambers and/or ducts at the compressor inlet or exit.

All the authors provide linearized stability analyses but some examine some of the

nonlinear aspects of the problem as well. Most authors recognize the importance of the slope of the compressor pressure-flow characteristic at the equilibrium operating point as a prime determinant of the compression system stability. Greitzer [17] also found global conditions on the compressor slope which must be satisfied to maintain surge oscillations. In addition, Greitzer showed the importance of the relative amount of fluid compliance to inertia (which he captured in his nondimensional B parameter[1].). More recent nonlinear analyses include those of Oliva and Nett [36] who looked at Hopf bifurcation phenomena and those of Simon and Valavani [45] who performed a Lyapunov stability analysis of a simple compression system.

The validity of these models has also been examined by a number of authors who all show that this simple modeling approach can capture both the qualitative and quantitative aspects of the surge phenomena for a broad class of turbomachines. Using a centrifugal compressor, Emmons [9] found reasonable agreement between linear theory for both the experimentally predicted onset of instability (the neutral stability point occurred near the peak of the compressor characteristic) and for the dependence of the system instability frequency on the system parameters. Greitzer [18] performed tests using a low speed axial flow fan and found good agreement for the predicted nonlinear behavior when the system exhibited large amplitude surge oscillations. In particular, he verified the theoretical prediction of the importance of the B parameter in determining whether a system would experience sustained surge

[1]The B parameter is defined by $B = \frac{u_T}{2\bar{a}_p}\sqrt{\frac{\bar{V}_p}{(\mathcal{L}_c A_c)}}$, where: u_T is the tip speed, $\bar{a}_p$ is the speed of sound in the plenum, $\bar{V}_p$ is the volume of the plenum, $\mathcal{L}_c$ is the equivalent inertial length of the compressor duct, and A_c is the compressor inlet area.

oscillations in annulus averaged mass flow or operate steadily (without surging) in a condition known as rotating stall. He showed good agreement between the predicted and actual time histories of the system when it was experiencing sustained oscillations. Hansen [21], using a small centrifugal compressor, also showed that a model similar to Greitzer's was able to accurately predict the nonlinear surge behavior. Fink [13, 14] performed an in depth study of surge, also using a centrifugal compressor, and showed impressive agreement between predicted and measured behavior. Finally, Bons [5] found a good comparison between experiment and theory using the same modeling approach for a centrifugal pump, thus demonstrating that the usefulness of the model is not limited to gaseous compression systems.

The models proposed by the above authors are all lumped parameter models, that is the system is represented by a finite number of ordinary differential equations. A distributed parameter model of a fan-duct-plenum system, forced by modulating dampers, has been developed and validated by Goldschmied and Wormley [16]. Their model uses a one-dimensional lossless acoustic transmission line representation for the duct, rather than a lumped fluid inertia. This is a more appropriate model for their system in which the acoustic wavelength at the higher forcing frequencies was less than the length of their duct. The fan and plenum were modeled using an approach similar to the other authors. The overall agreement between prediction and experimental measurements was found to be acceptable.

The most important general finding which is common to all of these studies is that it is not necessary to model the detailed, and very complex, flow phenomena occurring in the compressor itself in order to accurately predict the overall system behavior.

The pressure-rise versus flow characteristic of the compressor apparently provides a sufficient description for predicting the overall system dynamics. This was true even though in many of the experiments the flow in the compressor was three dimensional and locally unsteady, with rotating stall occurring in the axial flow machines and various diffuser stalls occurring in the centrifugal machines.

1.2.2 Modeling of Compressors

The previously cited work provides indirect evidence that a quasi-steady or simple first order lag model for the compressor is adequate. There is also some direct experimental support for this modeling approach provided by researchers who have attempted to measure the transfer function of the compressor. Ohashi [35] performed both an analytical and experimental study of the frequency response of turbo-pumps. He made a careful distinction between the unsteady behavior which is due only to fluid inertia effects and those due inherently to the unsteady pump performance. He found experimentally that the pump performance deviated significantly from the quasi-steady predictions when the reduced frequency (based upon convection time through the blade row) of the pump was greater than 0.1. Above this frequency the unsteady response of the compressor could be only roughly approximated by a first order lag. Abdel-Hamid [1] measured the frequency response of a low speed, single stage centrifugal blower with a tip diameter of 660mm operating in air at a tip Mach number of 0.36. His basic result was a polar plot showing the real and imaginary parts (in-phase and quadrature components) of the sinusoidal transfer function relating flow perturbations to pressure perturbations (This is the impedance of the compressor al-

though he did not call it that.) Over the range of frequencies and flows which he studied, the real part of the impedance varied only slightly while the imaginary part increased strongly with forcing frequency. He attributed this to a fluid inertia effect. However, the equivalent compressor length required to explain this data was a function of the mean flow rate, which does not seem physically plausible given that equivalent compressor length is a purely geometric quantity. The variation in the real part of the transfer function also would not be expected from quasi-steady theory which predicts that the real part remain constant at the value of the quasi-steady slope corresponding to the mean flow. Another attempt to characterize the unsteady response of a compressor was reported by Paulon [38] who studied a low speed single stage axial flow compressor, but no clear conclusions were reached.

Review of the available literature thus indicated the need for the direct assessment of the validity of simple lumped element models of the compressor and such an assessment was performed as part of the current research effort described in this thesis.

1.2.3 Feedback Stabilization of Compression Systems

There have been a number of demonstrations that the stable operating range of a compressor can be extended by modifying the overall dynamics of the system. Such modification can always be interpreted as providing a stabilizing feedback mechanism. In terms of implementation, these methods can be divided into two general categories: unilaterally coupled and bilaterally coupled (see for example [53]).

In a unilaterally coupled feedback system, power flows essentially one way; from

the actuator into the controlled plant. A typical example of a unilaterally coupled feedback consists of a silicon strain gauge pressure transducer measuring pressure in a plenum which sends an electrical signal to a computer which drives (through an amplifier) a speaker connected to the plenum. In contrast, power flows both ways in a bilaterally coupled feedback system. For example, if the transducer, computer and speaker of the previous example were replaced by a spring loaded, movable plenum wall, a bilaterally coupled feedback mechanism would be obtained. These two types of implementations are also commonly distinguished as active and passive[2].

The idea of stabilizing a compressor using unilateral feedback was proposed by Epstein et al [11]. An initial theoretical investigation of surge stabilization was conducted by Chen [6] who examined the stabilization of compression system using a movable plenum wall and a variable throttle area at the plenum exit using linear stability theory. Chen also investigated the use of nonlinear sliding mode control with a plenum exit control valve and concluded that the approach was promising. A reference available in Russian [22] also discusses application of unilateral feedback stabilization of compression systems.

Two experimental investigations (Pinsley et al [40] and Ffowcs Williams and Huang [12]) demonstrate that a unilateral feedback control can be used to allow a compressor to operate steadily at naturally unstable points on the compressor map. Both control schemes were based upon a linearization of a lumped element model

[2]The terms active and passive already have useful precise definitions in the electrical circuit literature (See for example Wyatt et al [52].) which do not necessarily coincide with this common usage. Although unilaterally coupled feedback systems are typically active and bilaterally system are typically passive (in the electrical circuit sense) this correspondence need not hold in general. Thus, to avoid confusion, this terminology will not be used here.

similar to the type described in the previous section. Ffowcs Williams and Huang used a measurement of plenum pressure to provide a feedback signal which was used to drive a speaker mounted on the plenum wall, effectively changing the plenum volume in response to perturbations in plenum pressure. Pinsley also used measurements of plenum pressure to provide a feedback signal, but used it to drive a servo-actuated valve at the plenum exit. In both cases, the feedback control law (compensator) was implemented using a linear, frequency dependent, analog network.

Both investigators were successful at moving the surge line appreciably in some regions of the performance map but not in others; in particular, little effect was found at higher wheel speeds. Both researchers indicate that their inability to obtain control at higher speeds was attributable to diminished effectiveness of their actuated variable, although no detailed analysis was performed. Neither researcher considered the dynamics of the feedback components except to study the effect of changing the compensator gain and phase at a single frequency (the open loop system natural frequency).

There have been basically two types of bilateral implementations: close-coupled resistances and tuned absorbers. Dussourd [8] showed experimentally that adding a flow resistance immediately downstream of the compressor exit extended the surge free mass flow range. He found that, for compressors whose pressure-rise versus flow characteristics were not too steeply positively sloped, substantial increases in surge free operating range could be achieved with a relatively small pressure drop penalty. Further, the stability limit of the overall system could be well predicted based upon the simple criterion that the slope of the combined pressure-rise versus

flow characteristic of the compressor and valve be zero at instability. (This would be expected from the simple lumped element model for systems with a reasonably large value of B parameter.) It should be noted that this result was apparently well known, at least empirically, as long ago as the 1930's with commercially available devices providing throttling at the compressor inlet as described by Kearton [23].

At least two tuned resonator approaches have been reported in the literature. Bodine [4] used a no moving parts Helmholtz resonator (a plenum chamber with a short neck) mounted at the compressor exit to extend the stable flow range but did not provide any detailed analysis. Gysling [20] used a mechanical resonator to extend the stable flow range. In Gysling's purely aero-mechanical scheme, the compression system was coupled to a mass-spring-dashpot arrangement through a movable plenum wall. Functionally, plenum pressure was fed back to produce changes in plenum volume.

Gysling modeled both the dynamics of the mass-spring-dash pot system and the compression system using simple lumped element models and showed that an appreciable surge line shift (20-30% in mass flow) could be obtained by optimizing the choice of system parameters. Gysling's design was based upon a linearization of the system dynamic model which was then checked using a nonlinear simulation. Good agreement was shown between the experimental and theoretical range of stabilization.

1.3 Current Research Objectives

The specific objectives identified for the research reported in this thesis are classified into two main categories: modeling and model validation related objectives and those concerned directly with feedback stabilization. In this section, the identified objectives in both of these categories are first motivated, and then are briefly summarized.

1.3.1 Modeling and Model Validation

Although an established approach for modeling compression system surge instabilities is available, two research goals involving modeling related work would be beneficial were identified as useful to pursue. The first was to develop control oriented models which would include a variety of attractive actuation and sensing schemes. Many of the currently available models are oriented toward studying the autonomous system dynamics and do not include any actuators and sensors. Development of models in a form readily amenable to performing control system design and analysis was thus a necessary step for the subsequent thesis work described here. Availability of such models also provides the benefit of making this interesting problem accessible to other researchers.

The second modeling related research goal was to experimentally assess in detail, the widely used approach of modeling the compressor as a quasi-steady actuator disk coupled to a one-dimensional incompressible duct. Although indirect evidence, based upon studies of overall system dynamics, exists to support this modeling approach, there have been few unambiguous studies of the compressor alone. Since it is

the compressor behavior which drives the surge instability, accurate modeling of the compressor is an item of key importance. Thus, the results of such an experimental validation would provide an important contribution.

1.3.2 Feedback Stabilization

Work to date on controlling compression system instabilities has focused on analyzing and or implementing particular control schemes, and little of the available, and apparently applicable, control theory has been used to study this problem. Several research objectives were accordingly identified.

The first was to establish and quantify the fundamental theoretical limits to stabilizing a compression system. The second objective was to evaluate a variety of potentially attractive control schemes and to identify the most promising generic stabilization approach to pursue. The third objective was to obtain a detailed understanding of the most promising concepts and to experimentally demonstrate the viability of this option.

1.3.3 Summary

The basic objectives of this research are briefly summarized as follows:

- Assess experimentally the quasi-steady compressor model.
- Develop control oriented system dynamic models of the compression system for the more attractive actuation and sensing options

- Characterize and establish quantitative limits to feedback stabilization of compression systems
- Determine the most promising generic approach to stabilizing compression systems.
- Develop a detailed understanding of the most promising stabilization approach and experimentally demonstrate its viability

1.4 Overview of Thesis

To accomplish these research objectives a combined analytical and experimental approach was taken. This section provides a brief overview of the overall thesis organization.

- Chapter 1 - Introduction and Background

  The general problem of compressor instability and motivation for stabilizing compression systems is introduced. Potential benefits and risks are discussed. Previous work is reviewed to establish the starting point for this research. Research objectives are outlined.

- Chapter 2 - Experimental Facility

  This chapter provides an overall description of the experimental facility utilized for experiments described in the thesis.

- Chapter 3 - Modeling of Actuation and Sensing

  This chapter develops the models necessary for performing control system design

or analysis for the compression system using the various actuation and sensing schemes which were considered. Inclusion of fuel modulation and mass injection amongst the set of potential actuators requires some extensions to the simple model presented initially and these are made here and explained. For example, the isentropic plenum assumption must be dropped introducing an additional states. Models of actuation and sensing previously developed must also be modified to be consistent with the new assumptions and this is also done here. The models are put into a form readily amenable to control system design and analysis.

- Chapter 4 - Compressor Model Validation

  Modeling of the unsteady behavior of the compressor itself is the most fundamental aspect of an overall compression system model. To directly assess our ability to model this behavior, the frequency response of a representative centrifugal compressor was determined. This chapter presents both the experimental technique and data analysis methods which were developed for this purpose and the comparison of experimental results with theoretical predictions.

- Chapter 5 - Limitations to Stabilization of Compression Systems

  This chapter establishes and quantifies some fundamental limitations to stabilization of compression systems. First it is established that achieving nominal linear stability is not generally problematic; with most choices of actuator and sensor the system is controllable and observable so the poles may be placed arbitrarily in the left half plane. This point had not previously been clearly es-

tablished. With this issue clarified, attention is directed at what actually limits our ability to control such systems. This is the topic of the second part of the chapter where more fundamental limits to stabilization imposed by practical considerations such as bounded actuation and model uncertainty are characterized and quantified.

- Chapter 6 - Evaluation of Alternative Stabilization Strategies

  In this chapter a side by side quantitative assessment of a representative assortment of potential pairings of actuators and sensors is performed. The results presented here serve two main purposes. First, they provide a rational basis for selecting the more viable options for more intense scrutiny. Second, they establish, in a concrete manner, the real impact that choice of actuator and sensor location has. This fact, particularly regarding sensor selection had not been recognized previously.

- Chapter 7 - Close-Coupled Control Theory and Design

  The use of an actuator and sensor close-coupled to the compressor can have significant advantages as could be qualitatively anticipated from the model physics and quantitatively established in Chapter 6. In this chapter, the rational design of a particular implementation (a valve close-coupled to the compressor exit with mass flow measurement) is analyzed in detail and experimentally evaluated for the first time. A nonlinear, Lyapunov stability analysis of this close-coupled control strategy is also provided in Appendix E. This analysis is useful when considering the effect of large disturbances acting on the system.

- Chapter 8 - Summary and Conclusions

  In this final chapter the overall research effort is summarized, a final set of conclusions conclusions are provided, and suggestions for further research are outlined.

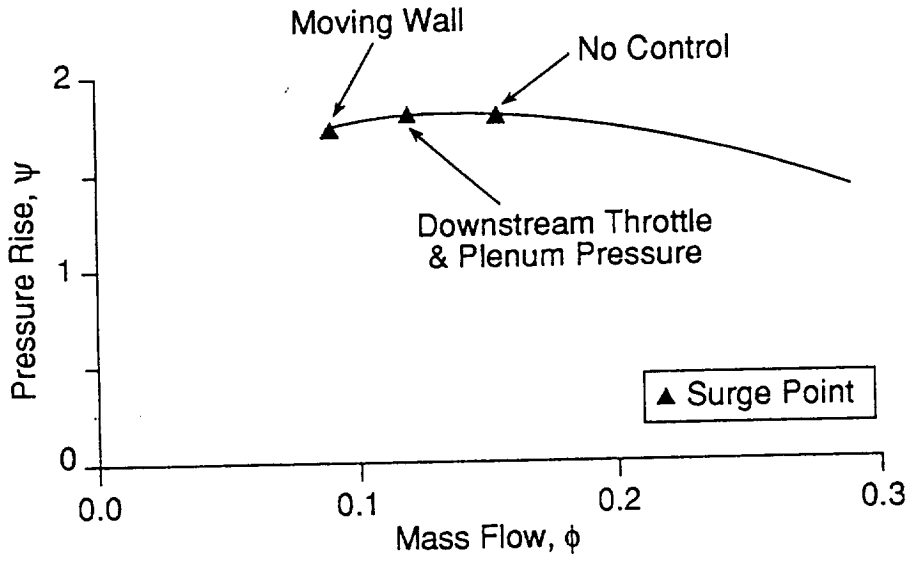

Figure 1-1: Extended range of surge free operation provided by feedback stabilization. (Data of Gysling [20], and Pinsley, [38])

Chapter 2

Experimental Facility

A turbocharger consisting of a single stage centrifugal compressor driven by a radial inflow turbine was used for the experimental phases of the present work. An overview of the experimental facility is provided by Figure 2-1 which shows schematically the arrangement of the various subsystems, which are listed below.

Compression System The compression system consists of the compressor itself, a plenum chamber and connecting ductwork.

Actuation System The actuation system is made up of a valve which controls flow through the compression system, along with a high bandwidth D-C servo motor, servo-amplifier and motor position controller.

Measurement System The measurement system consists of the various transducers (pressure, temperature, speed, etc.) along with their power supplies, and signal conditioning hardware.

Data Acquisition and Control System The data acquisition and control system consists of a digital computer, A/D (analog to digital converter), D/A (digital to analog converter), user interface, mass storage, and software.

Auxiliary Support System The auxiliary support system includes the drive turbine, high pressure air supply (used for the turbine drive), oil supply, cooling water and cooling air supply for the servo motor.

The basic facility was originally constructed by Pinsley, and is described in detail in [39]. The compression system and auxiliary support systems have not been significantly modified and Pinsley [39] can be referred to for full details. The actuation system, measurement system, and data acquisition system components have been either extensively modified or replaced for the purpose of performing the experiments described here. A full description will therefore be provided in the following sections for these systems.

2.1 Compression System

The compression system consists of the following components: inlet duct, compressor, compressor exit duct, plenum chamber, throttle valve and metering duct.

2.1.1 Flow Path

The arrangement of these components and air flow path is shown in Figure 2-2. Ambient air enters the system through a bellmouth at the entrance of the inlet duct. The air passes through the inlet duct into the compressor which discharges into the

inlet duct diameter	5.2 cm
annular inlet area	12.5 cm^2
hub to tip radius ratio	0.37
exit tip diameter	5.5 cm
exit duct diameter	4.4 cm

Table 2.1: Compressor Geometry

compressor exit duct. The air then passes through the compressor exit duct into the plenum chamber. The air exits from the plenum chamber through the throttling valve into the metering duct. In the metering duct the flow passes through a series of perforated plates and finally discharges through a sharp-edged ASME orifice into the room. The servo-controlled valve could be located either at the plenum entrance or exit as described subsequently.

2.1.2 Description of Compressor

A Holset Model H1D turbocharger was used for all tests. In this turbocharger the compressor and drive turbine are mounted on a common shaft. The compressor is a centrifugal type, with a vaneless diffuser, a volute and no inlet guide vanes. The impeller has 6 blades and 6 splitter vanes. An exploded view of the compressor (reprinted from the Holset Manual) is shown in Figure 2-3. Some specifications of the compressor geometry, taken from Pinsley [39], are given in Table 2.1. The compressor has a peak rated pressure ratio of 3.1 at 140,000 rev/min at a flow rate of approximately 0.10 kg/s. The tests described here were done at approximately 90,000 rev/min, with a pressure ratio of approximately 1.75. An overall performance map from [39] is shown in Figure 2-4.

2.1.3 Flow Path Components

The inlet duct is constructed from 2" PVC Schedule 40 piping. Different inlet lengths were used and the length of the inlet used for each particular test is specified subsequently when these tests are described. The plenum is constructed of 10" 304 Stainless Steel Schedule 10S pipe. The plenum volume is adjustable and the actual volume used is provided in the description of the individual tests. A $1\frac{1}{2}$" Jenkins Ball Valve located at the plenum exit was adjusted manually to throttle the flow. The metering duct consists of a 1.07 m section of 4" Schedule 10, Type 304-L pipe, baffled with 3 perforated plates terminating in a 1.75 inch (4.4 cm) ASME standard sharp edged orifice plate.

2.2 Actuation System

The actuation system provides the means to impose control actions upon the compression system. The actuation system consists of the following components: 1) a custom made rotary valve, 2) Pacific Scientific Model 4VM81-220-1 Low Inertia, Permanent Magnet D.C. servo motor, 3) Copley Controls Corporation Model 240 D.C. servo amplifier 4) Galil Model $DMC-400-10$ Digital Motion Control Board, and, 5) BEI Motion Systems Model BEI-MX-213-18-1024 optical shaft encoder. The angular control valve was constructed previously by G. Guenette and J.E. Pinsley and a detailed description is provided in [39]. For completeness, the valve is shown in Figure 2-5. The remaining components form a position control loop for the valve. This position control loop operates cyclically at a rate of 2000 cycles/sec as follows:

1. The digital motion control board reads its input buffer to obtain the commanded valve position.

2. The digital motion control board decodes the shaft encoder signal to obtain the shaft position

3. The digital motion control board generates an error signal by subtracting the actual shaft position from the commanded value

4. The error signal is input to a digital filter which implements a PID (Proportional-Integral-Plus-Derivative) control algorithm.

5. The output of the PID controller is converted to a 0 to 1 volt analog signal which is input to the D.C. servo amplifier

6. The D.C. servo amplifier outputs a pulse width modulated current to the servo motor. The time mean value of the amplifier output current is proportional to its voltage input.

7. The current supplied to the D.C. motor produces an accelerating torque which rotates the valve towards the desired position.

The small signal closed loop bandwidth (the frequency at which the ratio of the actual valve position to that commanded becomes less than unity with a small sinusoidal drive signal) of the valve position control loop is approximately 100 Hz.

2.3 Measurement system

The measurement system is comprised of the transducers, transducer excitation, and signal conditioning devices. Both high and low frequency response measurements were made to determine the time resolved and steady-state behavior, respectively, of the system. Measurements were made of the following quantities:

1. inlet duct mass flow rate, temperature and wall-static pressure
2. compressor rotational frequency, exit total pressure and exit static temperature
3. control valve angular position and total to static pressure-drop (differential pressure)
4. plenum wall-static pressure
5. orifice upstream temperature and differential pressure

The location of these sensors is shown schematically in Figure 2-6. Each channel of data was sampled at a rate of 1 KHz (1000 samples/sec/channel) by an analog to digital converter. A full description of the A/D is is given in a subsequent section. To prevent aliasing all time resolved measurements were low-pass filtered using 8-pole Butterworth Filters with a -3 dB cutoff frequency of 500 Hz.

2.3.1 Inlet Duct Instrumentation

Time Resolved Mass Flow Rate

The time resolved (instantaneous) mass flow rate was obtained using a DISA Type 55D01 Constant Temperature Anemometer with a TSI-1210-T1.5 hot-wire sensor located on the duct center line, 120 mm (approximately 2 duct diameters) downstream of the bellmouth inlet. The anemometer was directly calibrated statically against the ASME orifice at the start of each test. To obtain good resolution of the hot wire signal, it was offset using a TSI Model 1057 Signal Conditioner (the filters on the Model 1057 were not used) which provided a 0-1 volt output over the flow range of interest. This signal was then low-pass filtered at 500 Hz and amplified by a factor of 10 using a Frequency Devices 901F 8-pole Butterworth filter. The conditioned anemometer output, which now ranged from 0-10 volts over the flow range of interest, was terminated in the A/D converter. At the start of each test the mass flow was measured using both the ASME orifice and the anemometer at ten steady operating points over the flow range of interest and the data were fit with a fourth order polynomial. The calibration curve thus obtained provided mass flow rate directly as a function of conditioned anemometer output voltage.

Time-Averaged Inlet Temperature

The time averaged temperature of the air entering the system was measured using a a type-K unshielded thermocouple inserted 65 mm downstream of the bellmouth inlet, radially located 6 mm from the duct wall. The thermocouple output was conditioned

using an Analog Devices 3B47 Isolated Linearized Thermocouple Input Module which provided a linear high level 100 degree-K/volt output to be read by the A/D.

Time Averaged Inlet Wall-Static Pressure

Time averaged wall-static pressure was measured using a Druck-PDCR-820, 1 psi range, transducer located 65 mm downstream of the bellmouth inlet. The low level output of the Druck transducer was amplified using a Analog Devices 2B31K high performance strain gauge conditioner which also provided the required bridge excitation. The conditioned output provided a linear high level output of approximately 600 Pa/volt.

2.3.2 Compressor Instrumentation

Time Resolved Rotational Frequency

A magnetic pickup in conjunction with a magnetized nut on the compressor shaft provided a sinusoidal signal at the rotor frequency. This sinusoidal signal was then fed to an Analog Devices Model 451 F/V (frequency to voltage) Converter. The F/V converter provided a linear high level voltage output of approximately 250 Hz/volt. This signal was then low pass filtered at 500 Hz with a Frequency Devices 901-F 8-pole Butterworth Filter. For the compressor frequency response measurements, greater resolution of the rotational frequency was required. For this purpose, the F/V output signal was split into two separate channels. One channel was used to determine the time-averaged rotational frequency the other was offset and then further amplified.

Time-Resolved Total Pressure

Time-resolved total pressure at the compressor exit was measured using a 50 psi, Kulite XCE-093-50D pressure transducer connected to a modified United Sensor KB-6 Kiel Head Probe. The Kiel Probe was inserted 65 mm downstream of the compressor exit with the head of the probe at the duct center line. The modified probe arrangement is shown in Figure 2-7. As shown in Figure 2-7, the Kiel probe was modified by removing 3 inches (76mm) from the probe stem. The Kulite transducer was cemented with epoxy into a short section of 1/8" thin-walled stainless steel tubing with the sensing face of the transducer flush with the end of the stainless tube. The tube with the transducer is mated to the Kiel probe using a Scanivalve quick release connector. (This arrangement allowed for future re-use of the Kulite transducer.) The low level signal from the Kulite transducer was amplified using an Analog Devices 2B30K amplifier which also provided excitation for the transducer. The resulting output was a linear high level signal of approximately 14000 Pa/volt.

Time-averaged Static Temperature

Time averaged compressor exit static temperature was measured with a type-K unshielded thermocouple inserted 65 mm downstream of the compressor exit at a radial location 6 mm from the the duct wall. The thermocouple output was conditioned using an Analog Devices 3B47 Isolated Linearized Thermocouple Input Module. This module provided a linear high level 100 degree-K/volt output to be read by the A/D.

2.3.3 Control Valve Instrumentation

Time-resolved Valve Position

The angular position of the valve was measured using a BEI-MX-213-18-1024 optical shaft encoder. The shaft encoder provided a resolution of 4096 quadrature counts per revolution. The encoder signal was decoded by the Galil Model DMC-400-10 motion control board.

Time-averaged Total to Static Pressure-Drop

Time averaged total to static pressure drop across the control valve was measured using a Druck 20 psi PDCR-120/35-WL differential pressure transducer. The high pressure port of this transducer was connected to the Kiel probe described in Section 2.3.2 and the low pressure port is connected to a wall static tap in the plenum chamber into which the valve discharges. The time-resolved compressor exit total pressure and time-averaged control valve pressure drop were never both measured for the same test allowing the Kiel probe to be shared for the two purposes. The low level signal from the Druck transducer was amplified using an Analog Devices 2B30K amplifier which also provided excitation for the transducer. The resulting output was a linear high level signal of approximately 14000 Pa/volt.

2.3.4 Plenum Chamber Instrumentation

Time-resolved Wall Static Pressure

The time resolved wall static pressure in the plenum chamber was measured using a 30 psi Druck PDCR-820-0479 transducer. The low level signal from the Druck transducer was amplified using an Analog Devices 2B30K amplifier which also provided excitation for the transducer. The resulting output was a linear high level signal of approximately 20000 Pa/volt.

2.3.5 Metering Duct Instrumentation

Time-averaged Orifice Differential Pressure

The time averaged differential pressure across the ASME orifice was measured using a 2.5 psi Druck PDCR-811 transducer. The pressure tap for the transducer was located in the wall of the upstream flange. (Details are given in [39]). The low level signal from the Druck transducer was amplified using an Analog Devices 2B30K amplifier which also provided excitation for the transducer. The resulting output was a linear high level signal of approximately 900 Pa/volt.

Time-averaged Orifice Temperature

The temperature of the air entering the orifice was measured with a type-K unshielded thermocouple inserted upstream of the orifice. The thermocouple output was conditioned using an Analog Devices 3B47 Isolated Linearized Thermocouple Input Module. This module provided a linear high level 100 degree-K/volt output to

be read by the A/D.

2.4 Digital Data Acquisition and Control System

The digital data acquisition and control system has two basic functions: 1) Closing the compression system stabilization feedback loop with a digital control, and 2) storing data for further analysis. Due to limitations of the available hardware, it was necessary to integrate these two functionally independent tasks into a single system. The hardware system consists of: 1) Data Translations Model DT2801 A/D (Analog to Digital) converter, 2) 20MHz Intel 80386 microprocessor based Hewlett Packard Model HP-Vectra-RS/20 Microcomputer with a 120Mbyte Hard-disk, and, 3) Burr-Brown Model PCI-20093W-1 Analog Output Board (D/A converter).

2.4.1 System Operation

The cyclical operation of the system can be described functionally as follows:

1. Measurements from the compression system are sampled by the A/D converter and put into a digital format

2. The sampled signals are converted to engineering units.

3. A new valve position command is computed based upon the most recent and (possibly previous) measurements.

4. The valve position command is sent over the communication bus to the valve position controller (Galil digital motion control board).

5. Selected channels are output by the D/A converter to provide real time monitoring on an oscilloscope.

6. Data for selected channels is stored in the volatile memory (RAM) of the microprocessor.

At completion of the test, data stored in volatile memory is transferred to the hard disk for permanent storage.

2.4.2 Loop Timing

Details of the loop timing are given to help provide and understanding of the data reduction procedures employed. The overall data acquisition and control cycle actually involves a number of independent, concurrent, processes. These processes are: 1)The software loop, 2) the A/D conversion process and, 3) the actuator position control process.

The actuator position control process is executed by the Galil digital motion control board as described in Section 2.2. The A/D conversion process involves the Data Translation A/D board and the DMA (Direct Memory Access) controller of the Intel 80386 Microprocessor. The A/D board executes an endless loop, in which it successively samples the first, second, third, up to the n^{th} measurement channel, and then repeats. The board contains an internal clock and at each "tick" of this clock the next channel is sampled. After each channel is sampled, the DMA controller transfers the digitized value directly into the memory of the 80386 Microprocessor. There is a single, fixed memory location in the 80386 assigned to each A/D channel

and this memory location is overwritten each time the A/D obtains a new digitized sample for that channel. Thus, if there are a total of n channels of data which are measured, and the clock ticks at a uniform rate of f ticks/sec, each channel will be sampled every n/f seconds and, correspondingly, each assigned memory location in the 80386 will also be overwritten every n/f seconds. The amount of time, n/f will be referred to as the A/D cycle time or sampling period, T_s. With this system, if n channels of data are read by the A/D in each scan, then the first and last channel in a data scan are separated by a time interval of $T_s - 1/f$.

For control and data analysis purposes it is preferable to sample all the channels simultaneously. The process described above was adopted by necessity to accommodate various limitations imposed by the available hardware.

The software loop is a program which is executed by the 80386 microprocessor itself. It is responsible for processing the data obtained by the A/D, converting it to engineering units, implementing the digital control algorithm, storing data to an in memory buffer, sending commands to the actuator position control, and communicating with the user via keyboard input. This program operates as an endless loop (until it is terminated by keyboard input from the user.) The cyclic operation of the software loop is as follows:

1. The program enters a "tight loop", checking if all of the A/D channels have been updated (overwritten) that is, it waits until the completion of the next A/D cycle.

2. As soon as it has been determined that an A/D cycle is completed, all the

updated A/D channels are "read" i.e. they are copied to another memory location where they will not be overwritten. This set of values is called the current A/D scan.

3. The valve position command is computed.

4. The program enters a tight loop, polling the Galil DMC (digital motion control) board to determine if it is ready to communicate. The DMC board communicates at uniform time intervals of 0.5msec, corresponding to its internal 2KHz cycle time. This clock is not synchronized with the clocks on either the 80386 or the Data Translations A/D board. At the end of each DMC cycle, it sends the current motor shaft position and receives the current position command. Since the DMC uses the same register in the 80386's I/O address space for sending and receiving data, the shaft position must be read before the command can be sent.

5. Once the DMC board is ready to communicate, the current shaft position is read and the new position command is sent. Both the incoming and outgoing data must be sent one byte at a time with "hand-shakes" occurring after each byte. Thus, the 80386 is unavailable for other tasks until all the data is transferred.

6. Once the data transfer is completed, the current A/D scan is converted to engineering units, and the digital control law calculation is performed.

For control and data analysis purposes it is necessary to have the cycle time for the software loop the same as that of the A/D. Since the steps described above are

executed serially, it can be seen that the total amount of time required for the software loop to execute can be considered to be the sum of three time periods: 1) the waiting time for the A/D cycle to complete, 2) the waiting time for the communication with the DMC to complete and, 3) the computational time for implementing the digital control and other auxiliary calculations, such as conversion to engineering units. To insure proper timing of the software loop, the A/D cycle time thus had to be longer than the sum of the DMC waiting time and the computational time. This put an upper bound on the A/D cycle time of 1msec providing a sampling rate of 1KHz per channel.

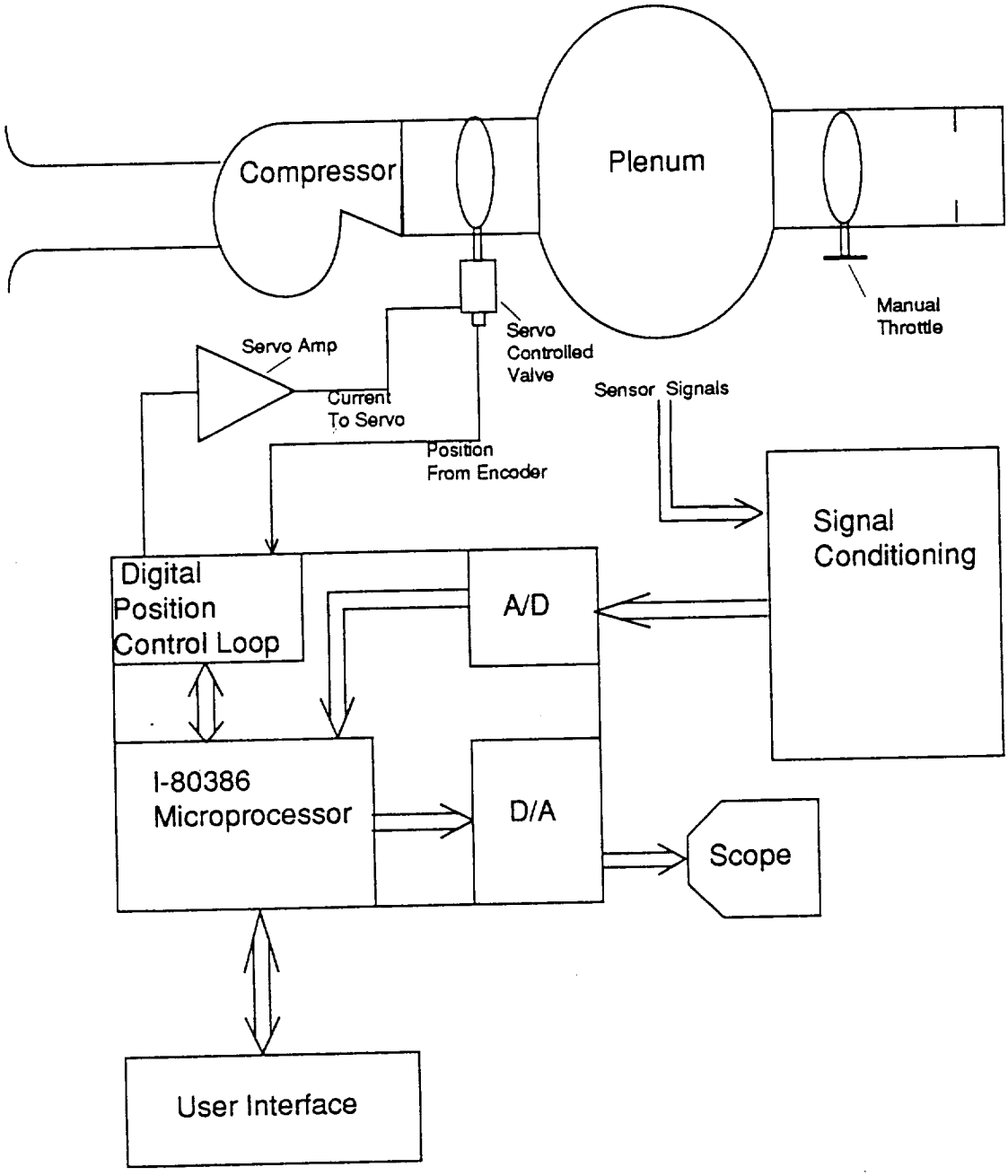

Figure 2-1: Overview of experimental facility

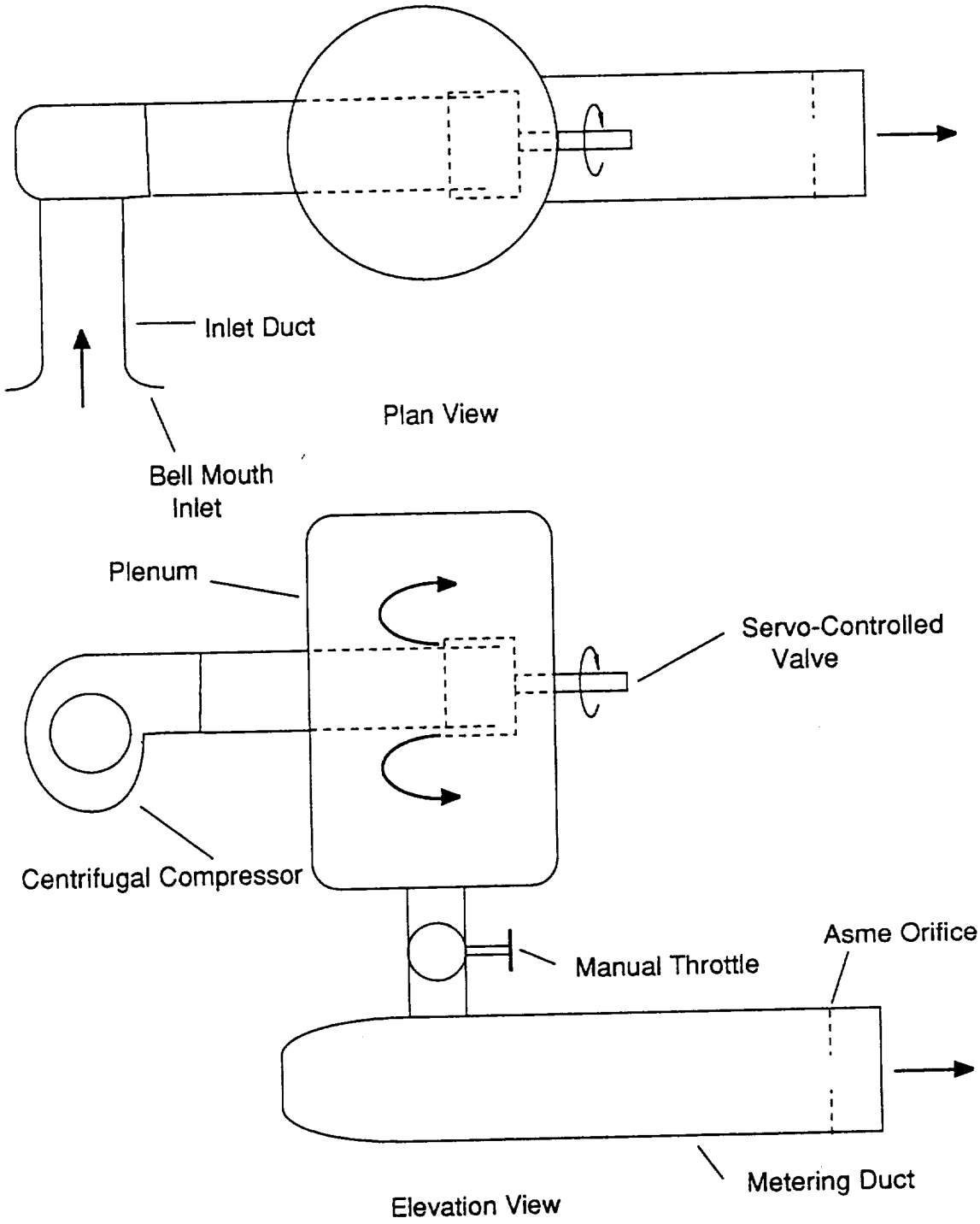

Figure 2-2: Compression system arrangement and flow path

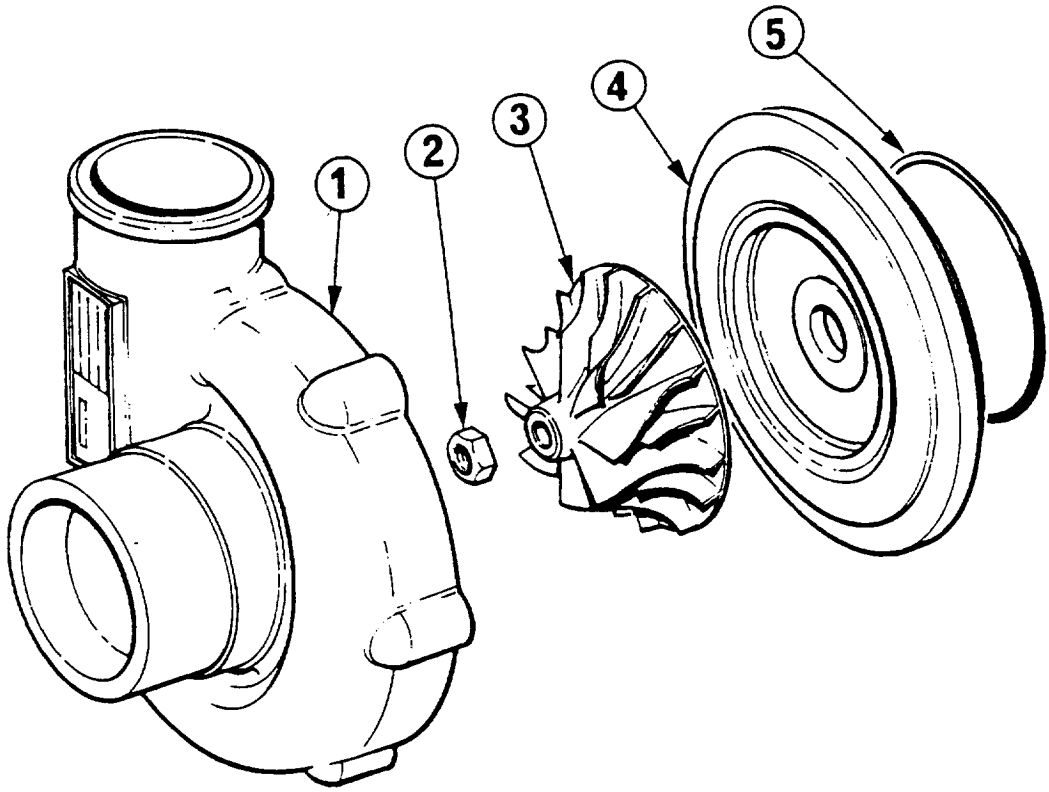

Figure 2-3: Exploded view of turbocharger used for experiments

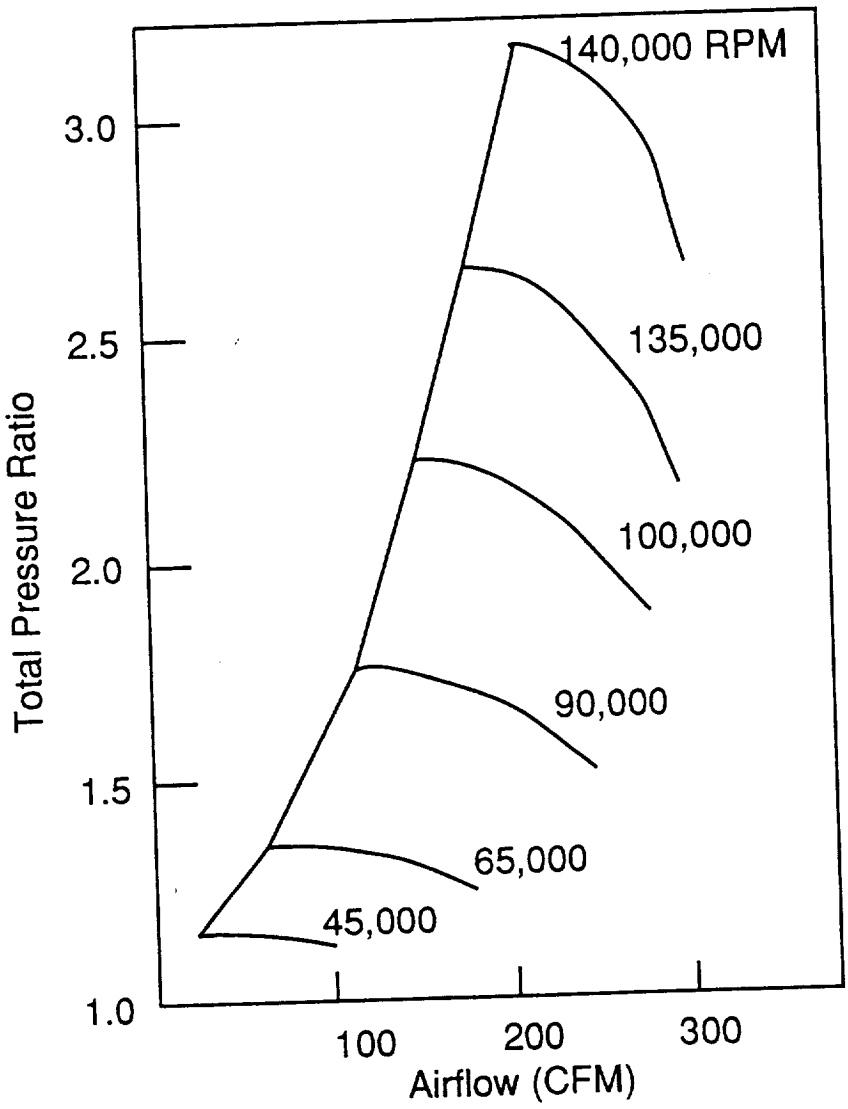

Figure 2-4: Overall Performance Map for Holset H1D Compressor

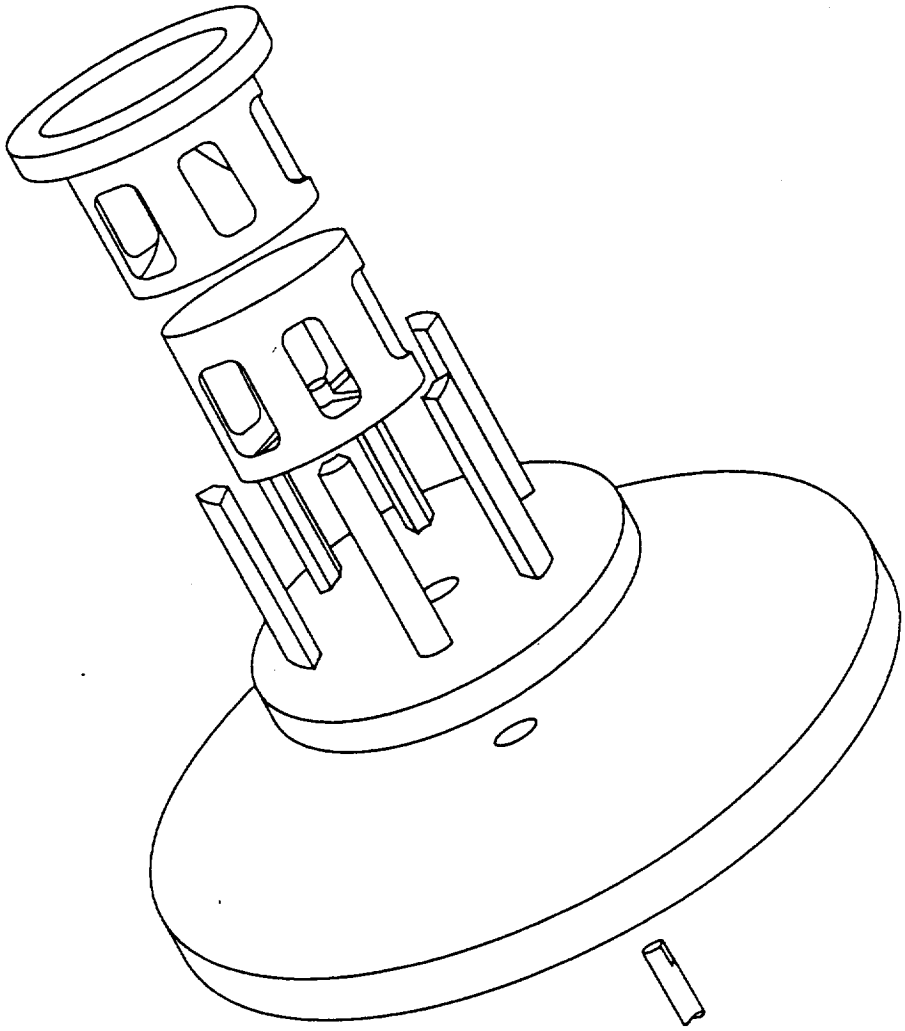

Figure 2-5: Control valve used for experiments

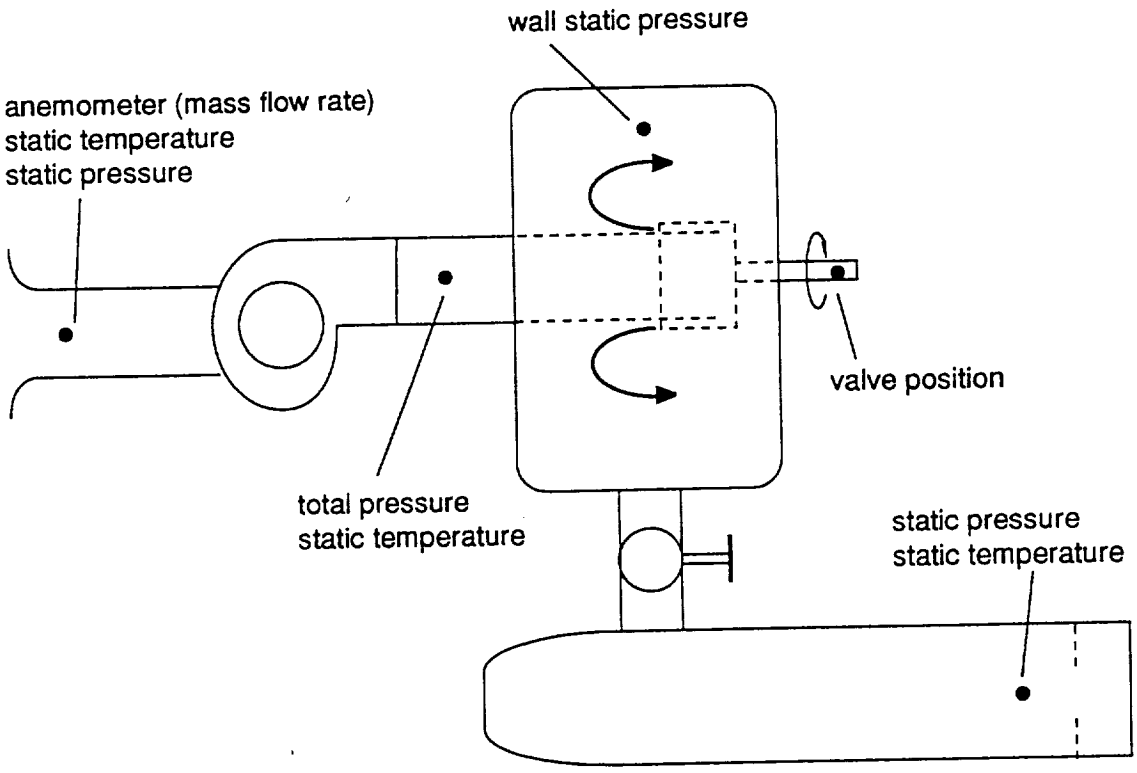

Figure 2-6: Sensor locations for experimental studies

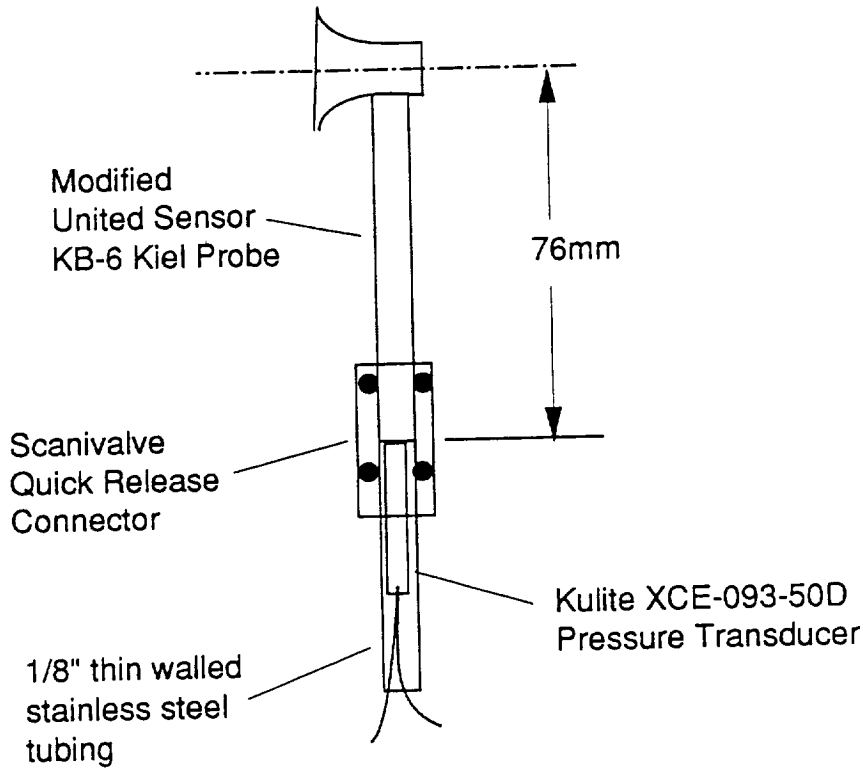

Figure 2-7: Modified Kiel Probe used to measure compressor exit total pressure

Chapter 3

System Modeling

In this chapter the system dynamics of a compression system equipped with a number of actuators and sensors are modeled in a form suitable for control design and analysis.

3.1 Description of System

The compression system to be studied is shown schematically in Figure 3-1. The system consists of an inlet duct, compressor, plenum chamber and throttle valve, and a number of actuators and sensors. This configuration is typical of that found in a gas turbine engine where the plenum chamber would represent the combustor and the throttle represents the turbine nozzles. All of the actuators and sensors shown here for implementing a stabilizing control would not, however, be found on a production engine.

Ambient, low pressure gas is drawn into the inlet duct where it flows to the compressor. The compressor then raises the pressure of the gas, discharges the pressurized

gas into the plenum chamber, where combustion occurs, raising the gas temperature. Hot, pressurized gas exits the plenum chamber, through the turbine nozzles, and is exhausted through the turbine to the ambient surroundings.

The system to be analyzed is equipped with five actuators which provide alternative means to influence the behavior of the system and four sensors to provide feedback signals. This set of actuators and sensors were selected as being representative of a diverse number of potentially attractive options. In the inlet duct upstream of the compressor is an *injector* which can be used to inject additional gas into the compressor inlet. The flow through the injector is controlled by modulating the injector supply pressure. A *close-coupled valve* is located immediately downstream of the compressor. The pressure drop across the valve is controlled by modulating the open area of the valve. A *plenum bleed valve* located in the plenum wall discharges high pressure gas from the plenum to ambient conditions. Flow through the valve is controlled by modulating the open area of the valve. A piston, which will be referred to as the *movable plenum wall*, is used to vary the volume of the plenum. The volume of the plenum is controlled by inserting or retracting this piston. The fifth means of influencing the system is to vary the rate of heat addition to the plenum. In a gas turbine this could be accomplished by varying the fuel flow.

Four sensors are available to measure the behavior of the system. Total and static pressure sensors are located at the compressor face. A mass flux sensor (such as a hot wire or hot film) also located in the compressor inlet, is used to obtain the instantaneous mass flow rate through the compressor. Since one-dimensional axial flow will be assumed, the radial locations of the transducers in the duct need not be

specified. A pressure sensor in the plenum wall provides measurements of the static pressure in the plenum. Since uniform pressure in the plenum is assumed, it is not necessary to specify the location of the sensor. All of the sensors are assumed to provide perfect measurements of the sensed quantities, free of noise and any other inaccuracy. This considerable idealization can be relaxed later by further augmenting the model.

3.2 Component Models

The dynamics of the compression system described above will be approximated with the lumped parameter model depicted in Figure 3-2. The model is constructed using a number of components which will be first modeled individually and then interconnected. All locations (flow stations) referred to in the following derivation are identified in figure 3-2. The presentation here will be brief, highlighting the major assumptions and the basic physics of the model.

3.2.1 Ducts

The inlet duct is broken into two separate ducts; one upstream and one downstream of the injector. These will be referred to as the upstream and downstream ducts respectively.

Assumptions

Flow in the ducts is assumed to be incompressible, inviscid, and one-dimensional[1]. The duct area is not assumed to be constant but must vary slowly enough to justify the one-dimensional flow assumption.

Mathematical Model

With these assumptions, the flow in the duct is completely described by specifying the mass flow, $\dot{m}$ through the duct and this will be used as a state variable. The time rate of change of the mass flow through the upstream duct, $\dot{m}_u$, is found from the axial momentum balance:

$$d\dot{m}_u/dt = \frac{1}{\mathcal{L}_u/A_c}(p_{0_1} - p_{0_2}), \tag{3.1}$$

where p_{0_1} and p_{0_2} are total pressures at station-1 and station-2 respectively; A_c is the annular inlet area of the compressor, and $\mathcal{L}_u$ is the equivalent length of the upstream duct computed using A_c as the reference area[2]. Similarly for the downstream duct:

$$d\dot{m}_d/dt = \frac{1}{\mathcal{L}_d/A_c}(p_{0_3} - p_{0_4}), \tag{3.2}$$

[1]By one-dimensional it is meant that at all points in the duct the fluid moves only in the axial direction, and at any given axial location the axial velocity is constant across the duct cross section.

[2]The equivalent duct length for a duct of non-constant cross sectional area is defined to be the length of duct with a given constant area which would experience the same acceleration as the non-constant area duct when the same total pressure difference was applied. Using the compressor annular inlet area as the reference area, the equivalent length, $\mathcal{L}$, of a duct of length L, is given by: $\mathcal{L} = A_c \int_0^L 1/A(x)\,dx$, where $A(x)$ prescribes the variation of duct area as a function of axial distance along the duct center line.

The equivalent length of the downstream duct, $\mathcal{L}_d$, includes the flow path through the compressor.

3.2.2 Plenum

Assumptions

All fluid properties in the plenum are assumed to be spatially uniform, that is, the plenum is *well mixed.* Fluid velocities in the plenum are assumed to be negligible. The effect of combustion is idealized as a specified rate of heat addition to the gas contained in the plenum. Ideal gas behavior[3], with constant specific heat is assumed.

Mathematical Model

With the above assumptions, the plenum behavior is fully described by specifying the mass, m_p, internal energy, U_p, and volume, V_p of the gas in stored in the plenum, which may vary with time due to the movable wall. These quantities will thus be used as the state variables for the plenum.

The time rate of change of the mass of gas, m_p, in the plenum is found from the mass balance:

$$dm_p/dt = (\dot{m}_6 - (\dot{m}_7 + \dot{m}_8)), \tag{3.3}$$

where $\dot{m}_6$ is the incoming mass flow, and $\dot{m}_7$ and $\dot{m}_8$ are the mass flows exiting through the throttle and bleed valve respectively.

The time rate of change of internal energy, U_p, of the gas in the plenum is found

[3]The pressure, temperature and density are related by $p = \rho RT$

from the energy balance:

$$dU_p/dt = \dot{m}_6 C_p T_{0_6} - \dot{m}_7 C_p T_{0_7} - \dot{m}_8 C_p T_{0_8} + Q + p_p A_w u_w, \tag{3.4}$$

where, C_p is the specific heat at constant pressure, T_{0_6}, T_{0_7}, and T_{0_8} are the absolute total temperatures of the entering and exiting streams, Q is the heat addition rate, p_p is the absolute static pressure in the plenum, A_w is the projected area of the movable wall and u_w is the velocity of the wall.

The time rate of change of the volume of the plenum is given by:

$$dV_p/dt = A_w u_w \tag{3.5}$$

3.2.3 Compressor

Assumptions

The compressor is modeled as an actuator disk, that is, a region of infinitesimal axial extent producing a discontinuity in total pressure and temperature. Any fluid inertia associated with the flow passages of the actual compressor is included in the equivalent length, $\mathcal{L}_d$, of the duct attached to its upstream flange. The actuator disk assumption implies that no mass can accumulate in the compressor. Unless otherwise noted, the instantaneous total pressure-rise and total temperature ratio of the compressor are assumed to be the same as the steady state values for the same inlet conditions. This will be referred to as the *quasi-steady assumption.*

Mathematical Model

The total to total pressure rise, (p_{0_5}-p_{0_4}), of the compressor is given by:

$$p_{0_5} - p_{0_4} = 1/2\rho_a {u_T}^2 \, \Psi_c(\dot{m}_4/(\rho_a u_T A_c), u_T/a), \tag{3.6}$$

where ρ_a is the ambient density, u_T is the tip speed of the compressor, $\dot{m}_4$ is the mass flow through the compressor, a is the speed of sound at ambient conditions, and Ψ_c is the non-dimensional compressor pressure rise characteristic. Ψ_c is an empirically determined function which must be measured for the compressor of interest. Similarly, the compressor temperature ratio, T_{0_5}/T_{0_4}, is given by:

$$T_{0_5}/T_{0_4} = \Theta_c(\dot{m}_4/(\rho_a u_T A_c), u_T/a) \tag{3.7}$$

where, Θ_c is the total temperature ratio characteristic of the compressor. This is also an empirically determined function.

In some cases, we will not make the quasi-steady assumption. Instead, we will assume that the instantaneous, non-dimensional pressure rise of the compressor, $\psi(t)$, is given by: $\psi(t) = \Psi_{ci} - \psi_l(t)$, where $\Psi_{ci}(\dot{m}_4/(\rho_a u_T A_c), u_T/a)$ is the theoretical, ideal pressure rise of the compressor, and $\psi_l(t)$ is the instantaneous non-dimensional total pressure loss due to viscous effects and other non-idealities. The losses will be assumed to evolve in time according to:

$$d\psi_l/dt = \frac{1}{t_l}\left(\Psi_{ci}(\dot{m}_4/(\rho_a u_T A_c), u_T/a) - \Psi_c(\dot{m}_4/(\rho_a u_T A_c), u_T/a) - \psi_l(t)\right), \tag{3.8}$$

where t_l is an empirically determined time constant. This will be referred to as the unsteady loss model.

3.2.4 Throttle

Assumptions

The throttle flow is assumed to be quasi-steady, one dimensional, compressible, and isentropic.

Mathematical Model

The throttle is modeled as a quasi-steady one-dimensional isentropic converging nozzle. The mass flow through the throttle, $\dot{m}_7$ is given by:

$$\dot{m}_7 = \rho_a u_T A_c \Phi_t(p_p/p_a, T_p/T_a, A_t/A_c), \tag{3.9}$$

where, p_p and T_p are, respectively, the absolute temperature and pressure in the plenum, p_a and T_a are the ambient absolute pressure and temperature and A_t is the exit area of the throttle. The function, Φ_t is the non-dimensional throttle flow characteristic which is obtained assuming one-dimensional, steady, compressible flow. The nozzle model is applicable for both choked and non-choked conditions.

3.2.5 Plenum Bleed Valve

Assumptions

The plenum bleed valve was also modeled as a quasi-steady, isentropic, converging nozzle in exactly the same manner as described for the throttle.

Mathematical Model

The mass flow rate through the bleed valve is given by:

$$\dot{m}_8 = \rho_a u_T A_c \, \Phi_b(p_p/p_a, T_p/T_a, A_b/A_c), \tag{3.10}$$

where A_b is the bleed valve area, and the function Φ_b is the non-dimensional bleed valve flow characteristic. (It is actually the same function as Φ_t.)

3.2.6 Close-Coupled Valve

Assumptions

The close-coupled valve, as its name implies, is located immediately at the exit of the compressor. It is assumed that mass flow rates entering and leaving the close-coupled valve are at all times equal to each other and to the flow through the compressor. That is, there is no accumulation of mass in the close-coupled valve or between it and the compressor. Pressure loss across the close-coupled valve is assumed to be small enough for the flow through the valve to be accurately modeled as incompressible. The valve is assumed to discharges into the plenum with negligible static pressure

recovery.

Mathematical Model

The total pressure drop across the valve, (p_{0_5}-p_{0_6}) is given by

$$(p_{0_5} - p_{0_6}) = 1/2\rho_a {u_T}^2 \Psi_v(\dot{m}_5/(\rho_a u_T A_c), \alpha_c), \tag{3.11}$$

where, $\dot{m}_5$ is the flow through the valve, α_c is the valve fraction open (the area of the valve divided by the area of the valve when wide open), and Ψ_v is the non-dimensional pressure drop characteristic of the close-coupled valve. This function is either estimated analytically or measured empirically.

3.2.7 Injector

The section of duct between station-2 and station-3 along with the injection tube will be referred to as the injector.

Assumptions

It is assumed that the injector behaves quasi-steadily, that is, that the steady state characteristics continue to hold even when the upstream and downstream mass flows or supply pressure are unsteady. It is assumed that the mass of fluid contained in the injector duct remains constant, and that the axial velocity is spatially uniform at station-3, (i.e., the flow is fully mixed out at the exit of the injector). The flow between station-2 and station-3 is not necessarily one-dimensional. All of the fluid

inertia of the injector is included in $\mathcal{L}_u$.

Mathematical Model

The injector must be characterized as a two port device. Specifically, the difference in pressure between station-2 and the injector supply, $(p_{0_2} - p_{0_i})$, is given by:

$$p_{0_2} - p_{0_i} = 1/2\rho_a {u_T}^2 \Psi_{i_u}(\dot{m}_2/(\rho_a u_T A_c), \dot{m}_3/(\rho_a u_T A_c)), \tag{3.12}$$

where Ψ_{i_u} is defined as the non-dimensional injector upstream pressure characteristic, and $\dot{m}_2$ and $\dot{m}_3$ are the upstream and downstream mass flows, respectively. Similarly, the difference in pressure between station-3 and the injector supply, $(p_{0_3} - p_{0_i})$, is given by:

$$p_{0_3} - p_{0_i} = 1/2\rho_a {u_T}^2 \Psi_{i_d}(\dot{m}_2/(\rho_a u_T A_c), \dot{m}_3/(\rho_a u_T A_c)), \tag{3.13}$$

where Ψ_{i_d} is defined as the non-dimensional injector downstream pressure characteristic.

Analytical expressions which are used for the steady characteristics Ψ_{i_u} and Ψ_{i_d} are derived in appendix A.

3.3 System Model

The component models described in the previous section must be interconnected to form an overall system model. Applying continuity, matching pressures at component

interfaces, and using the spatially uniform plenum assumption gives:

$$
\begin{aligned}
d\dot{m}_u/dt &= \frac{1/2\rho_a {u_T}^2}{\mathcal{L}_u/A_c}\left(\frac{(p_a - p_{0_i})}{1/2\rho_a {u_T}^2} - \Psi_{i_u}\right) \\
d\dot{m}_d/dt &= \frac{1/2\rho_a {u_T}^2}{\mathcal{L}_d/A_c}\left(\Psi_{i_d} + \frac{(p_{0_i} - p_a)}{1/2\rho_a {u_T}^2} + \Psi_c - \Psi_v - \frac{(p_p - p_a)}{1/2\rho_a {u_T}^2}\right) \\
dm_p/dt &= \rho_a u_T A_c\,(\dot{m}_d/(\rho_a u_T A_c) - \Phi_t - \Phi_b) \\
dU_p/dt &= \left(\dot{m}_u C_p T_a \Theta_c - \rho_a u_T A_c(\Phi_t C_p T_{0_p} + \Phi_b C_p T_{0_p}) + Q + p_p A_w u_w\right) \\
dV_p/dt &= (u_w A_w)\,.
\end{aligned}
\tag{3.14}
$$

For brevity, the arguments of the various characteristic functions have been suppressed. The system model, Equations 3.14, is put into non-dimensional form by normalizing the various dimensional quantities by the reference values given in Table 3.1 to form the non-dimensional quantities listed in Table 3.2. For example, non-dimensional time, τ, is defined as the ratio of the physical time, t, to the reference time, $(\sqrt{\mathcal{L}_c \bar{V}_p})/(\bar{a}_p\sqrt{A_c})$, from Table 3.1 to give:

$$
\tau = \frac{t}{\left(\frac{\sqrt{\mathcal{L}_c \bar{V}_p}}{\bar{a}_p\sqrt{A_c}}\right)}.
$$

quantity	reference value
time	$\frac{\sqrt{\mathcal{L}_c \bar{V}_p}}{\bar{a}_p \sqrt{A_c}}$
pressure(differential)	$1/2\rho_a {u_T}^2$
pressure(absolute)	p_a
mass flow rate	$\rho_a u_T A_c$
temperature	T_a
heat addition	$\rho_a u_T A_c C_p T_a$
area	A_c
plenum mass	$\rho_a \bar{V}_p$
plenum energy	$\rho_a \bar{V}_p C_v T_a$
plenum volume	$\bar{V}_p$
tip speed	a
length	$\mathcal{L}_c = \mathcal{L}_u + \mathcal{L}_d$
wall displacement rate	$u_T A_c$

Table 3.1: Reference quantities for non-dimensionalizing the system model

It is also useful to utilize the B parameter[4] which is defined by:

$$B = \frac{u_T}{2\bar{a}_p}\sqrt{\frac{\bar{V}_p}{(\mathcal{L}_c A_c)}} \tag{3.15}$$

The resulting non-dimensional equations are then given by:

$$\begin{aligned} d\phi_u/d\tau &= \frac{-B}{\mathcal{L}_u/\mathcal{L}_c}\left(\psi_i + \Psi_{i_u}(\phi_u, \phi_d)\right) \\ d\phi_d/d\tau &= \frac{B}{\mathcal{L}_d/\mathcal{L}_c}\left(\Psi_{i_d}(\phi_u, \phi_d) + \psi_i + \Psi_c(\phi_d, M_T) - \Psi_v(\phi_d, \alpha_c) - \psi_p\right) \\ d\tilde{m}_p/d\tau &= \frac{{M_T}^2}{2B\bar{\theta}_p}\left(\phi_d - (\Phi_t(\pi_p, \theta_p) + \Phi_b(\pi_p, \theta_p))\right) \end{aligned} \tag{3.16}$$

[4]One could also define a stability parameter, $(B\psi_{peak})/\phi_{peak}$, where ϕ_{peak} is the flow coefficient at which the peak compressor pressure rise occurs and ψ_{peak} is the peak pressure rise. For classes of compressors where the slope of the compressor characteristic roughly scales with ψ_{peak}/ϕ_{peak}, this stability parameter provides a useful means to compare the stability characteristics of compression systems containing compressors whose pressure-rise differs greatly.

non-dimensional quantity	symbol
time	τ
pressure (differential)	ψ
pressure (absolute)	π
mass flow rate	ϕ
temperature (absolute)	θ
heat addition	$\tilde{Q}$
area	$\tilde{A}$
plenum mass	$\tilde{m}_p$
plenum energy	$\tilde{U}_p$
plenum volume	$\tilde{V}_p$
tip speed	M_T
wall displacement rate	ξ
length	$\tilde{L}$
Greitzer B parameter	B

Table 3.2: Non-dimensional symbols for the system model

$$
\begin{aligned}
d\tilde{U}_p/d\tau &= \frac{{M_T}^2\gamma}{2B\bar{\theta}_p}\left(\phi_u\Theta_c(\phi_d, M_T) - (\Phi_t(\pi_p,\theta_p) + \Phi_b(\pi_p,\theta_p))\theta_p + \tilde{Q} + \pi_p\xi\right) \\
d\tilde{V}_p/d\tau &= \frac{BM_wM_T}{2\bar{\theta}_p}\xi,
\end{aligned}
$$

To obtain closure, some auxiliary relations are required to allow all the quantities appearing on the right hand side of equation 3.16 to be determined in terms of the state and input variables. Using the definitions of the non-dimensional variables and routine algebra gives the required relations as:

$$\pi_p = \tilde{U}_p/\tilde{V}_p \tag{3.17}$$

$$\psi_p = 2(\tilde{U}_p/\tilde{V}_p - 1)/(\gamma {M_T}^2) \tag{3.18}$$

$$\theta_p = \tilde{U}_p/\tilde{m}_p \tag{3.19}$$

3.3.1 Model Reduction

The model order is reduced if either the injector or movable wall is not used. Without the injector, the flow through the upstream and downstream ducts is the same and the model reduces to:

$$
\begin{aligned}
d\phi/d\tau &= B\left(\Psi_c(\phi_d, M_T) - \Psi_v(\phi_d, \alpha_c) - \psi_p\right) \\
d\tilde{m}_p/d\tau &= \frac{{M_T}^2}{2B\bar{\theta}_p}\left(\phi_d - (\Phi_t(\pi_p, \theta_p) + \Phi_b(\pi_p, \theta_p))\right) \\
d\tilde{U}_p/d\tau &= \frac{{M_T}^2\gamma}{2B\bar{\theta}_p}\left(\phi_u\Theta_c(\phi_d, M_T) - (\Phi_t(\pi_p, \theta_p) + \Phi_b(\pi_p, \theta_p))\theta_p + \tilde{Q} + \pi_p\xi\right) \\
d\tilde{V}_p/d\tau &= \frac{BM_wM_T}{2\bar{\theta}_p}\xi,
\end{aligned}
\tag{3.20}
$$

where ϕ_u is now the common mass flow through both the up and downstream duct. With a fixed plenum volume, the system equations reduce to:

$$
\begin{aligned}
d\phi_u/d\tau &= \frac{-B}{\mathcal{L}_u/\mathcal{L}_c}\left(\psi_i + \Psi_{i_u}(\phi_u, \phi_d)\right) \\
d\phi_d/d\tau &= \frac{B}{\mathcal{L}_d/\mathcal{L}_c}\left(\Psi_{i_d}(\phi_u, \phi_d) + \psi_i + \Psi_c(\phi_d, M_T) - \Psi_v(\phi_d, \alpha_c) - \psi_p\right)
\end{aligned}
\tag{3.21}
$$

$$
\begin{aligned}
d\tilde{m}_p/d\tau &= \frac{{M_T}^2}{2B\bar{\theta}_p}\left(\phi_d - (\Phi_t(\pi_p, \theta_p) + \Phi_b(\pi_p, \theta_p))\right) \\
d\tilde{U}_p/d\tau &= \frac{{M_T}^2\gamma}{2B\bar{\theta}_p}\left(\phi_u\Theta_c(\phi_d, M_T) - (\Phi_t(\pi_p, \theta_p) + \Phi_b(\pi_p, \theta_p))\theta_p + \tilde{Q}\right).
\end{aligned}
\tag{3.22}
$$

With no injection and a fixed plenum volume, the system equations become:

$$
d\phi/d\tau = B\left(\Psi_c(\phi_d, M_T) - \Psi_v(\phi_d, \alpha_c) - \psi_p\right) \tag{3.23}
$$

$$
\begin{aligned}
d\tilde{m}_p/d\tau &= \frac{{M_T}^2}{2B\bar{\theta}_p}\left(\phi_d - (\Phi_t(\pi_p,\theta_p) + \Phi_b(\pi_p,\theta_p))\right) \\
d\tilde{U}_p/d\tau &= \frac{{M_T}^2\gamma}{2B\bar{\theta}_p}\left(\phi_u\Theta_c(\phi_d,M_T) - (\Phi_t(\pi_p,\theta_p) + \Phi_b(\pi_p,\theta_p))\theta_p + \tilde{Q}\right)
\end{aligned}
\tag{3.24}
$$

Removing any of the other actuators does not require a change in the number of states. If the close-coupled valve is not used, the valve pressure drop characteristic, Ψ_v is held fixed at zero. When no bleed valve is present, the plenum bleed characteristic, Φ_b, is set to zero. With no unsteady heat addition $\tilde{Q}$ is held constant, although not necessarily zero.

3.4 Simplified System Model

The system model can be further simplified by assuming that the thermodynamic process occurring in the plenum is isentropic, i.e., p/ρ^γ = constant, where γ is the ratio of specific heats. With this assumption, and considering only the close-coupled valve and plenum, the following second order (two state) model is obtained:

$$
d\phi/d\tau = B\left(\psi_1 - \psi_p + \Psi_v - \Psi_c\right) \tag{3.25}
$$

$$
d\psi_p/d\tau = \frac{1}{B}(\phi_d - (\Phi_t + \Phi_b)). \tag{3.26}
$$

This model, given by Equations 3.25 and 3.26, will be referred to as the *basic compression system model.*

3.5 Linearized System Model

The preceding nonlinear models are valid for perturbations of arbitrary amplitude. For many purposes it is useful to have simpler models which are valid for small perturbations about an equilibrium operating point. Throughout, when such models are required they are obtained by the usual Taylor series expansion about an equilibrium point (see for example [24]). We will subsequently have need to refer to the linearized basic compression system model which is given by:

$$\begin{bmatrix} d\widehat{\phi_c}/d\tau \\ d\widehat{\psi_p}/d\tau \end{bmatrix} = \begin{bmatrix} m_C B & -B \\ \frac{1}{B} & -\frac{1}{Bm_T} \end{bmatrix} \begin{bmatrix} \widehat{\phi_c} \\ \widehat{\psi_p} \end{bmatrix} + \begin{bmatrix} Bv_c & 0 \\ 0 & -\frac{v_b}{B} \end{bmatrix} \begin{bmatrix} \widehat{\alpha_c} \\ \widehat{\alpha_b} \end{bmatrix}, \quad (3.27)$$

where, $m_C = \frac{\partial \Psi_c}{\partial \phi_c}$, $m_T = 1/(\frac{\partial \Phi_t}{\partial \psi_p})$, $v_c = \frac{\partial \Psi_u}{\partial \phi_c}$, and, $v_b = \frac{\partial \Phi_b}{\partial \psi_p}$, are evaluated at the equilibrium operating point of interest.

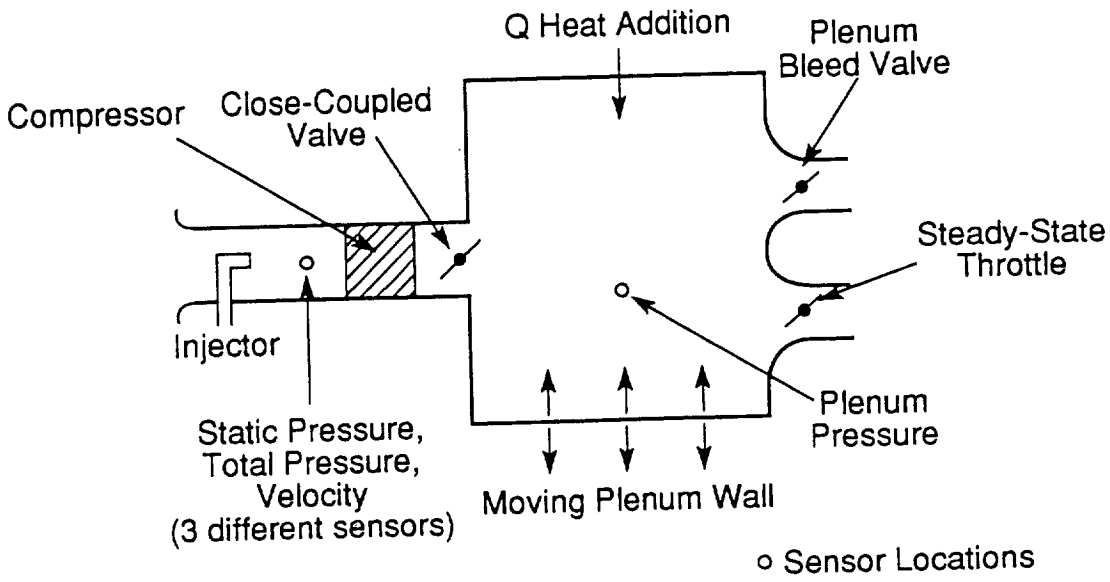

Figure 3-1: Compression system equipped with actuators and sensors

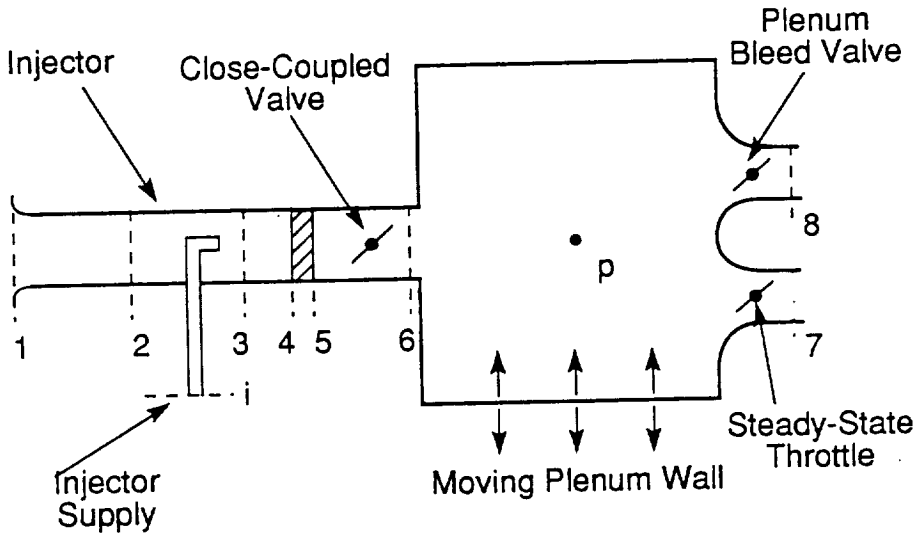

Figure 3-2: Flow stations for for modeling compression system

Chapter 4

Validation of Compressor Model

4.1 Introduction

Central to the modeling of the compression system is the treatment of the compressor itself. As discussed in previous chapters, most compression system models assume that the compressor can be represented by a possibly nonlinear fluid-resistor (quasi-steady actuator disk) in series with some amount of fluid-inertia. In some cases, this model is elaborated slightly by using a first order lag to relate the compressor instantaneous pressure rise and the quasi-steady value at the same flow rate. The use of a low order, lumped element, (finite number of ordinary differential equations) representation is common to both these approaches, however, representing a considerable simplification of the detailed behavior of the flow field existing in an actual compressor. Although much indirect support for this approach is provided by the success of the overall models which incorporate these assumptions, little direct validation of this modeling approach has been done previously. To provide such a direct validation, a set

of experiments have been performed in which the transfer function between sinusoidal pressure perturbations across the compressor (input) and the mass flow perturbations through the compressor (output) was measured. The measured frequency response could be directly compared with that predicted by a lumped model.

In the following sections the theoretical frequency response of the compressor is first obtained for the compressor with and without a first order lag. Next, the experimental methodology used to obtain experimental measurements of the compressor transfer function is given. Finally, the experimental measurements and theoretical response are compared and the results interpreted.

4.2 Theoretical Compressor Frequency Response

4.2.1 Background- Admittance, Impedance, and Phasors

Consider the compressor shown schematically in Figure 4-1. Let us assume that the the non-dimensional mass flow rate at inlet and exit, ϕ_1 and ϕ_2 are at all time equal and refer to this common flow as ϕ. Suppose that the difference (exit minus inlet) in non-dimensional total pressure, ψ, across the compressor is caused to fluctuate sinusoidally about some mean value $\overline{\psi}$, with amplitude, ψ_m, so:

$$\psi(t) = \overline{\psi} + \widehat{\psi}(t),$$

where:

$$\widehat{\psi}(t) = \psi_m \cos(\omega t + \theta_1)$$

For a linear time invariant system, which is assumed here, the resulting perturbations in mass flow rate, $\widehat{\phi}(t)$, are also sinusoidal at the same frequency with amplitude, ϕ_m and phase angle θ_2:

$$\widehat{\phi}(t) = \phi_m \cos(\omega t + \theta_2)$$

It is convenient (and quite standard, see for example Chua [7]) to represent these real valued, time domain, sinusoidal signals as phasors. That is, we associate the unique complex number (phasor), $\boldsymbol{\psi} = \psi_m e^{j\theta_1}$ with the pressure signal, $\psi(t)$ and the unique complex number $\boldsymbol{\phi} = \phi_m e^{j\theta_2}$ with the mass flow rate signal $\phi(t)$. (Note that bold face will be used to distinguish phasor quantities.) The corresponding time domain signals can be uniquely recovered using: $\psi(t) = \mathcal{R}e\{\boldsymbol{\psi} e^{j\omega t}\}$ and, $\phi(t) = \mathcal{R}e\{\boldsymbol{\phi} e^{j\omega t}\}$, where, $\mathcal{R}e\{\}$, indicates the real part of a complex number. Using the phasor notation, we define (in analogy to electrical system terminology) the complex valued, frequency dependent admittance, $Y(j\omega)$, of the compressor as the ratio of the flow phasor, $\boldsymbol{\phi}$, and the pressure phasor, $\boldsymbol{\psi}$

$$Y(j\omega) = -\boldsymbol{\phi}/\boldsymbol{\psi}. \tag{4.1}$$

The sign convention adopted here means that the direction of positive power flow is into the element. Thus, the magnitude of $Y(j\omega)$ is given by: $|Y(j\omega)| = \phi_m/\psi_m$ which is the amplitude ratio of the output flow perturbation to input pressure perturbation. Similarly, the angle of $Y(j\omega)$, which is given by: $\angle(Y(j\omega)) = \theta_2 - \theta_1$, represents the phase shift between the mass flow perturbations and pressure perturbations. It will also be useful to define the complex valued, frequency dependent impedance, $Z(j\omega)$,

of the compressor as the inverse of the admittance as given by:

$$Z(j\omega) = 1/Y(j\omega). \tag{4.2}$$

The frequency dependent behavior of either $Y(j\omega)$ or $Z(j\omega)$ will be referred to as the frequency response of the compressor.

Analytical expressions for the compressor frequency response will now be obtained for both the quasi-steady and the unsteady loss models of the compressor as described in Section 3.2.3.

4.2.2 Quasi-steady Model

From Section 3.2.3 we have for the linearized quasi-steady compressor:

$$d\phi/dt = u_T/(2\mathcal{L}_c)(\frac{\partial \Psi_c}{\partial \phi}\hat{\phi} - \hat{\psi}). \tag{4.3}$$

For now, we maintain the use of the physical time, t. Assuming a sinusoidal input pressure perturbation and flow response, substituting into Equation 4.3 and performing routine manipulations yields:

$$Y(j\omega) = \frac{1/R_c}{\frac{2\mathcal{L}_c}{R_c u_T} j\omega + 1}, \tag{4.4}$$

where the compressor resistance, R_c is defined as $R_c = -\frac{\partial \Psi_c}{\partial \phi}$. The impedance can then be obtained by applying Equation 4.2 to Equation 4.4, giving:

$$Z(j\omega) = R_c + j2\mathcal{L}_c\omega/u_T \tag{4.5}$$

Thus, for the quasi-steady model, the real part of the impedance is (within an algebraic sign) simply the compressor slope, and is independent of the forcing frequency. As a function of frequency, the imaginary part of the impedance would plot as a straight line with a slope in direct proportion to the equivalent duct length (fluid inertia). The impedance representation thus isolates the two important physical effects, flow dependence of the compressor pressure rise and fluid inertia, into real and imaginary parts, respectively, of the compressor frequency response. This provides a means for directly checking the validity of the quasi-steady assumption. Non-quasisteady behavior effecting the compressor pressure rise will manifest itself as a frequency dependence on $\mathcal{R}e\{Z(j\omega)\}$, and and $d\mathcal{I}m\{Z(j\omega)\}/d\omega$.

4.2.3 Unsteady Loss Model

Using model described in Section 3.2.3 the linearized model for the compressor with unsteady losses can be obtained as:

$$d\hat{\phi}/dt = u_T/(2\mathcal{L}_c)(\frac{\partial \Psi_{ci}}{\partial \phi}\hat{\phi} - \widehat{\psi_L} - \hat{\psi}) \tag{4.6}$$

$$d\widehat{\psi_L}/dt = \frac{\overline{\phi} u_T A_c}{\tau_L V_c}((\frac{\partial \Psi_{ci}}{\partial \phi} - \frac{\partial \Psi_c}{\partial \phi})\hat{\phi} - \widehat{\psi_L}), \tag{4.7}$$

where τ_L is defined as the ratio of the loss time lag to the compressor flow through time. We will only be concerned here with radial bladed machines for which the ideal pressure rise is a constant, independent of flow, so that, $\frac{\partial \Psi_{ci}}{\partial \phi} = 0$. Once again defining $R_c = -\frac{\partial \Psi_c}{\partial \phi}$ the admittance and impedance can be obtained as in the preceding section. The admittance is then given by:

$$Y(j\omega) = 1/R_c \frac{(1 + \frac{\tau_L V_c}{\phi u_T A_c} j\omega)}{(\frac{-2\mathcal{L}_c \tau_L V_c}{R_c u_T{}^2 A_c} \omega^2 + 1) + \frac{2\mathcal{L}_c}{R_c u_T} j\omega}. \tag{4.8}$$

This reduces to the quasi-steady model, given by Equation 4.4 as the flow-through time becomes small with respect to the drive frequency, i.e. $\tau_L \omega \rightarrow 0$. The impedance is found from $Z(j\omega) = 1/Y(j\omega)$ and is given by:

$$Z(j\omega) = \frac{R_c + j((2\mathcal{L}_c/u_T - \frac{R_c \tau_L V_c}{\phi u_T A_c})\omega + 2\mathcal{L}_c/u_T (\frac{\tau_L V_c}{\phi u_T A_c})^2 \omega^3}{1 + (\frac{\tau_L V_c \omega}{\phi u_T A_c})^2} \tag{4.9}$$

As previously noted, with the unsteady behavior modeled, the real part of the impedance becomes frequency dependent. In the limit, as the frequency approaches zero, the real part of the impedance approaches the slope of the compressor pressure rise characteristic but at high frequency it approaches the slope of the ideal pressure rise characteristic, which is zero in the present case. The derivative with respect to frequency (slope) of the imaginary part of the impedance, is frequency dependent. For the unsteady model, even at low frequencies, the slope of the imaginary part of the impedance is dependent on the time mean flow coefficient as well as geometry.

4.2.4 Frequency Normalization

The expressions for the theoretical frequency response of the compressor derived in the preceding sections have been in terms of dimensional angular frequency (e.g. radians/sec). It is useful in interpreting data to normalize the driving frequency to some relevant physical time scale. For this problem there are two different important time scales. The first, is the exponential growth (decay) time constant inherent in the linearized, quasi-steady model given by:

$$t_q = |2\mathcal{L}_c/(R_c u_T)|, \tag{4.10}$$

which is seen to be a function of the compressor slope and fluid inertia (equivalent length) of the the compressor duct. This is analogous to the L/R time constant of an electrical circuit consisting of a an inductor with inductance (L) in series with a resistor with resistance (R). Based on this time constant, we define ω_q, the quasi-steady normalized frequency by:

$$\omega_q = \omega/(1/t_q). \tag{4.11}$$

The other relevant time scale is t_u, the flow through time of the compressor. The flow through time is defined here as the compressor volume, V_c, divided by the volume flow rate of fluid, which can be expressed in terms of the flow coefficient and tip speed as:

$$t_u = V_c/(\phi_c u_T A_c), \tag{4.12}$$

from which the reduced frequency ω_u is defined as:

$$\omega_u = \omega/(1/t_u). \tag{4.13}$$

The flow through time, as defined by Equation 4.12, is the amount of time it would take a fluid particle in a constant density, axisymmetric flow (plug flow) to pass from the inlet to the exit of a conduit whose volume matched that of the compressor. Note that the cross sectional area of the conduit is irrelevant for this calculation. It is remarked that the flow through time of a centrifugal compressor with a volute is a somewhat poorly defined quantity in that the flow through time is dependent on the particular path taken through the compressor, and the density is not in fact perfectly constant. Thus, the definition of flow through time adopted here is by no means unique, but this representation should provide the correct order of magnitude and capture the major dependence on mean flow and geometric scaling. The volume of the Holset H1D compressor used for the experiments was estimated at $V_c = 2.36 \text{ x } 10^{-4}\text{m}^3$, based upon a rough approximation of the annular volume bounded by the centrifugal impeller hub and the casing.

4.3 Experimental Methodology

4.3.1 Summary

Experimental frequency response measurements were obtained for the Holset H1D centrifugal compressor described in Chapter 2 using the short inlet configuration.

The frequency response was measured at four different time mean operating points along a constant corrected speed line with $M_T = 0.76$, as shown in Figure 4-2. The flow coefficients at these time mean operating points, which range from 0.1 to 0.2, were chosen to include both negatively and positively sloped portions of the compressor characteristic. For the latter, the downstream valve acted to stabilize the system, thus allowing the compressor to operate without surging even on the positively sloped portions of its characteristic.

To obtain frequency response data, the compressor was forced sinusoidally by modulating the area of a valve located immediately downstream of the compressor exit. The system was driven at 25, logarithmically spaced, values of frequency, ranging between 1 Hz and 100 Hz. This provided data on the compressor behavior from the low to high frequency asymptotic limits based upon the quasisteady time scale given by Equation 4.10. For each drive frequency, the system was operated for several minutes prior to taking data which allowed any transient behavior associated with the start up of the forcing to die away.

Time resolved measurements were made of the total pressure difference imposed across the compressor (inlet to exit) and the resulting flow rate fluctuations through the duct. The compressor exit minus atmospheric inlet pressure difference was measured using the high response total pressure probe described in Chapter 2. Flow rate measurements were derived from a single hot wire anemometer located at the duct center line, several duct diameters upstream of the compressor. The locations of the instruments are shown in Figure 4-3.

The signals were Fourier analyzed to obtain their amplitude and phase at the drive

frequency, from which the desired frequency response was then directly calculated.

4.3.2 Detailed Test Procedure

The basic configuration used for the frequency response measurements is shown schematically in Figure 4-3 with the various instruments and transducers as described in in Chapter 2. The frequency response data for the compressor was obtained at four different time mean operating points along a line of constant compressor speed ($M_T = 0.76$) as shown in Figure 4-2. The time mean flow was set to the desired value by adjusting the nominal area of the control valve. (The throttle at the plenum exit was wide open for these tests) A series of test runs were then performed in which the system was driven at a particular fixed forcing frequency by the control valve.

A collection of such runs at a fixed time mean operating point will be referred to as a test. Each test consisted of 25 runs in which the frequency was varied between 1 Hz and 100 Hz which gave data over a wide range of reduced frequencies for the quasi-steady model; from the low frequency to high frequency asymptotic limits. A logarithmic frequency spacing was used. The drive frequency was set using the analog Wavetek signal generator which was then sampled by the computer and used as an input to the digital controller which, in turn, drove the servo-motor position control loop.

The length of time and sampling rate of the runs was varied according to the drive frequency (at least 10 samples per period) to provide sufficient spectral range and total number of cycles (at least 50 cycles) to obtain sufficient spectral resolution. The cutoff frequency of the low pass anti-aliasing filters was set at one half the sampling

frequency, to avoid aliasing.

The amplitude of the drive signal was adjusted at each frequency to the minimal value required to obtain a clearly distinguishable flow perturbation as determined by direct observation with a digital storage oscilloscope. This method was adopted to minimize the effects of non-linearity, which increase with signal amplitude, while maintaining a large signal to noise ratio. Post-test, spectral analysis showed that the resulting sinusoidal amplitude of the flow coefficient perturbation at the drive frequency varied between 0.005 and 0.038 over all the tests conducted. Amplitude of the forcing pressure coefficient perturbations at the drive frequency ranged from 0.01 to 0.1.

To account for effects of rotor speed fluctuation, it was also necessary to experimentally obtain estimates of the rate of change of the compressor time mean pressure-rise characteristic with speed i.e., $\frac{\partial \Psi_c}{\partial M_T}$. This data was obtained at the four time mean flow coefficients at which the frequency response was measured. At each flow coefficient, the compressor steady state pressure rise was determined at ten different rotational frequencies equally spaced to cover a range of $\pm 15 Hz$ nominally centered at the time mean rotational frequency as used for the frequency response tests. (This range of flows was chosen to reflect the observed maximum fluctuations in rotational frequency) At each rotational frequency the throttle was adjusted to maintain the desired time mean flow coefficient. Over the small range of speed variations, the resulting data showed an essentially linear variation of pressure-rise with rotor speed, as would be expected. The slope of a straight line fit to this data was

used accordingly to provide an estimate of $\frac{\partial \Psi_c}{\partial M_T}$.

4.4 Signal Processing and Data Analysis

The overall goal of the signal processing and data analysis was to obtain an accurate measurement of the frequency response of the compressor from the raw, time series (digitally sampled) data. Specifically, for each drive frequency at which the compressor was tested it was desired to obtain both the magnitude ratio and phase difference between the input pressure signal and output fluctuation in the compressor mass flow. The methods applied for this purpose will now be described.

Drive Frequency Determination

The first step in the data analysis was to determine the actual drive frequency, f_d. Because the drive frequency signal was generated externally by the Wavetek signal generator and its frequency was not known exactly. The drive frequency was determined by using the DFT (Discrete Fourier Transform) of the finite length sequence, $x[n]$, obtained by sampling the drive signal over the duration of a run, where the DFT is defined as in Oppenheim [37], for a length N sequence by:

$$X[k] = \sum_{n=0}^{N-1} x[n] e^{-j(2\pi/N)kn}.$$

For computational efficiency, the DFT was actually computed using a FFT (Fast Fourier Transform) algorithm rather than directly from the definition above. The

drive frequency was then given by the spectral component of the DFT with the greatest magnitude. As discussed in Oppenheim [37, Example 11.5], the frequency corresponding to an isolated spectral peak can be more accurately determined by zero padding the sequence (i.e. extending the length by appending a sequence of zeros) prior to computing the DFT. An iterative procedure was implemented for this purpose which would double the sequence length by zero padding until successive estimates of the peak magnitude agreed within a prescribed tolerance. (A value of 1% was used for the analysis reported here.) The frequency corresponding to this peak was then taken as the drive frequency for that run. Based upon the minimal spectral resolution obtained with this procedure the resulting relative error in the frequency determination is conservatively estimated at less than $\pm 1\%$.

Magnitude and Phase Determination

Once the drive frequency, f_d, was determined, the magnitude and phase of each signal was computed by evaluating the DTFT (Discrete Time Fourier Transform) at the drive frequency. For the length N, real sequence $x[n]$, the DTFT of $x[n]$, denoted, $X(e^{j\omega})$ evaluated at the frequency ω is given as in Oppenheim by:

$$X(e^{j\omega}) = \sum_{n=0}^{N-1} x[n]e^{-j\omega n}.$$

If the physical drive frequency, f_d, has dimensions of cycles per unit time and the sampling period is T, then ω in the above expression is defined by $\omega = 2\pi f_d T$. Denoting the real and imaginary part of $X(e^{j\omega})$ by a and b, respectively, the amplitude, A, and

phase angle, θ, of the signal at the drive frequency is then found using: $A = \sqrt{a^2 + b^2}$ and $\theta = \arctan(b/a)$.

A/D Skew Correction

As discussed in Chapter 2 there is a known, fixed, inter-channel time delay (A/D skew) between the various signals. For the situation of interest here, a sinusoidal signal at a known frequency, f_d, this effect was easily correctable. For a delay time, t_d, the phase lag due to the delay is given by $\delta\theta = 2\pi f_d t_d$. The phase lag was calculated in this way for each channel and then subtracted off to restore all channels to a common time base.

4.5 Experimental Results

4.5.1 Quasi-steady Model

The simple quasi-steady model, as expressed by Equation 4.4, requires two parameters, compressor slope $\frac{\partial \Psi_c}{\partial \phi}$ and equivalent duct length, $\mathcal{L}_c$. These parameters were identified, i.e. their numerical values were determined, by varying them to obtain a good fit between the calculated and experimentally measured frequency response.

Since the equivalent compressor length (fluid inertia) is a purely geometric parameter, which does not vary with the time mean flow, a common value was used to fit the frequency response data for all four operating points. The compressor slope in general is expected to vary with the operating point and so different values were allowed for each operating point. The values obtained were $\mathcal{L}_c = 0.75m$ for all flows

and $\frac{\partial \Psi_c}{\partial \phi} = 1.5,\ 0.80,\ 0.38,\ -2.1$ corresponding to $\phi = 0.10,\ 0.12,\ 0.15$ and0.20 respectively. Independent estimates for these parameter values, based purely on known compressor geometry and steady state data, are consistent with these identified values, as detailed subsequently in this section.

The frequency response plots comparing the measured admittance with the theoretical response using these parameter values are shown in Figure 4-4. The "Bode Plot" format (log magnitude versus log frequency and phase angle versus log frequency) used here was selected as the most relevant for control design purposes as it gives a direct indication of the required compensation and associated gain and phase margins. Theory and measurement are seen to agree well over the higher frequency range but not at lower frequencies.

The poor agreement at low frequencies can be attributed to the fluctuations in rotor speed which occur at the lower frequencies. This is demonstrated by the improved agreement at low frequency shown in Figure 4-5 where the data has been corrected, as described below, to account for the measured rotor speed fluctuations. At higher forcing frequencies, the inertia of the rotor tends to maintain a constant rotational speed, so the correction has little effect.

To obtain this plot, the measured rotor speed fluctuations were accounted for by assuming that the compressor responds linearly (so that superposition applies) and quasi-steadily to rotor speed fluctuations. Using the measured speed fluctuation phasor, M_T, and sensitivity, $\frac{\partial \Psi_c}{\partial M_T}$ (obtained by the procedure described in Section 4.3.2) the pressure rise fluctuation phasor due to speed fluctuation alone, ψ_{M_T}, was cal-

culated using, $\psi_{M_T} = \frac{\partial \Psi_c}{\partial M_T} M_T$. The effect of this was considered as an additional forcing term acting on the compressor duct which was then superimposed, using phasor addition, to obtain the net driving pressure. With the speed fluctuations accounted for, overall agreement between the simple quasi-steady model and measured data is quite good. Unless otherwise noted, in the remaining data presented in this chapter, speed fluctuations are accounted for in this manner.

A number of qualitative features shown by the data in Figure 4-5 warrant further comment. The magnitude of the admittance is seen to be essentially monotonically decreasing with frequency, in agreement with theory. This indicates that, over the tested range of frequencies, there are no unexpected resonances. Thus, if any higher order dynamics have been neglected by the simple model over this frequency range, they are well damped and unlikely to cause closed loop stability problems. For the flow coefficients where the compressor slope is positive, ($\phi = 0.10, 0.12, 0.15$) the phase angle characteristics are seen to monotonically increase while for the operating point on the negatively sloped portion of the characteristic, $\phi = 0.20$, the phase angle decreases monotonically. This difference in behavior can be understood by considering Equation 4.4 in which the phase of the admittance is given by $\arctan(\frac{-2\mathcal{L}_c}{R_c u_T})$, showing that the algebraic sign of the phase depends upon the slope of the compressor characteristic. Alternatively, this change is indicative of the migration of the system's pole from the right to the left half of the complex plane as the compressor slope changes sign with increasing flow. Finally it is noteworthy that the "break frequency", where the relatively constant portion of experimentally determined magnitude of the frequency

response begins to decrease ("roll-off"), occurs at a normalized frequency, ω_q of unity, for all the flows, in agreement with the theoretical curves. Physically, the break frequency occurs at the transition between quasi-steady behavior with negligible fluid inertia effects at low frequency to inertia dominated behavior at high frequency. The agreement between experiment and theory indicates that the relevant time scale is in fact set by the fluid inertia and compressor slope as defined by Equation 4.10.

As previously noted, the parameter values for this model were also estimated independently to provide a check on the reasonableness of the values identified from the frequency response data. An estimate of the equivalent length based purely on geometry gave a value of $\mathcal{L}_c = 0.63(\text{m})$ compared with the identified value of $0.75(\text{m})$. Differentiating a fourth order polynomial fit of the steady state compressor speed line to obtain estimates of the compressor slope gives values of $\frac{\partial \Psi_c}{\partial \phi} = 1.5,\ 0.86,\ -0.05,\ -4.1$ in order of increasing flow coefficient, compared to the corresponding identified values of $\frac{\partial \Psi_c}{\partial \phi} = 1.5,\ 0.80,\ 0.38,\ -2.1$. Thus, considering the relative crudeness of the independent estimates, the identified and estimated parameters appear to agree well, lending additional support to the conclusion that the important physics are properly captured by the model. Note that without this confirmation, the compressor might still be adequately modeled by a first order system with the same functional form of Equation 4.4, but be governed by an entirely different set of physics. The difference between the identified and estimated values indicates that, for detailed control design purposes, it may be worthwhile to perform the system identification as done here rather than to rely on a priori estimates.

4.5.2 Unsteady Model

For basic control design purposes, the quasi-steady model appears to provide an adequate representation of the compressor as shown in the preceding section. However, in many compression system dynamic studies, for example, Greitzer [17], Fink [14] and Bons [5] the existence of some unsteady lag in the compressor response has been assumed.

The experimental frequency response data obtained here was therefore examined to determine if there were direct evidence of such lagging behavior. To do this, the theoretical quasi-steady impedance, Equation 4.5, was first compared with the observed data. The previously identified values of the slope and equivalent length were used to compute the theoretical response. For this comparison, the impedance rather than the admittance was used, as it provides a more sensitive and diagnostic measure of the unsteady effects, as discussed in Section 4.2.2.

The result is shown in Figure 4-6 where the real and imaginary parts of the impedance are plotted against the reduced frequency, ω_u, based on flow through time as defined by Equation 4.13. As discussed in Section 4.2.4, ω_u would be expected to provide the relevant frequency scaling for unsteady aerodynamic effects.

Two observations are made regarding Figure 4-6. First, the real part of the impedance, which is predicted by the quasi-steady theory to be a constant, numerically equal to the slope of the compressor pressure rise characteristic, but opposite in algebraic sign, in fact varies with frequency. In particular, for the three operating points on the positively sloped portion of the characteristic, the real part of

the impedance goes from a negative value at low frequency to a positive value at high frequency. The second observation is that the imaginary part of the normalized impedance, $\mathcal{I}m\{Z(j\omega)/\overline{\phi}\}$, which is predicted to be proportional to the frequency (with the constant of proportionality independent of operating point) actually varies with the time mean flow coefficient.

To determine whether a relatively simple model of the unsteady compressor response could account for the observed deviations from quasi-steady behavior, the experimental data was compared to the theoretical impedance of the unsteady model described by Equation 4.9. Along with the the compressor slope and equivalent length of the quasi-steady model, the unsteady model contains a single additional parameter, τ_L, the ratio of lag time and flow through time. Leaving the original parameters unchanged, the time lag parameter, τ_L, was set to a value of 1.4 which gave the best overall agreement between theory and experiment.

The results are shown in Figure 4-7, which compares the experimental impedance with the unsteady model predictions. It can be seen that the unsteady model predictions are consistent with both the previously observed trends, that is: the frequency dependence of the real part of the impedance and the mean flow dependence of the slope of the imaginary part of the impedance. Although the agreement is not perfect, particularly for the real part of the impedance at the highest frequencies and flow rates, it can be concluded that, overall, the observed behavior appears consistent with the hypothesized unsteady loss model. Considering the probable complexity of the loss development process, it is not surprising that such a crude model, which lumps all of the loss development into a single time lag, is not adequate for accurate

prediction as reduced frequency approaches unity. The unsteady loss model, based on flow through time accounts well for the dependence of the imaginary part of the impedance on the time mean flow rate.

This dependence on mean flow had also been observed by Abdel-Hamid [1] who accounted for it as a flow dependent equivalent compressor length. Since equivalent length is a purely geometric quantity this explanation is not physically plausible. In contrast, the simple unsteady loss model appears to offer a physically reasonable explanation for the observed trend.

4.5.3 Relevance of Unsteady Behavior for Control Design

Finally, from a control design perspective, it is interesting to examine the Bode Plots of the admittance computed with the unsteady loss model. This is done in Figure 4-8, which compares the experimentally measured admittance with the theoretical response using the unsteady loss model and the previously identified parameters. Comparison with the quasi-steady model results given in Figure 4-5 shows that the unsteady model provides a marginally better match to the experimental data, particularly the phase. This would reduce the required phase margin in the control design. Thus, for detailed design and fine tuning, use of the unsteady loss model may be warranted by the additional fidelity which it provides.

The more significant aspect of the observed unsteady behavior is that it suggests a physical upper bound on the required control bandwidth which does not exist for the quasi-steady model. Specifically, the data shows that the real part of the impedance becomes positive at high frequencies. This implies that the system cannot support

sustained oscillations above some finite high frequency limit.

4.6 Summary and Conclusions

The results of the compressor model validation study are summarized as follows:

- The experiments show that this class of compressor can be well represented using a lumped parameter, linear model for small sinusoidal disturbances over the frequency range of interest.

- The quasi-steady theory provides a good approximation which is useful for control design purposes.

- For the particular drive arrangement used for these experiments fluctuations in rotor speed occurred at low frequencies. Effects of the speed fluctuations can be accounted for by superimposing the quasi-steady response to measured rotor speed fluctuations.

- A simple unsteady loss model gives good agreement with data and can be used to account for departures from quasi-steady behavior at intermediate reduced frequencies.

- The experimental data shows that when operating on the positively sloped portion of its characteristic, at reduced frequencies (based on flow through time) much less than unity the compressor impedance (as defined by Equation 4.2) is negative. As the reduced frequency approaches unity, the compressor impedance becomes positive.

- The observed high frequency change in the algebraic sign of the compressor impedance, which is not predicted by the quasi-steady model, indicates that the quasi-steady model will be conservative in terms of predicting the required control system bandwidth.

C-2

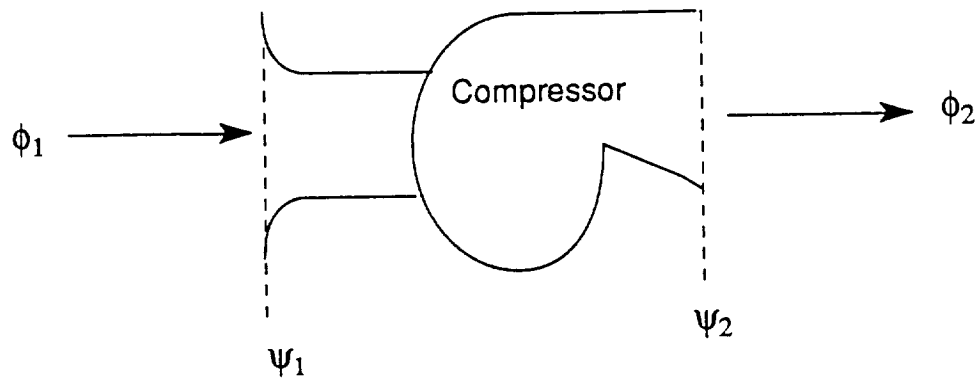

Figure 4-1: Schematic representation of compressor for frequency response model

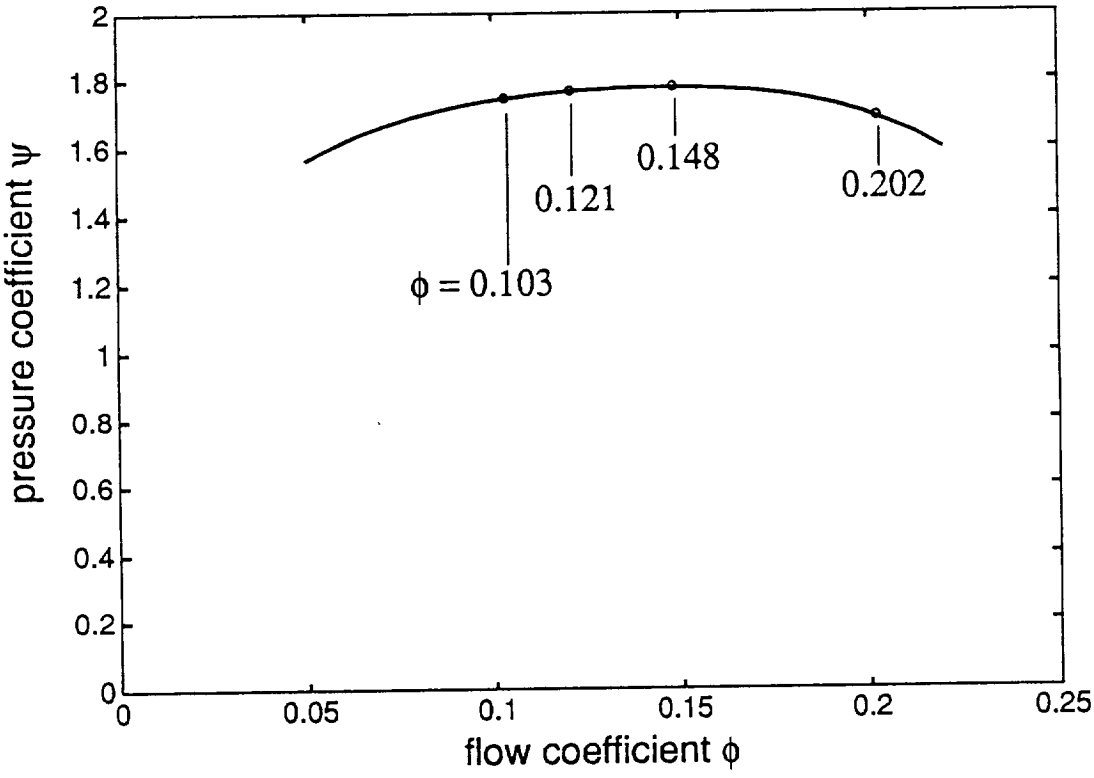

Figure 4-2: Operating points at which frequency response was measured

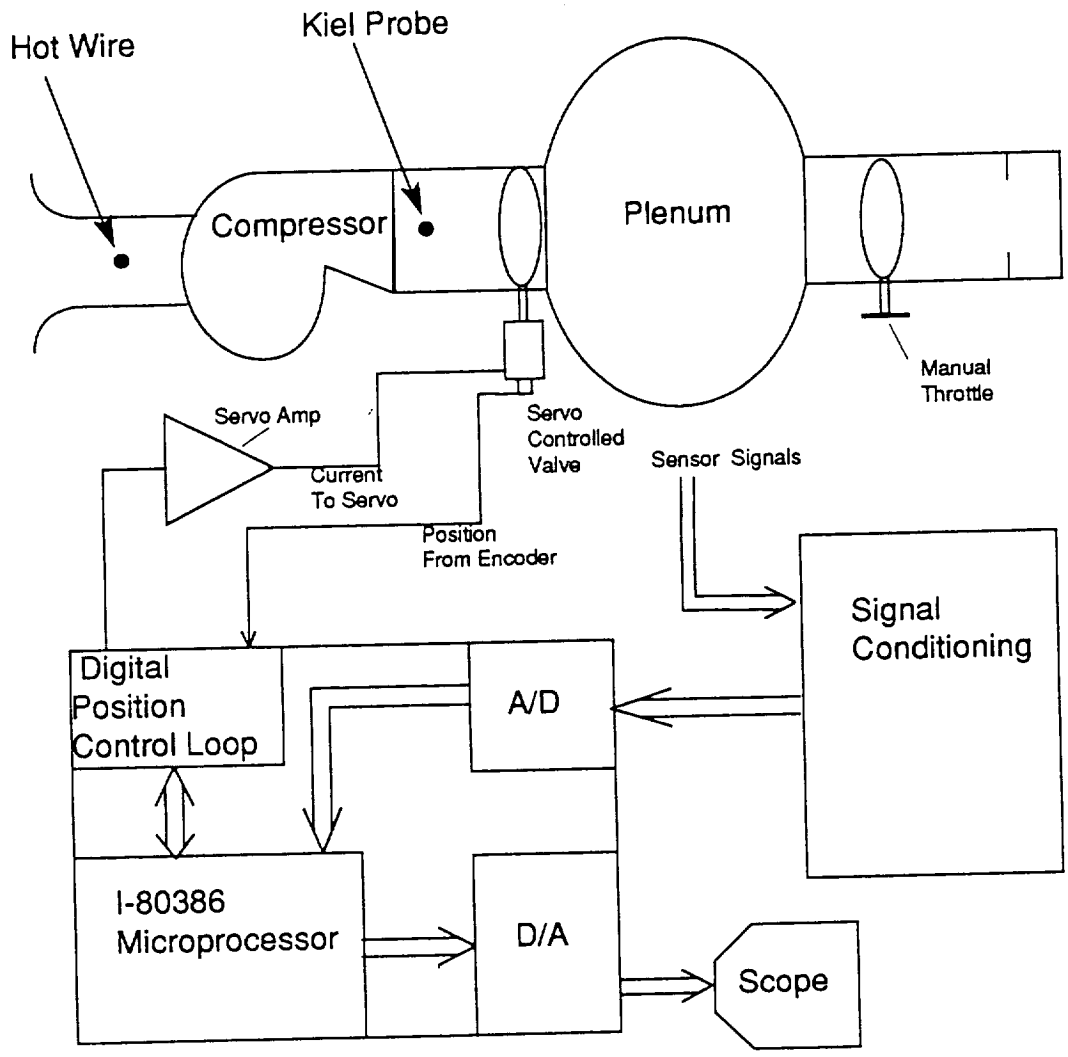

Figure 4-3: Equipment configuration for frequency response measurement

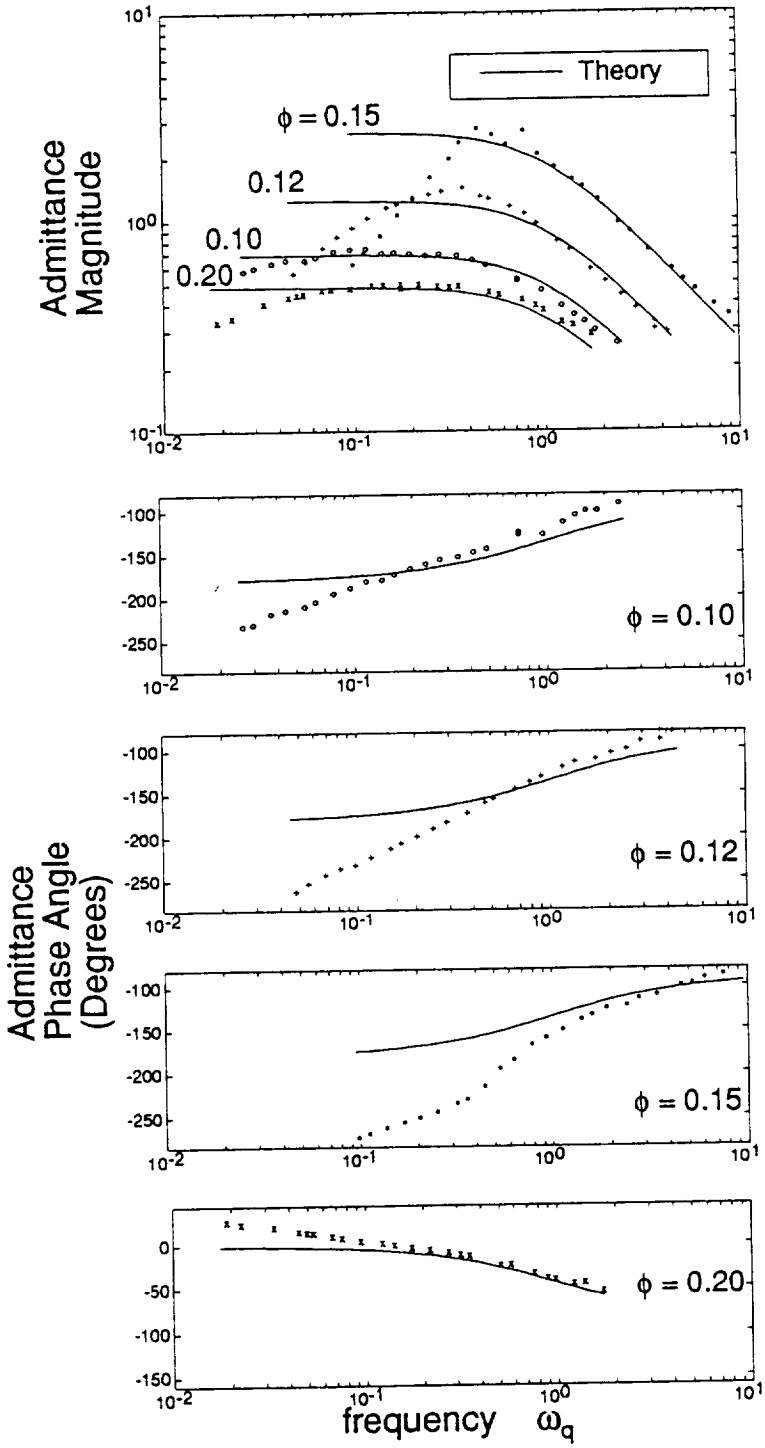

Figure 4-4: Comparison of experimentally determined compressor admittance with quasi-steady theory (without accounting for rotor speed fluctuation)

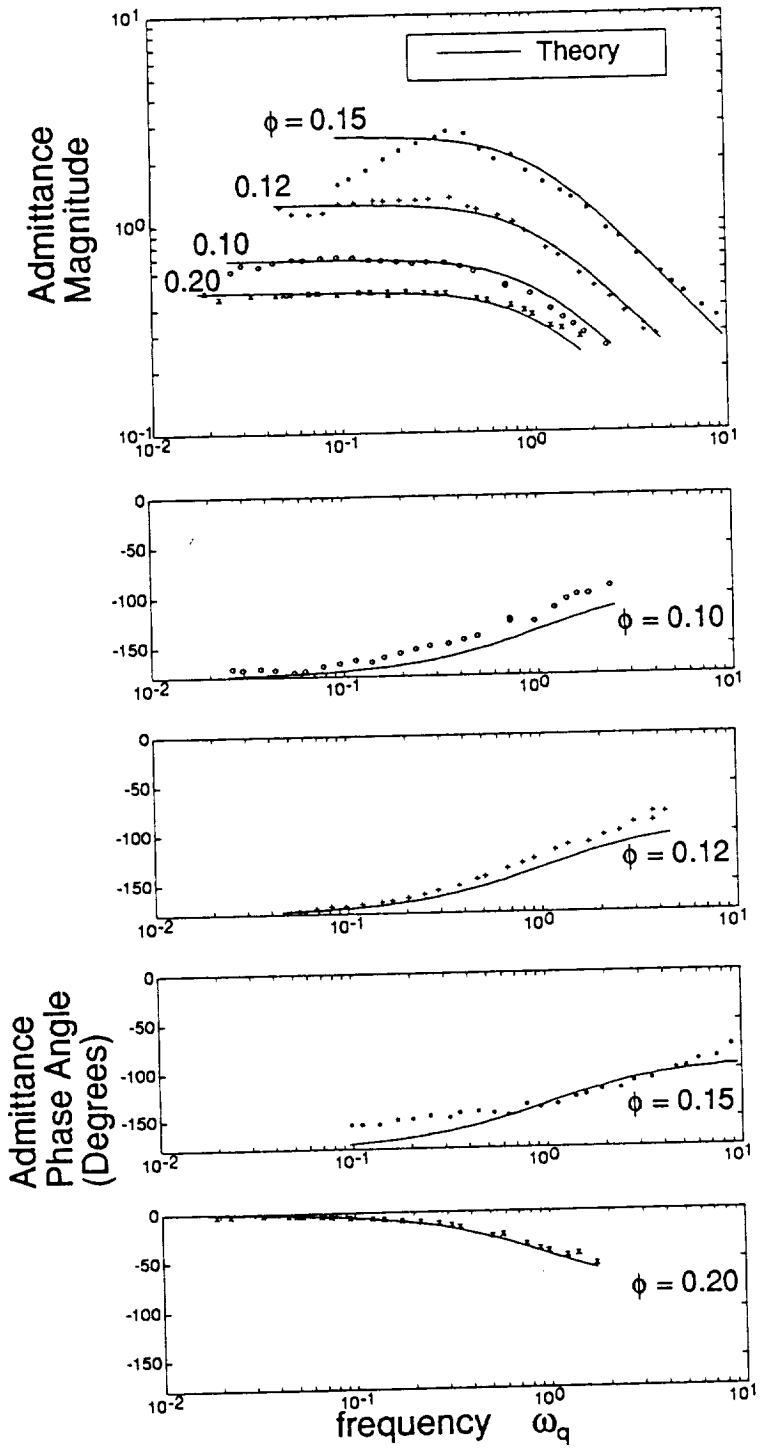

Figure 4-5: Comparison of experimentally determined compressor admittance with quasi-steady theory (accounting for rotor speed fluctuation)

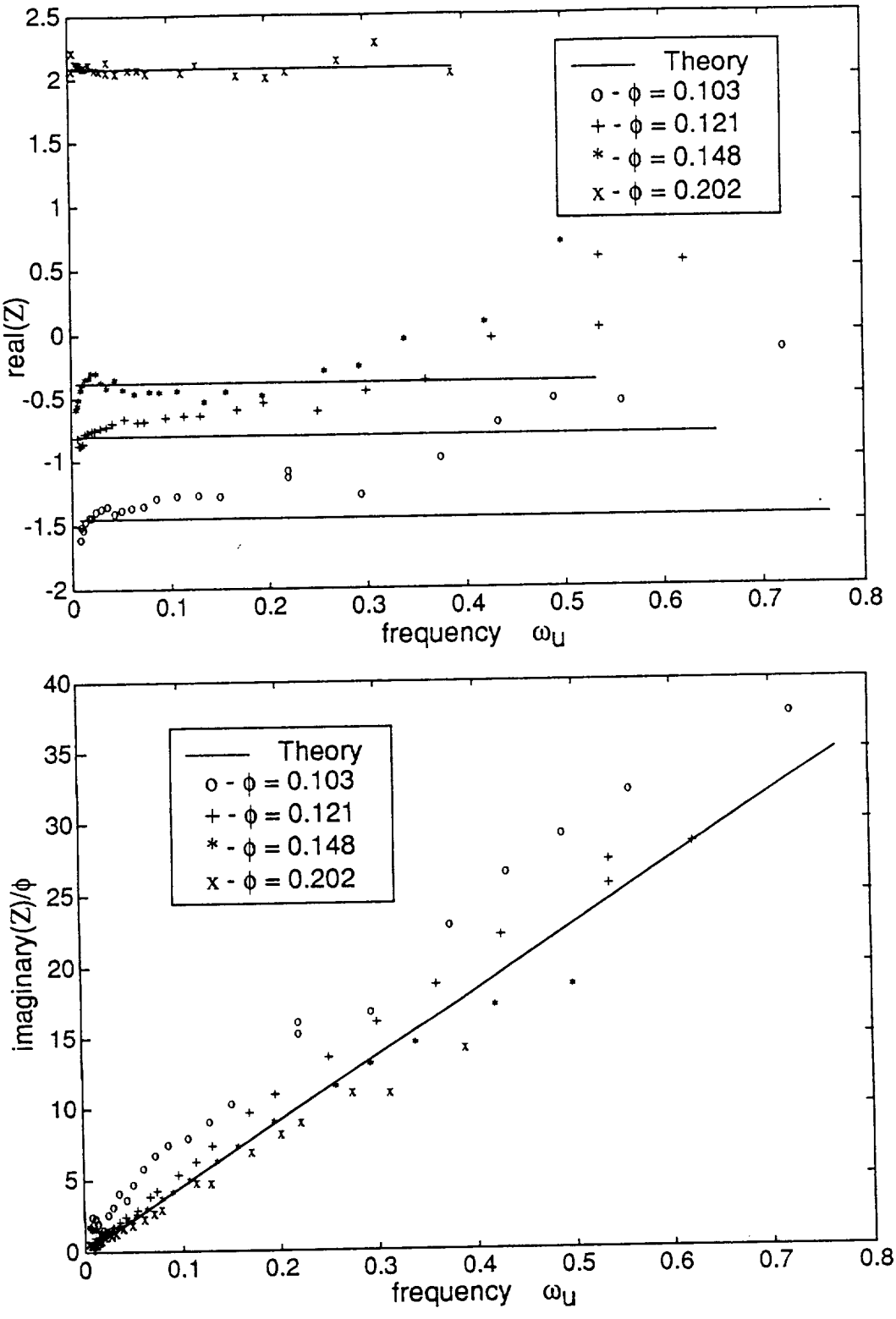

Figure 4-6: Comparison of experimentally determined compressor impedance with quasi-steady theory

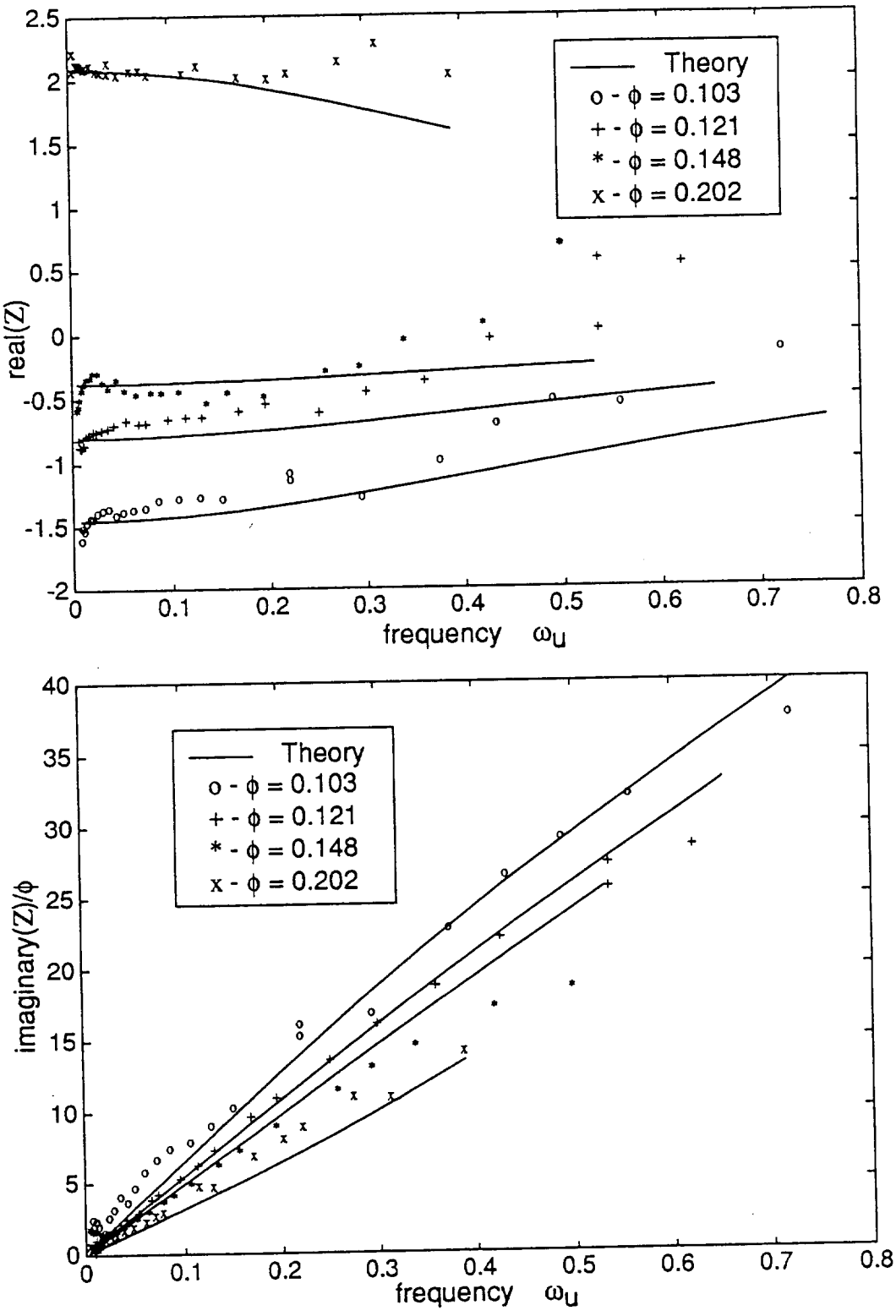

Figure 4-7: Comparison of experimentally determined compressor impedance with unsteady theory

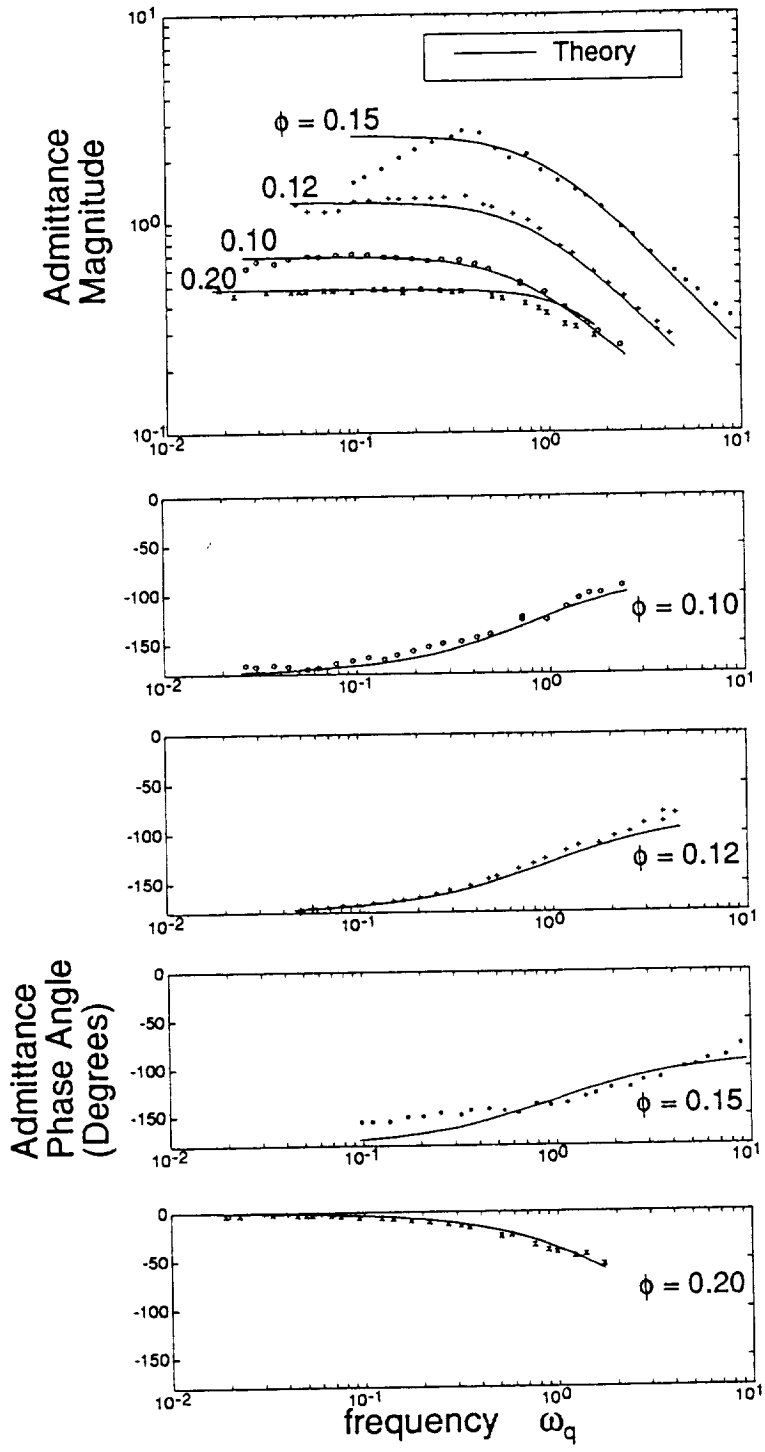

Figure 4-8: Comparison of experimentally determined compressor admittance with unsteady theory

Chapter 5

Limits to Compression System Stabilization

Previous experimental and analytical work ([12, 20, 40] has shown that feedback can be used to extend the stable (surge free) operating range of a compression system. These studies have also indicated that, for the particular schemes investigated, there were limits to the range of system parameters (flow coefficient, B parameter, compressor slope etc.) over which the control remained effective. Motivated by these findings, an investigation has been carried out to determine what fundamentally limits the ability to stabilize a compression system. Relevant control theory is developed and applied to illuminate the nature and extent of these limitations.

5.1 Nominal Stabilization

The most basic requirement of the feedback control used to extend the operating range of the compression system is that the resulting closed loop system be stable to infinitesimal perturbations, that is, linearly stable. In designing such a control, the true system is idealized with a model. If this model, when coupled with the feedback control, is linearly stable, the system is said to be nominally stabilized. Because of the approximations involved in the modeling process, nominal stability does not ensure that the actual system with the same control will also be stable, but, from the point of view of performing a rational design, nominal stability is a minimal requirement.

Additional measures must be taken to ensure that the implementation shares the stability properties of the nominal model. This is the *stability robustness problem* of control design and will be addressed subsequently. In this section the more basic requirement of achieving nominal stability for the basic compression system model will be addressed.

5.1.1 Theoretical Background

We will consider linear, time invariant, SISO (single input single output) system models of the form:

$$\begin{aligned} \dot{\mathbf{x}} &= \mathbf{A}\mathbf{x} + \mathbf{b}u \\ \mathbf{y} &= \mathbf{c}\mathbf{x}, \end{aligned} \tag{5.1}$$

where, the vector $\mathbf{x}$ denotes the system state, u is the scalar control input, y is the scalar output and $\mathbf{A}$,$\mathbf{b}$,$\mathbf{c}$, are appropriately dimensioned constant matrices. It is well known (see for example [24, Theorem 5.2]) that the system, given by Equation 5.1, can be stabilized using a linear time invariant, finite dimensional, feedback control if and only if it is both stabilizable and detectable (The terminology here follows [24] but is fairly standard.) If the stronger conditions of controllability and observability are met, then not only can the system be stabilized but, in addition, the closed loop poles of the system can in fact be placed arbitrarily in the left half plane. Complex poles must, however, be placed as complex conjugate pairs. Such stabilizing controllers can readily be synthesized using standard design techniques and numerical algorithms.

For our purposes therefore, the question of whether a compression system can be nominally stabilized is reduced to determining under what conditions its linear system model is stabilizable and detectable. These properties, in turn, depend upon the particular choice of actuators and sensors, which determine $\mathbf{b}$ and $\mathbf{c}$ respectively in Equation 5.1, as well as the homogeneous system dynamics expressed by the system $\mathbf{A}$ matrix.

5.1.2 Application of Theory to Compression Systems

The theoretical results outlined in the preceding section will now be applied to the question of nominally stabilizing a compression system using a single actuator and and a signal sensor. Note that, u and y in Equation 5.1 are scalars. Correspondingly, $\mathbf{b}$ and $\mathbf{c}$ are column and row vectors respectively. Consider the linearization of the basic compression system model with two states given by Equation 3.25 with an as

yet unspecified sensor and actuator. The system is described by:

$$\begin{bmatrix} d\widehat{\phi_c}/d\tau \\ d\widehat{\psi_p}/d\tau \end{bmatrix} = \begin{bmatrix} m_c B & -B \\ \frac{1}{B} & -\frac{1}{Bm_T} \end{bmatrix} \begin{bmatrix} \widehat{\phi_c} \\ \widehat{\psi_p} \end{bmatrix} + \begin{bmatrix} b_1 \\ b_2 \end{bmatrix} u \tag{5.2}$$

$$y = \begin{bmatrix} c_1 & c_2 \end{bmatrix} \begin{bmatrix} \widehat{\phi_c} \\ \widehat{\psi_p} \end{bmatrix}, \tag{5.3}$$

which is of the form of Equation 5.1. The (as yet unspecified) input and output matrices, $\mathbf{b}$, and $\mathbf{c}$, are determined by the particular choice of actuator and sensor. The compression system can be stabilized if it is controllable and observable[1]. Applying standard rank tests on the controllability and observability matrices shows that this second order system is controllable if and only if

$$\text{rank}(\begin{bmatrix} \mathbf{b} & \mathbf{Ab} \end{bmatrix}) = 2$$

and it is observable if and only if

$$\text{rank}(\begin{bmatrix} \mathbf{c} \\ \mathbf{cA} \end{bmatrix}) = 2.$$

Before considering special cases, i.e. particular choices of $\mathbf{b}$ and $\mathbf{c}$, it is noteworthy that if the open loop poles are complex, i.e. have non-zero real part, then these conditions will be met by any actuator/sensor pair. This can be seen by noting that

[1] As previously discussed in Section 5.1.1 it need only be stabilizable and detectable. However, the more conservative requirement of controllability and observability is somewhat more straight forward to check and will therefore be used here.

if,

$$\text{rank}(\begin{bmatrix} \mathbf{b} & \mathbf{Ab} \end{bmatrix}) < 2,$$

then, $\mathbf{b}$ and $\mathbf{Ab}$ are linearly dependent, which implies that $\mathbf{b}$ is an eigenvector of $\mathbf{A}$. But since $\mathbf{A}$ and $\mathbf{b}$ are real, this is impossible unless the eigenvalue is also purely real. A similar argument holds for the observability matrix. Thus, for any operating point and set of characteristics for which the open loop system $\mathbf{A}$ has complex poles, a stabilizing control can be designed for any choice of actuator and sensor. Limitations on the allowable range of parameters over which a particular choice of actuator and sensor can be used to nominally stabilize a compression system will, therefore, only occur for parameter values which result in purely real open loop poles.

From the rank tests it is seen that limitations occur if $\mathbf{b}$ or $\mathbf{c}$ are aligned with an eigenvector of $\mathbf{A}$ or $\mathbf{A}^T$ respectively. Fortunately, for most specific choices of actuator and sensor, this cannot occur for any physically meaningful value of the system parameters.

As a practical example, consider a variable plenum exit throttle actuator with plenum pressure sensing. This corresponds to Pinsley's [40] experiment. In this case we have:

$$\mathbf{b} = \begin{bmatrix} 0 \\ -\frac{1}{B}\frac{\partial \Phi_t}{\partial \alpha} \end{bmatrix} \tag{5.4}$$

$$\mathbf{c} = \begin{bmatrix} 0 & 1 \end{bmatrix} \tag{5.5}$$

For this two dimensional case, if,

$$\det(\begin{bmatrix} \mathbf{b} & \mathbf{Ab} \end{bmatrix}) \neq 0,$$

then,

$$\operatorname{rank}(\begin{bmatrix} \mathbf{b} & \mathbf{Ab} \end{bmatrix}) = 2.$$

Similarly,

$$\det(\begin{bmatrix} \mathbf{c} \\ \mathbf{cA} \end{bmatrix}) \neq 0,$$

implies that,

$$\operatorname{rank}(\begin{bmatrix} \mathbf{C} \\ \mathbf{CA} \end{bmatrix}) = 2.$$

From which we obtain the condition for controllability:

$$\frac{1}{B}(\frac{\partial \Phi_t}{\partial \alpha})^2 \neq 0, \tag{5.6}$$

which will be satisfied for any finite value of B so long as the mass flow through the throttle valve (with pressure drop held constant) is a strictly increasing function of the valve area, which will always be the case. Similarly, the condition for observability can be obtained :

$$\frac{1}{B} \neq 0, \tag{5.7}$$

which again holds for any finite value of B. Thus it has been shown that, for all physically reasonable values of the system parameters, the compression system can be

nominally stabilized using a variable area throttle at the plenum exit as the actuator and a plenum pressure sensor. It should be noted that limitations in terms of the maximum B-parameter which can be stabilized exist if the control law is restricted to a simple proportional control (see for example Pinsley [40]). In order to nominally stabilize this system for any value of B-parameter a dynamic compensator (see [24, Chapter 5]) will be required.

Similar calculations can be done to show that many other reasonable choices of actuator and sensor also yield systems which are both controllable and observable.

This calculation does point out, however, that as B becomes infinitely large the system would in the limit no longer be controllable or observable. It should then be anticipated that large but finite values of B will be difficult to control with this choice of actuator and sensor.

The main point which has been established is that the nominal stabilization of the basic compression system does not generally set a fundamental limit to control. This is an important theoretical result because it points out that, as a means of comparison between various actuation and sensing strategies, the ability to nominally stabilize the system provides little discrimination.

5.2 Bounded Actuation

In the analysis presented in the previous section, it is assumed that there is no bound on the allowable magnitude of the control signal u. This section considers the more realistic situation where the control is bounded.

5.2.1 Theoretical Background

Suppose that a stabilizing feedback control is connected to the linear system described by Equation 5.1. Then, with no bound on the control signal, any initial state will be driven back to the origin by the controller. This is not the case if the control magnitude is bounded, ie., $u_{\min} \leq u \leq u_{\max}$. With the control bounded and the plant open loop unstable, the system cannot be restored to equilibrium for all initial states.

The set of initial states which can be restored to equilibrium subject to the constraint on the control magnitude includes only a limited region in the overall state space. This region (which will be more precisely defined subsequently) will be referred to as the *recovery region*[2]. For a control system to be effective, in practical situations, the recovery region cannot be too small.

To make the previous notions more precise, consider the linear discrete time system[3]:

$$\mathbf{x}_{n+1} = \mathbf{A}_d \mathbf{x}_n + \mathbf{b}_d u_n, \tag{5.8}$$

which describes the behavior at the sample points of the continuous time system, Equation 5.1 driven by a discrete time controller[4]. Let the control sequence be

[2]The concepts of recovery region and degree of controllability were developed independently in the course of this thesis research and were only later found to coincide with Schmitendorf's [42] work. Schmitendorf's terminology will be used here.

[3]A similar analysis can be performed for the continuous time control case; however, the analysis is not so straight forward.

[4]It is assumed that the input to the plant is held constant over the sampling interval.

bounded by the constraint,

$$u_{\min} \leq u_i \leq u_{\max} \; i = 1, 2, 3 \ldots \tag{5.9}$$

Following Schmitendorf[5] [42], $\mathcal{R}(nT)$, the recovery region at time nT is defined as the set of all initial states, $\mathbf{x}(0)$, which can be driven back to the origin using a control sequence $u_1, u_2, \cdots, u_n$ satisfying the constraint equation 5.9 in the time interval, $0 \leq t \leq nT$ where T is the sampling period of the discrete time control. The degree of controllability ϱ is then defined as the shortest distance between the origin and the boundary of the recovery region, i.e.,

$$\varrho = \inf\{\|\mathbf{x}\| : \mathbf{x} \in \mathcal{R}^c(nT)\}, \tag{5.10}$$

where, $\mathcal{R}^c(nT)$ is the complement of the recovery region, $\mathcal{R}(nT)$, and $\inf\{\}$ is defined as the greatest lower bound on the indicated set.

For a system with two states, for example the basic compression system model, the degree of controllability is simply the radius of the largest circle centered at the origin (equilibrium point) which can be contained in the recovery region. In general, it is the radius of the largest hypershere centered at the origin which can be contained inside of the recovery region. Every initial state inside this circle, or hypersphere for the general case, can be returned to the origin.

For open loop unstable systems, the degree of controllability approaches a finite

[5]Schmitendorf defined these terms terms for the continuous control case and his terminology has been adapted to the discrete time case treated here.

limit as the number of steps, n increases to infinity. That is, due to the bounded actuation, some initial states cannot be driven back to the origin no matter how long a time we allow. If for some choice of actuator and set of system parameters the magnitude of $\varrho(nT)$ as $n \rightarrow \infty$ is small, with respect to the expected magnitude of initial conditions, (assuming an appropriately scaled set of state variables is used) an actual system using this actuator cannot be expected to be effective. In such a case, the slightest perturbation in the initial system state could place the system into a region which could not be returned to equilibrium.

The magnitude of the degree of controllability thus provides a figure of merit for assessing the relative effectiveness of various actuators. Since the analysis assumes a linear plant model, it is most appropriately employed as a means for distinguishing ineffective actuators, as opposed to determining the most effective actuators. This can be understood by considering that for an ineffective actuator the degree of controllability will be small, and even small initial perturbations, for which the linearized dynamics are accurate, cannot be returned to equilibrium. If the degree of controllability is too small it is, therefore, unlikely that the system will work in practice. On the other hand, it is important to note that one cannot assume that an actuator with an extremely large degree of controllability would actually achieve this radius as nonlinear effects may become important.

Finally, it is noted that the recovery region is the largest possible region that can be returned to the origin without violating the control constraints. It is thus the best that can be done with any control law, linear or nonlinear, and any choice of sensor. The degree of controllability thus provides a means of comparing the effectiveness of

various actuators which is independent of the choice of control law or sensor.

5.2.2 Numerical Results for Compression System

A numerical algorithm to calculate the boundary of the recovery region and the degree of controllability was developed and implemented. The method taken closely follows the continuous time approach described in [42], but has been adapted for a discrete time control (see Appendix B). To illustrate the basic concepts for a practical case of interest, recovery regions, $\mathcal{R}(nT)$, calculated for various values of nT for an unstable compression system with a plenum bleed valve actuator, are shown in Figure 5-1. The maximum fluctuations in bleed flow are constrained to be less than $\pm 1\%$ of the mean mass flow. In the planar case shown here, the degree of controllability at time nT is defined as the radius of the largest circle centered at the origin which can be contained inside of the recovery region at time nT. It can be seen that, for increasing values of the recovery time, the size of these circles and, therefore, the degree of controllability, approaches a limiting value as expected for an open loop unstable system.

It is apparent that the degree of controllability is dependent upon the scaling of the state variables and input. For a clear physical interpretation, the degree of controllability should be based on an appropriately scaled set of state variables. That is, a perturbation of unit magnitude should have the same physical significance regardless of its direction in state space. To this end, scaled state variables are chosen

as:

$$\begin{aligned} \tilde{x}_1 &= \frac{(\phi_c - \overline{\phi_c})}{\overline{\phi_c}} \\ \tilde{x}_2 &= \frac{(\psi_p - \overline{\psi_p})}{\overline{\psi_p}}, \end{aligned}$$

with the input scaled as:

$$\tilde{u} = \frac{(\phi_b - \overline{\phi_b})}{\phi_{b\max}},$$

where $\overline{\phi_c}$, $\overline{\psi_p}$, and $\overline{\phi_b}$ are the values at the equilibrium operating point, and $\phi_{b\max}$ is the maximum bleed flow. The resulting scaled recovery region at time $nT = 2$, ie. two Helmholtz periods, and the corresponding circle whose radius defines the degree of controllability, are illustrated in Figure 5-2.

With this scaling, the degree of controllability for the plenum bleed valve is plotted as a function of system B parameter and compressor slope in Figure 5-3 for $nT = 10$. Additional computations using larger values of nT showed that no significant increases in the degree of controllability would be obtained by further increasing the recovery time. To help interpret the results, if the degree of controllability were equal to 0.01, then, with this scaling the maximum perturbation in initial plenum pressure or compressor flow must be less than 1% of the equilibrium value. Figure 5-3 shows that the degree of controllability decreases asymptotically towards zero as the B parameter and or compressor slope increases.

The analysis quantifies a trend which can be anticipated from the following phys-

ical considerations. As the compressor slope becomes increasingly positive, the force accelerating the compressor duct fluid for a given flow perturbation increases, and consequently so does the growth rate of the instability. As B increases, the relative compliance of the plenum increases which decreases the effectiveness of the bleed valve in influencing the compressor. Since the control is constrained, both of these trends require the allowable region of initial conditions to decrease, i.e., the degree of controllability is reduced. This calculation shows that even though the system can be nominally stabilized, the allowable set of initial conditions when the control is bounded becomes so restrictive that for practical purposes the system cannot be stabilized.

It is revealing to compare this to the case of an actuator close coupled to the compressor exit. The actuator (which could be a valve) is idealized here as a device which can produce a desired pressure rise (or drop) which is simply added to that of the compressor to obtain the overall pressure rise of the compressor and actuator. The resulting degree of controllability, assuming that the actuator could produce a maximum pressure perturbation of $\pm 1\%$ of the time mean compressor pressure rise (and otherwise using the same parameter values as for Figure 5-3) is shown in Figure 5-4.

In contrast to the plenum bleed actuator case, the degree of controllability for the close-coupled actuator does not asymptotically approach zero. On this basis, the plenum bleed valve can be rejected as being the less favorable option. It would be anticipated that bounded actuation will similarly severely limit the effectiveness of many control schemes which might appear viable if only nominal stabilization were

considered.

5.3 Limitations Imposed by Model Uncertainty

The approximations used in developing the simple lumped compression system model are valid over only a limited range of frequencies. Above this range of frequencies we would expect that the behavior of the system would depart significantly from that of the model. It is well known that these unmodeled high frequency dynamics can potentially result in instability when a feedback control loop is closed around the system, even though the nominal model with high frequency dynamics neglected is theoretically stable.

To prevent such instability, the feedback control must be properly designed. This is one aspect of what is known as the *stability robustness problem* and there is a large body of literature treating this subject. The basic approach to ensuring stability in the face of uncertain high frequency dynamics, which is common to many of these methods, is to impose limitations on the closed loop system bandwidth.

For an open loop unstable system, which is the main concern here, it is not clear to what extent this prescription can be followed. That is, can the closed loop bandwidth in fact be made arbitrarily small for such systems? Intuitively, one would expect problems to arise as the time scales of the instability approach the time scales at which the model becomes inaccurate.

In this section it is shown that this is in fact the case. The problem will be quantified as a design tradeoff between stability robustness to high frequency model error

and nominal performance. This is a fundamental control problem which apparently has not been previously addressed in this fashion and so the analysis is of some general interest. Focus will, however, be primarily maintained on the implications for the compression system, to which end specific numerical results will be given for an illustrative case.

The presentation is organized as follows. Section 5.3.1 provides a brief summary of relevant background concepts and theory. Section 5.3.2 applies the theory to formulate the desired quantitative design tradeoff and Section 5.3.3 gives some numerical results for the compression system application.

5.3.1 Theoretical Background

Closed Loop Transfer Functions

A frequency domain (Laplace Transform) description of the linearized system is used for the analysis. A block diagram of the system to be analyzed is shown in Figure 5-5. The notation used here follows [15] and is fairly standard. Laplace transformed quantities will be distinguished by the use of s, or $j\omega$ if evaluated on the imaginary axis, as their argument. Referring to Figure 5-5, $P(s)$ is the plant transfer function representing the compression system and $F(s)$ is the transfer function of the feedback system used to stabilize the loop. The *Loop Transfer Function*, $L(s)$, is defined by:

$$L(s) = P(s)F(s). \tag{5.11}$$

The *Sensitivity Transfer Function*, $S(s)$, and *Complementary Sensitivity Transfer Function*, $T(s)$, are defined respectively by:

$$S(s) = \frac{1}{1+L(s)} \tag{5.12}$$

$$T(s) = \frac{L(s)}{1+L(s)}. \tag{5.13}$$

The two are related by the identity:

$$S(s) \equiv 1 - T(s) \tag{5.14}$$

By expressing the closed loop response in terms of the Sensitivity and Complementary Sensitivity Transfer Functions, the role played by these functions in dictating the overall performance in the face of inevitable disturbances and sensor noise is made clear. Referring to the block diagram, Figure 5-5, the response of the plant output, $y(s)$, to disturbances at the plant input, $d_i(s)$, disturbances at the plant output, $d_o(s)$, sensor noise, $n(s)$, and reference command, $r(s)$, is given by:

$$y(s) = S(s)d_o(s) + P(s)S(s)d_i(s) + T(s)n(s) + T(s)r(s) \tag{5.15}$$

The response of the controller output, $u(s)$ to these inputs is given by:

$$u(s) = -S(s)F(s)d_o(s) - T(s)d_i(s) - S(s)F(s)n(s) + S(s)F(s)r(s) \tag{5.16}$$

Stability Robustness

Let $L(s)$ be the nominal loop Transfer Function, given by the approximate model, and $L'(s)$ be that of the actual system. It will be assumed that the nominal system is closed loop stable and that the true and nominal plant models are related by:

$$L'(s) = L(s)(1 + \varepsilon(s)) \ . \tag{5.17}$$

where, $\varepsilon(s)$ is a stable transfer function whose magnitude can be estimated but is otherwise unknown. This is known as a multiplicative representation of unstructured uncertainty, see for example [50]. The relative error between the nominal and true model is given by:

$$\left| \frac{L'(s) - L(s)}{L(s)} \right| = |\varepsilon(s)| \ . \tag{5.18}$$

Using the Nyquist Stability Criterion, it can then be shown, see for example [50], that the actual closed loop system will also be stable so long as the nominal Complementary Sensitivity Transfer Function evaluated along the entire $j\omega$ axis satisfies:

$$|T(j\omega)| < 1/|\varepsilon(j\omega)| \tag{5.19}$$

Thus, the Complementary Sensitivity Transfer Function gives an indication of stability robustness to unstructured multiplicative uncertainty as well as governing the nominal closed loop response to disturbances and noise.

Frequency Domain Design Specification

Ideally, the closed loop system would exactly follow the input command in the face of the various disturbances and noise sources. From Equations 5.15 and 5.16 it can be seen that, for the system output, $y(s)$, to follow the command and to keep the response to disturbances small, we should have $|T(s)| \approx 1$. On the other hand, to keep the response of the output to measurement noise small we should have $|T(s)| \ll 1$. From Equation 5.19 it is seen that for stability robustness we also require $|T(s)| \ll 1$ along the portions of the $j\omega$ axis where the modeling error is large.

If the commands and disturbances are limited to low frequencies and the sensor noise and model uncertainty are largely confined to high frequencies, then reasonably good performance can be achieved if $|T(s)|$ can be held close to unity at low frequencies and then made to decrease (roll off) above some high frequency cutoff. Such a specification is illustrated in Figure 5-6. It is demonstrated in the following section that, unfortunately, specifications of this sort cannot necessarily be satisfied for an open loop unstable plant.

Frequency Domain Integral Constraints

Freudenberg and Looze, [15], extending the approach pioneered by Bode, [3], have shown that the achievable closed loop transfer functions, $S(s)$ and $T(s)$, for plants with right half plane (unstable) poles, zeros, and time delays cannot be shaped arbitrarily. They have expressed these limitations in terms of integrals of the logarithm of the magnitudes of the $S(s)$ and $T(s)$ evaluated along the $j\omega$ axis. These will be called frequency domain integral constraints here. As a direct consequence, reductions in

the magnitude of $S(s)$ or $T(s)$ over one range of frequencies can only be achieved at the expense of increased magnitude at other frequencies.

5.3.2 Theoretical Stabilization Limitation

The general limitations implied by Freudenberg and Looze's frequency domain integral constraints can be used to obtain quantitative estimates of the price paid for high frequency model uncertainty for the basic compression system. Suppose that we wish to stabilize the compression system at an open loop unstable operating point. To obtain such a bound, let us assume that, above some high frequency cutoff, ω_c, the magnitude of the relative error between the nominal and actual frequency response is bounded above by ε_m. That is:

$$|\varepsilon(j\omega)| < \varepsilon_m \text{ for } |\omega| > \omega_c \text{ with } \varepsilon_m > 1. \tag{5.20}$$

Further, to satisfy the stability robustness condition, Equation 5.19, the closed loop is constrained to satisfy:

$$|T(j\omega)| < 1/|\varepsilon_m| \text{ for } |\omega| > \omega_c. \tag{5.21}$$

Let $p = a + jb$ denote the most unstable of the two open loop poles of the nominal compression system model. (That is the one with the largest real part.) If at the operating point of interest the system has two complex conjugate poles either one can be selected and called p. Let z_i, $i = 1, n_z$ denote the right half plane zeros, if any, of

$L(s)$.

With these assumptions, Freudenberg and Looze's results can be extended to show that the complementary sensitivity has a peak magnitude on the $j\omega$ axis, denoted by $\|T(j\omega)\|_\infty$, which is lower bounded by:

$$\|T(j\omega)\|_\infty \geq (\varepsilon_m^{(\pi-\theta(\omega_c))} k_z)^{\left(\frac{1}{\theta(\omega_c)}\right)}, \tag{5.22}$$

where

$$\theta(\omega_c) = \arctan\left(\frac{\omega_c - b}{a}\right) + \arctan\left(\frac{\omega_c + b}{a}\right) \tag{5.23}$$

and,

$$k_z = \begin{cases} \prod_{i=1}^{n_z} \left|\frac{(\bar{z}_i + p)}{(z_i - p)}\right| & ; n_z > 0 \\ 1 & ; n_z = 0 \end{cases} \tag{5.24}$$

Because $k_z \geq 1$ and by assumption $\varepsilon_m > 1$, Equation 5.22 shows that the peak complementary sensitivity must be greater than unity. Since $|T(j\omega) < 1|$ for $|\omega| > \omega_c$ the peak must occur at a frequency below ω_c. The true peak value is always at least as large as the estimate given by Equation 5.22.

It is noted that when the system has right half plane zeros, k_z is greater than unity, so that the situation is always made worse by the presence of these zeros. Whether or not there are any right half plane zeros depends on the choice of actuator and sensor. Inspection of the denominator of k_z shows that the peak complementary sensitivity will become extremely large when there is a near pole zero cancellation in the right half plane. Thus, the actual location as well as the mere presence of right half plane zeros and poles is important.

Due to the relationship between $T(s)$ and $S(s)$ given by Equation 5.14, the sensitivity transfer function must also have a peak value greater than unity when ever $\|T(j\omega)\|_\infty \gg 1$. This is shown as follows. Since,

$$\begin{aligned} \|S(j\omega)\|_\infty &= \|1 - T(j\omega)\|_\infty \\ &\geq \|T(j\omega)\|_\infty - 1 \end{aligned}$$

,

it can be seen that $\|S(j\omega)\|_\infty$ will be substantially greater than unity whenever $\|T(j\omega)\|_\infty \gg 1$.. A geometrical construction showing the function $\theta(\omega_c)$ as an angle in the complex plane is shown in Figure 5-7. From Equation 5.22 it is apparent that, for $\|T(j\omega)\|_\infty$ to be small, we must have $\theta(\omega_c) \approx \pi$.

From the geometrical construction shown in Figure 5-7, it can be seen that, for a fixed ω_c, as either the growth rate of the instability (real pole case) or the natural frequency of the instability (complex conjugate case) or both become large, with respect to ω_c, $\theta(\omega_c)$, will become small, implying a large $\|T(j\omega)\|_\infty$. Equation 5.22 can thus be used to quantify the intuitively anticipated trend that acceptable performance can only be achieved when the instability growth rate is small with respect to the high frequency limitation on the range of model validity.

5.3.3 Numerical Results for a Compression System

To appreciate the severity of the limitation imposed by the bound given by Equation 5.22 it is useful to compute numerical values for the basic compression system

model using some typical parameter values. The results of performing such a calculation are shown in Figure 5-8 for the case of a close-coupled valve actuator with measurement of compressor mass flow rate. For this pairing of actuator and sensor there are no zeros in the right half plane so that $k_z = 1$ in Equation 5.22. In this figure, the lower bound on $\|T(j\omega)\|_\infty$ is plotted as a function of compressor slope and ω_c/ω_h, the ratio of the high frequency cutoff to the system undamped natural frequency (Helmholtz Frequency). The maximum relative modeling error is held fixed at $\varepsilon_m = 2.0$ and the parameter B is held fixed at $B = 2$.

For the lower values of compressor slope, m_C, the open loop poles are complex conjugates and, as shown in Figure 5-8, the peak complementary sensitivity can be made reasonably close to unity even for relatively small values of ω_c/ω_h. That is, the model need only be good up to the Helmholtz frequency. For the steeper compressor slopes or larger values of B, the figure shows that we must have ω_c/ω_h greater than 8 to reduce the lower bound on $\|T(j\omega)\|_\infty$ to a reasonable value. In this case, the unstable open loop poles are real, the important time scale has become the growth rate of the fastest unstable pole, and the model must be accurate for these fast time scales.

For other choices of sensors and actuators, there are also right half plane zeros so that $k_z > 1$ and, from Equation 5.22, the limitation would be expected to be more severe.

High frequency modeling uncertainty, therefore, imposes an effective limit on the range of compressor slopes and B which can be robustly stabilized while maintaining acceptable performance. A means for estimating this bound has been derived and

numerical results utilizing this procedure have been presented to demonstrate the severity of the limitation for an illustrative case. The existence of right half plane zero increases the severity of these limitations and properly choosing actuators and sensors to eliminate such zeros is an important design consideration.

5.4 Summary

In this chapter, important theoretical limitations to stabilization of compression systems have been examined in detail. For many choices of actuators the compression system can be nominally stabilized. In the more realistic situation where actuators are bounded and high frequency modeling errors are considered the ability to stabilize the system may be severely restricted over the parameter ranges of practical interest. These limitations are more severe for some actuator and sensor pairs than others and, therefore, a proper choice of actuator and sensor is essential. This finding is further amplified and explored in detail in Chapter 6 where a systematic evaluation of various actuator sensor pairs is performed.

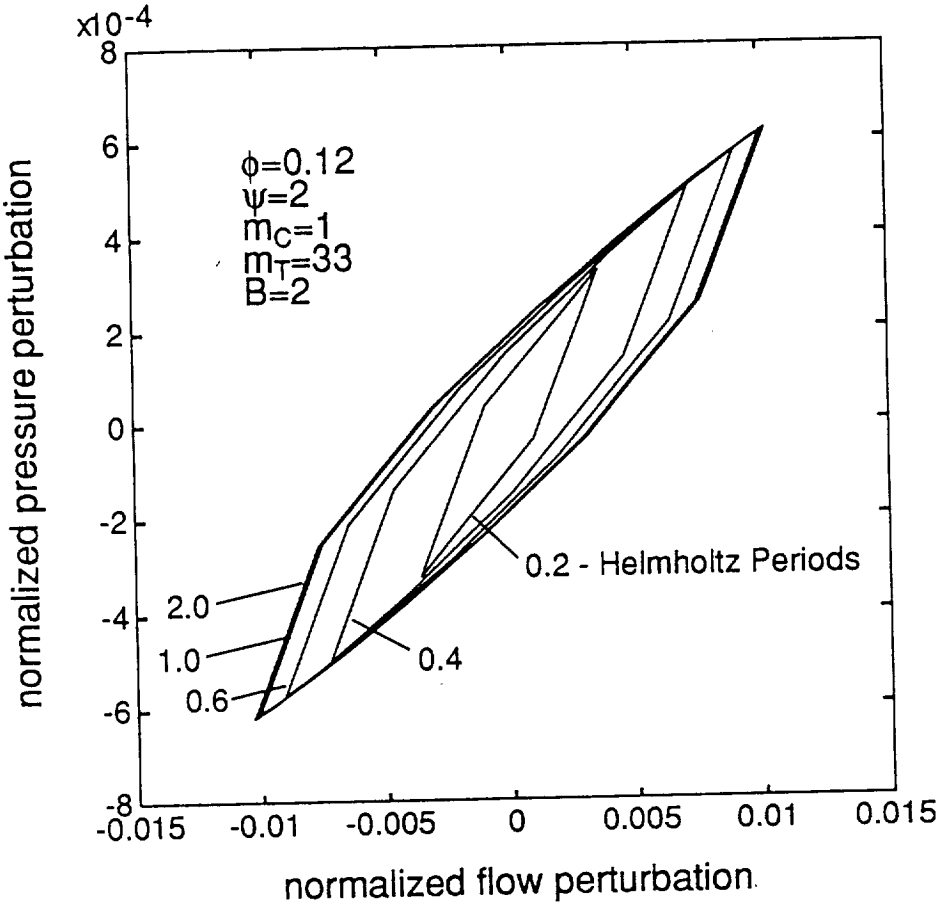

Figure 5-1: Recovery regions for plenum bleed actuator as function of recovery time (illustrative case)

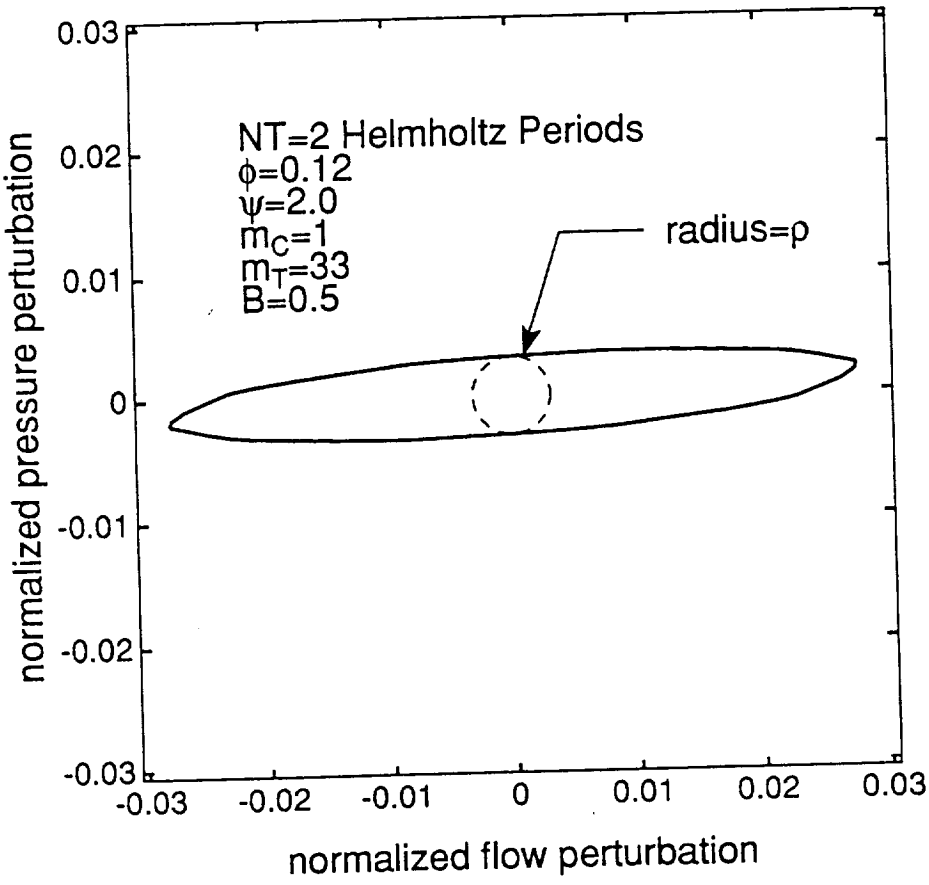

Figure 5-2: Recovery region for plenum bleed actuator showing circle whose radius determines degree of controllability (illustrative case)

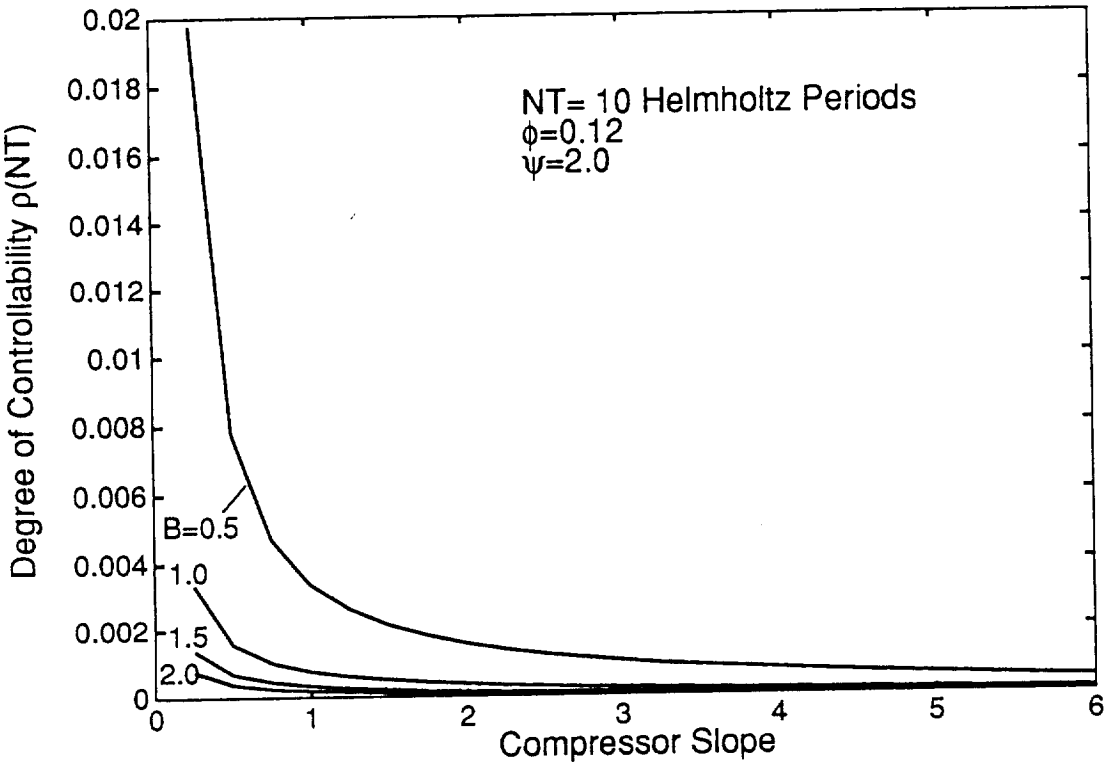

Figure 5-3: Degree of Controllability as function of system parameters for plenum bleed actuator

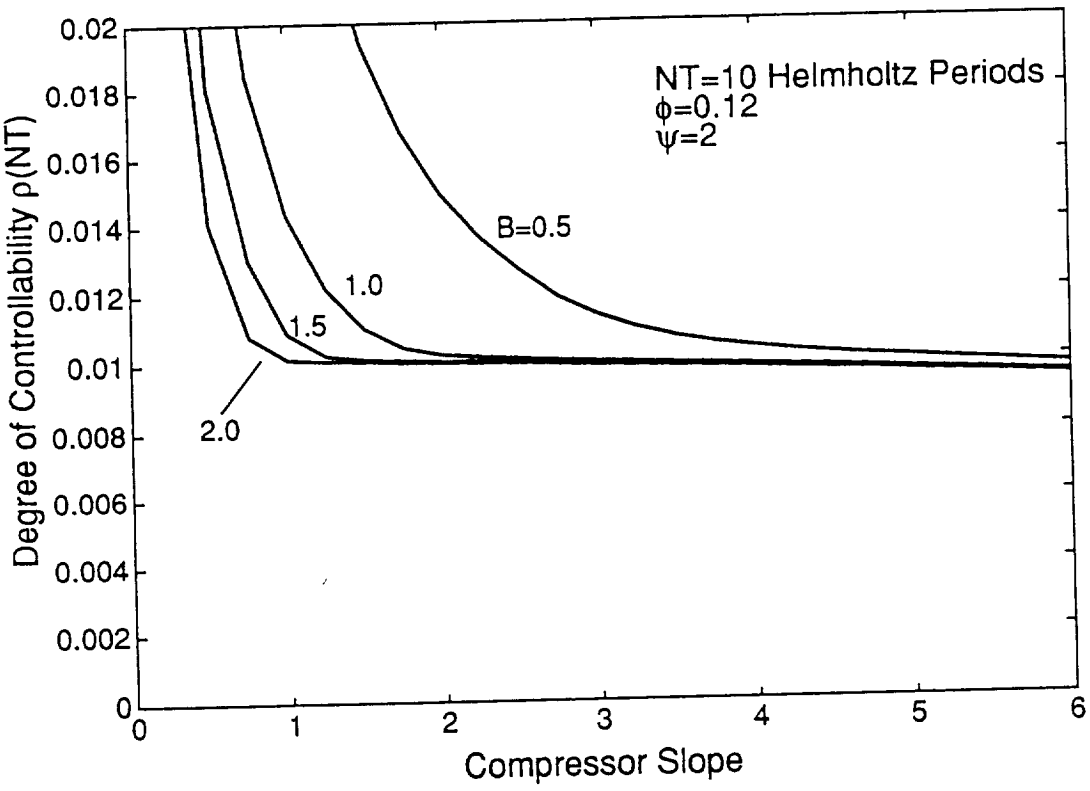

Figure 5-4: Degree of Controllability as function of system parameters for close-coupled actuator

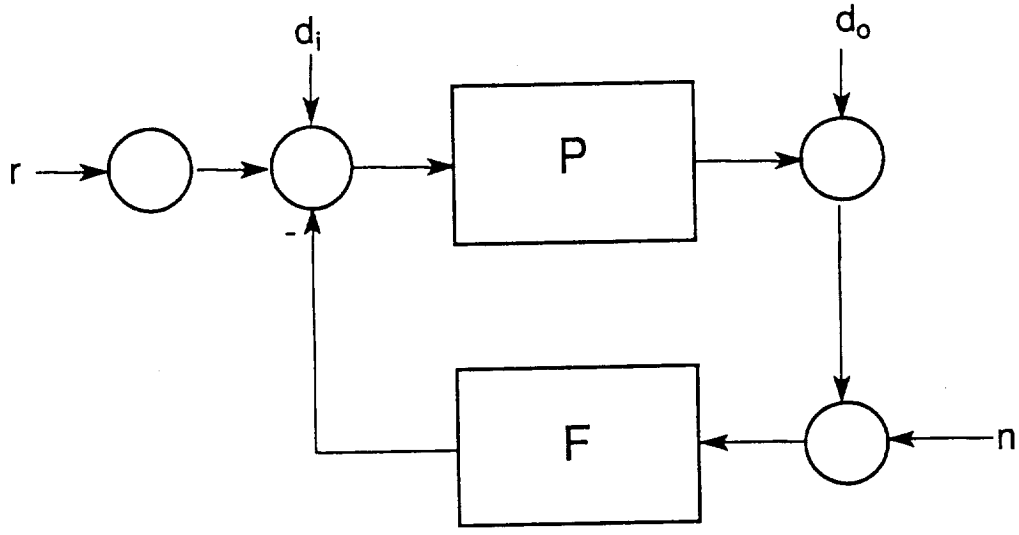

Figure 5-5: Block Diagram for defining closed loop transfer functions

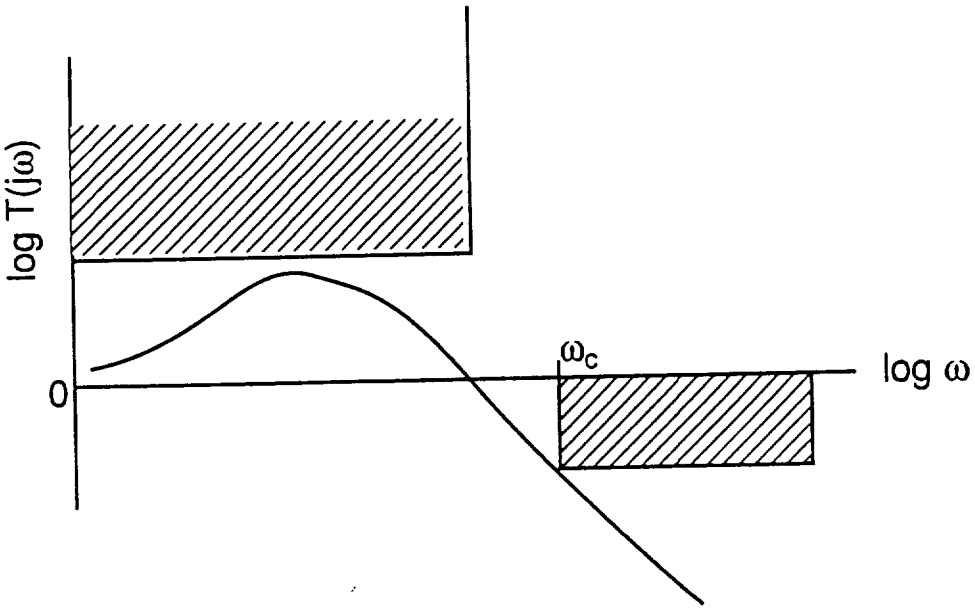

Figure 5-6: Typical frequency domain performance specification for the complementary sensitivity transfer function

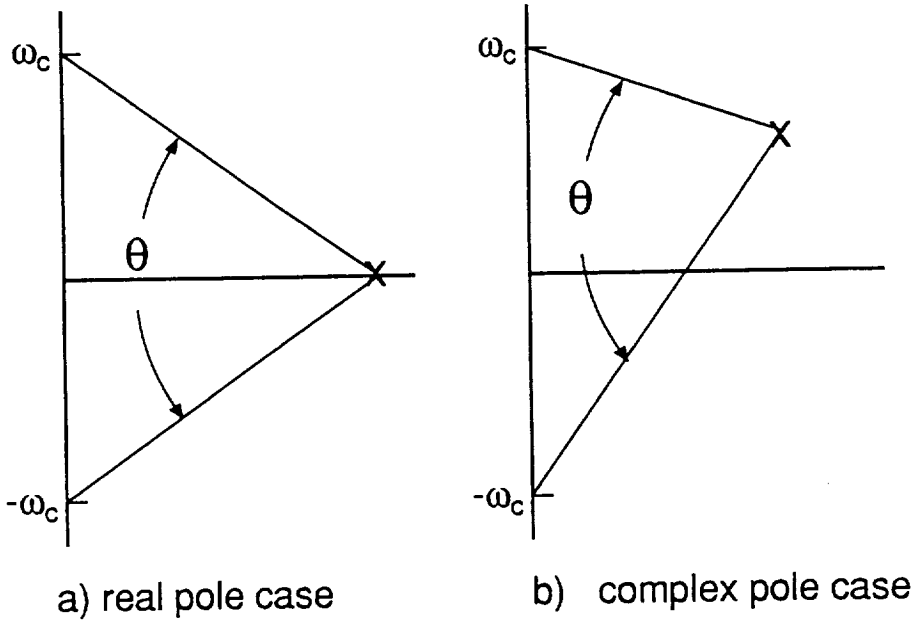

Figure 5-7: Geometrical Construction for the weighting function $\theta(\omega_c)$ a)real pole b)complex conjugate pole

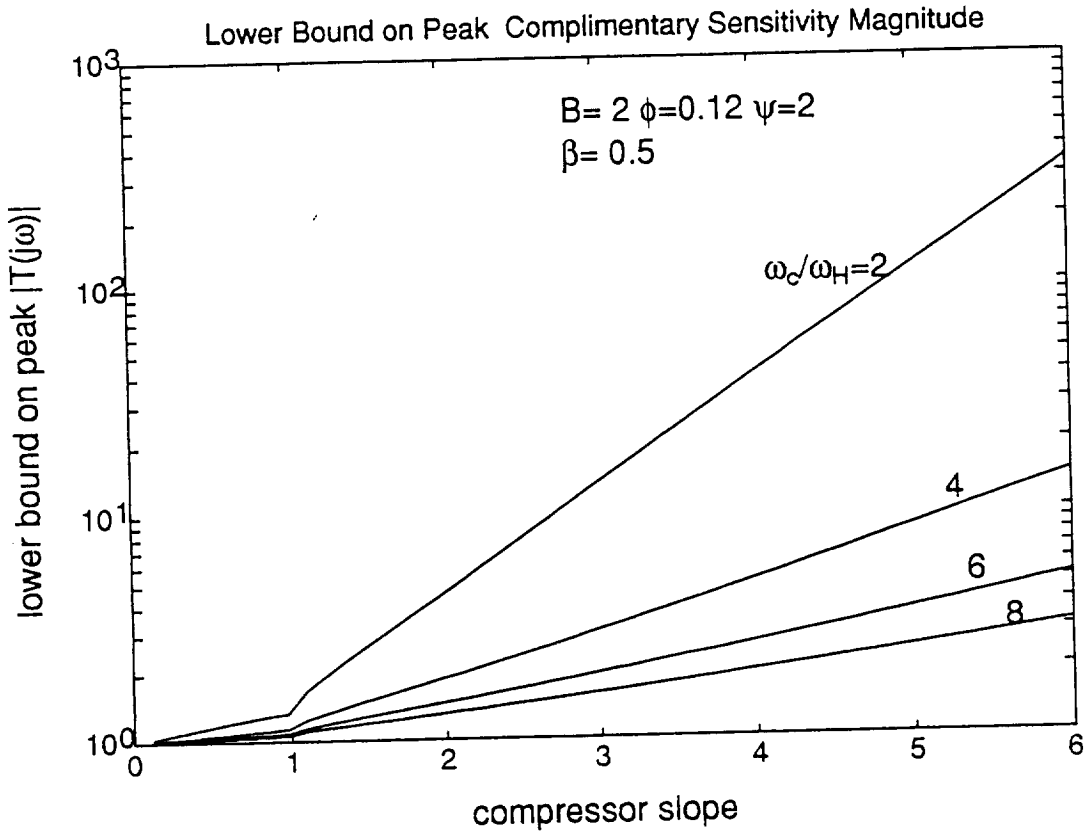

Figure 5-8: Lower Bound on peak complementary sensitivity for close-coupled valve with mass flow measurement

Chapter 6

Evaluation of Alternative Control Strategies

6.1 Introduction

Almost all research to date on the use of feedback stabilization of compression systems has been aimed at proof of concept of the technique, and only a few of the many possible actuators and sensors have been considered. In this chapter, we therefore present the first systematic definition of the influence of sensor and actuator selection on increasing the range of stabilized compressor performance[1]. The results show that proper choice of sensor as well as actuator crucially affects the ability to stabilize these systems and that, overall, those actuators which are most closely coupled to the compressor (as opposed to the plenum or throttle) are most effective. In addition,

[1]The work of this chapter was originally presented in a similar form by Simon et al [46] at the International Gas Turbine and Aeroengine Congress and Exposition, Cologne, Germany June 1-4, 1992.

the source of the disturbances driving the system (for example, unsteady compressor pressure rise or unsteady combustor heat release) has a strong influence on control effectiveness. This chapter both delineates general methodologies for the evaluation of compressor stabilization strategies and quantifies the performance of several approaches which might be implemented in gas turbine engines.

A compressor feedback stabilization system to prevent surge conceptually consists of sensors to detect fluid disturbances within the compression system, actuators to introduce desired perturbations, and a suitable control law connecting the two. Theoretically, only a single sensor and actuator are required, with many choices available for their type and location. Sensors may measure pressure, mass flow, velocity, or temperature within the compressor duct, upstream or downstream of the compressor, in the plenum, or at the throttle. Similarly, there are many methods to introduce unsteady fluid perturbations: varying throttle area, moving a plenum or duct wall, introducing or bleeding off mass flow, varying the heat addition in the plenum (when it is a combustor), as well as introducing a variable throttle between the compressor and plenum, to name a few. A representative list of sensing and actuation options is shown in Table 1.

The central point of the chapter is to show that selection of sensor and actuator type and location is a critical factor in determining the effectiveness and practicality of a stabilization system. Because of the practical interest in this question, the chapter presents a methodology to compare different implementation alternatives, as well as carries out this comparison for a number of candidate strategies. Each sensor/actuator pair when coupled to the compressor, forms a different physical system,

Actuation	Sensing
Injection in compressor duct	Inlet mass flow
Valve close-coupled to compressor	Plenum pressure
Plenum bleed valve	Compressor face Ptotal
Plenum heat addition	Compressor face Pstatic
Variable plenum volume	Plenum temperature
Variable inlet geometry	
Fast inlet guide vanes	
Tangential inlet injection	
Auxiliary compressor stage	
Plenum mass injection	
Inlet duct bleed	

Table 6.1: Sensing and Actuation Options

with differing dynamic behavior, physical limitations, and overall performance. The steps included in the evaluation of control strategies are thus as follows:

- Models of specific systems are analyzed to elucidate the relative performance sensitivities to non-dimensional system parameters.

- Numerical calculations are carried out to quantify the limits to control of various sensor/actuator pairs when connected by a simple proportional control law.

- Optimal control theory is used to evaluate actuator effectiveness, given complete knowledge of the system state.

It is noted that the methodology followed here was developed to obtain quantitative comparisons in a manner which was thought to be most accessible to the to the turbomachinery community. The general problem of actuator/sensor selection has also been considered by a number of researchers for other applications (see, for example, Norris and Skelton, [33]; Schmitendorf, [42]; Muller and Weber, [31]) and these

approaches should certainly be considered in future investigations of this type.

The goals of this work are to make clear the large influence that implementation (sensor/actuator selection) has on the effectiveness of a compressor stabilization control scheme and to elucidate the basic physical limitations to control. We thus do not consider all possible actuators and sensors but chose a representative selection of schemes which are potentially applicable for a large variety of compression systems.

6.2 Analytical Comparison

We use the simplified lumped parameter model of compression system dynamics, developed in Chapter 3 and linearize it about a particular operating point. The behaviors of systems with different sensor/actuator pairing are most clearly revealed from their transfer functions, which are defined as the ratio of the Laplace transformed system output (sensor signal) to input (actuator motion). Open loop transfer functions for three different actuators and four different sensors illustrated in Figure 3-1 are presented in Table 6.2. The transfer functions for all the sensor/actuator pairs in Table 6.2 have the same denominator polynomial denoted as $D(s)$ which is given by:

$$D(s) = s^2 + \left(\frac{1}{Bm_{T_e}} - Bm_{C_e}\right)s + \left(1 - \frac{m_{C_e}}{m_{T_e}}\right), \tag{6.1}$$

but the numerator polynomials differ so that the inherent differences are captured by the latter. For generality, the expressions given in Table 6.2 use the equivalent throttle slope, m_{T_e}, of a throttle in parallel with a bleed valve, and equivalent compressor slope, m_{C_e} of a compressor in series with a close-coupled valve. If no bleed valve is used,

	Close-Coupled Valve	Plenum Bleed Valve	Movable Wall
Compressor Mass Flow	$\frac{Bv_c\left(s+\frac{1}{Bm_{T_e}}\right)}{D(s)}$	$\frac{v_b}{D(s)}$	$\frac{G_w B}{D(s)}$
Plenum Pressure	$\frac{v_c}{D(s)}$	$\frac{\frac{-v_b}{B}(s-Bm_{C_e})}{D(s)}$	$\frac{G_w(s-Bm_{C_e})}{D(s)}$
Compressor Face Total Pressure	$\frac{-v_c s\left(s+\frac{1}{Bm_{T_e}}\right)}{D(s)}$	$\frac{\frac{v_b}{B}s}{D(s)}$	$\frac{G_w s}{D(s)}$
Compressor Face Static Pressure	$\frac{-v_c\left(s^2+\left(2\overline{\phi_c}B+\frac{1}{Bm_{T_e}}\right)s+\frac{2\phi_c}{m_{T_e}}\right)}{D(s)}$	$\frac{\frac{v_b}{B}\left(s+2\overline{\phi_c}B\right)}{D(s)}$	$\frac{-G_w\left(s+2\overline{\phi_c}B\right)}{D(s)}$

Table 6.2: Open Loop Transfer Functions

$m_T = m_{T_e}$. Similarly, if no close-coupled valve is used, $m_{C_e} = m_C$. In this section, we will use the simplest control law, a proportional relationship between input and output, to focus on the effects of actuator and sensor selection, but in a subsequent section, we will examine the impact of the form of the control law.

6.2.1 Stability Modification Using Proportional Control

System stability under the influence of a proportional control law is determined from the roots of the closed loop characteristic equation (this is derived in many texts; see, for example, Ogata, [34])

$$G_D(s) + KG_N(s) = 0 \tag{6.2}$$

In Equation 6.2, $G_N(s)$ and $G_D(s)$ are the numerator and denominator polynomials, respectively, of the transfer function given in Table 6.2 and the gain, K, is a real constant of proportionality in the control law. The system will be stable if and only

if all the roots of the characteristic equation have strictly negative real parts. For the present case, where the characteristic equation is a second order polynomial, this is equivalent to requiring all the coefficients of the closed loop characteristic equation to be strictly positive.

Equation 6.2 is the sum of two terms, $G_N(s)$ and $G_D(s)$. When the control is off (K set to zero), stability is determined from the roots of $G_D(s)$ only and, thus, is the same whatever the sensor/actuator pair. As the gain K is increased from zero, system stability becomes increasingly modified by the $G_N(s)$ term and, because the various sensor/actuator pairs have different numerator polynomials, $G_N(s)$, the effect of feedback also varies. This is best illustrated by several specific examples. The first two examples show the effect of sensor type, whereas comparison between behavior in the second and third illustrate the impact of the actuator.

Example 1: Close-Coupled Control Valve With Mass Flow Measurement

Using the appropriate transfer function from Table 6.2, substituting into the characteristic equation, Equation 6.2, and rearranging results in the closed loop characteristic equation:

$$s^2 + \left(\frac{1}{Bm_{T_e}} - Bm_{C_e} + KBv_c\right)s + \left(1 - \frac{m_{C_e}}{m_{T_e}} + \frac{Kv_c}{m_{T_e}}\right) = 0 \qquad (6.3)$$

For stability we require:

$$\left(\frac{1}{Bm_{T_e}} - Bm_{C_e} + KBv_c\right) > 0 \qquad (6.4)$$

and

$$\left(1 - \frac{m_{C_e}}{m_{T_e}} + \frac{K v_c}{m_{T_e}}\right) > 0 \tag{6.5}$$

All the parameters in these two inequalities are positive numbers except for the compressor slope, m_{C_e}. If $m_{C_e} < 0$, as it typically is for high flow rates, the system will be stable with no feedback, that is with K set equal to zero. As the flow rate becomes lower, m_{C_e} will become less negative, reaching zero at the peak of the compressor characteristic and then moving to a large enough positive value, so that the system will be unstable without feedback. For sufficiently large values of the gain K, however, both the inequalities expressed in Equations 6.4 and 6.5 can be simultaneously satisfied and the system can always be stabilized.

Example 2: Close-Coupled Valve With Plenum Pressure Measurement

In this case, as given in Table 6.2, the numerator polynomial of the transfer function contains only a constant term. The closed loop characteristic equation is:

$$s^2 + \left(\frac{1}{B m_{T_e}} - B m_{C_e}\right) s + \left(1 - \frac{m_{C_e}}{m_{T_e}} + K v_b\right) = 0 \tag{6.6}$$

The system can now only be stabilized if the equivalent compressor slope is small enough so that the term $\left(\frac{1}{B m_{T_e}} - B m_{C_e}\right)$ is positive; in other words, the equivalent compressor slope obeys the inequality $m_{C_e} < 1/(B^2 m_{T_e})$. The ability of proportional feedback to stabilize this system is thus limited to a certain range of parameters. For many applications, B is unity or larger and the throttle slope, m_{T_e}, is on the order of ten to one hundred, so the useful range can be quite small.

Example 3: Plenum Bleed Valve With Measurement of Plenum Pressure

From Table 6.2, the numerator polynomial for this case is

$$G_N(s) = -\frac{v_b}{B}(s - Bm_{C_e}) \tag{6.7}$$

and the closed loop characteristic equation is given by:

$$s^2 + \left(\frac{1}{Bm_{T_e}} - Bm_{C_e} - \frac{Kv_b}{B}\right)s + \left(1 - \frac{m_{C_e}}{m_{T_e}} + Kv_b m_{C_e}\right) = 0. \tag{6.8}$$

Whether the gain K is chosen to be positive or negative, it will have the desired effect on only one of the two coefficients of the characteristic equation. As a result, stabilization is limited to cases where $m_{C_e} < 1/B$. The limitation is associated with the sign change between the leading and the constant coefficient of $G_N(s)$, as given by Equation 6.7, which implies that $G_N(s)$ has a zero in the right half of the complex plane. Systems whose transfer functions have numerators with zeros in the right half of the complex plane are called non-minimum phase systems. As discussed in Section 5.3.1, the ability to control non-minimum phase systems is known to be subject to certain fundamental limitations (see also Freudenberg and Looze, [15]) and this is just one manifestation of the generally poor behavior encountered in such systems. The remaining sensor/actuator pairs whose transfer functions appear in Table 6.2 have also been analyzed. For stability, all coefficients in the closed loop characteristic equation must be positive; from this requirement, the capability of each scheme to extend the flow range to high values of compressor slope can be determined.

	Close-Coupled Valve	Plenum Bleed Valve	Movable Wall
Compressor Mass Flow	Unlimited Range Increase $K \sim \left(\frac{m_{C_e}}{v_c}\right)$ as $m_{C_e} \to \infty$ $K \sim \left(\frac{m_{C_e}}{v_c}\right)$ as $B \to \infty$	Limited Range Increase $m_{C_e} < \frac{1}{B^2 m_{T_e}}$	Limited Range Increase $m_{C_e} < \frac{1}{B^2 m_{T_e}}$
Plenum Pressure	Limited Range Increase $m_{C_e} < \frac{1}{B^2 m_{T_e}}$	Limited Range Increase $m_{C_e} < \frac{1}{B}$	Limited Range Increase $m_{C_e} < \frac{1}{B}$
Compressor Face Total Pressure	Limited Range Increase $m_{C_e} < m_{T_e}$	Limited Range Increase $m_{C_e} < m_{T_e}$	Limited Range Increase $m_{C_e} < m_{T_e}$
Compressor Face Static Pressure	Unlimited Range Increase $K \sim \left(\frac{m_{C_e}}{2v_c\phi_c}\right)$ as $m_{C_e} \to \infty$ $K \sim \left(\frac{m_{C_e}}{2v_c\phi_c}\right)$ as $B \to \infty$	Unlimited Range Increase $K \sim \begin{cases} \frac{m_{C_e}B^2}{v_b} \text{ if } \frac{1}{2\phi_c B^2 m_{T_e}} < 1 \\ \frac{m_{C_e}}{2v_b\phi_c m_{T_e}} \text{ otherwise} \end{cases}$ as $m_{C_e} \to \infty$ $K \sim \frac{B^2 m_{C_e}}{v_b}$ as $B \to \infty$	Unlimited Range Increase $K \sim \begin{cases} \frac{m_{C_e}B}{G_w} \text{ if } \frac{1}{2\phi_c B^2 m_{T_e}} < 1 \\ \frac{m_{C_e}}{2m_{T_e}G_w\phi_c B} \text{ otherwise} \end{cases}$ as $m_{C_e} \to \infty$ $K \sim \frac{B^2 m_{C_e}}{v_b}$ as $B \to \infty$

Table 6.3: Limitations on Compressor Flow Range Increase With Proportional Control

The behavior of the different pairs is shown in Table 6.3, which summarizes the limitations of each pair.

In some instances, for example, sensing compressor mass flow and actuating with a close-coupled valve, the range of parameters over which stabilization may be achieved is unlimited, although large values of gain may be required with a large compressor slope or large value of the B parameter. In these cases, the asymptotic behavior of the required gain is therefore given for large B and compressor slope, in order to show the trends to be expected in these regimes. Excessive gain must be avoided in practical situations as will be discussed below. As shown in Table 6.4, however,

the gain increases either linearly or quadratically with compressor slope and B and there will thus be a practical limitations on maximum slope or maximum B at which the system can be stabilized. An important point is that the limitations on nominal stabilization can, in most cases, be relaxed or removed by using a dynamic control law. Thus, the limitations expressed in this section reflect the combined properties of actuator, sensor, and control law taken together, and not necessarily of the individual elements. Within the restriction to a fixed control law maintained here, however, the comparison of different sensor/actuator pairs is both valid and useful.

6.3 Practical Limits To Control

The analytical results so far indicate that the ability to stabilize the system with proportional control depends strongly on proper pairing of actuator and sensor, as well as on the values of the system parameters, particularly the compressor slope m_C and B. In the above examples, however, we have considered ideal linear systems in which only the nominal system dynamics system are considered. To address the issue of implementation, it is also necessary to consider bandwidth limitations and actuator constraints (for example, servo dynamics and mechanical stops) which are encountered in any physical realization. As a matter of definition, by actuator we refer here to the entire actuation system including the flow train element (e.g. the valve), the motor that drives it, and any included feedback elements. The bandwidth limitations may be imposed by the sensors, processor, actuator, or some combination of the three. System bandwidth must also be constrained to maintain stability in

the presence of unmodeled high frequency dynamics (see Section 5.3). Unless the bandwidth of the actuator is much greater than that of the compression system, there is a non-negligible time lag between the command output of the control law and the response of the flow train element. The lags introduced by the actuator generally result in reduced control effectiveness although, to some degree, they can be compensated for by use of a control law more sophisticated than proportional control. Another constraint on control effectiveness is the need to avoid actuator saturation[2]. For example, valve areas can only be modulated between 0 and 100% (i.e. the valve must be somewhere between full open and full closed). This implies that control gains must be kept small enough to avoid saturation for the expected range of perturbations.

6.3.1 Sensor and Actuator Pairs and Fluid Model

In this section, the limitations imposed by gain and bandwidth constraints are quantified for specific cases. Five actuators and four sensors are studied as representative of a diverse set of implementation options. The selected actuators were: 1) injection in the compressor duct; 2) close-coupled control valve; 3) plenum bleed valve; 4) plenum heat addition; and 5) a movable plenum wall. The selected sensors were: 1) compressor duct mass flow; 2) plenum pressure; 3) compressor face static pressure; and 4) compressor face total pressure. These actuators and sensors are shown schematically in Figure 3-1. At the level of idealization used here, the close-coupled valve could be either at the compressor inlet or exit without changing the results. The linear

[2]An actuator is said to be saturated when its output reaches the limit of its allowable range.

lumped parameter models of the previous section were extended as required, because the various actuators imply additional system states. The differential equations that describe the system dynamics are obtained by performing balances on momentum in the ducts and mass and energy in the plenum as detailed in Chapter 3. The general description is nonlinear, but it is small perturbations which are of primary interest here, and the governing differential equations are linearized to yield sets of equations of the form:

$$\dot{\mathbf{x}} = \mathbf{A}\mathbf{x} + \mathbf{b}u. \tag{6.9}$$

The nonlinear output equations are also linearized to obtain the resulting vector of output perturbations y defined as

$$y = \mathbf{c}\mathbf{x} + \mathbf{d}u \tag{6.10}$$

In Equations 6.9 and 6.10 , the linearized state variables $\mathbf{x}$, the inputs u, and the outputs y, are perturbations from the corresponding equilibrium values, and $\mathbf{A}$, $\mathbf{b}$, $\mathbf{c}$, and $\mathbf{d}$ are appropriately dimensioned constant matrices. The state variables have been normalized as detailed in Table 6.4, so that unity magnitude for any of these perturbation variables has approximately the same physical significance.

All twenty pairings of the five actuators and four sensors have been evaluated with a proportional control law. Such a comparison provides two useful results. One is the identification of sensor/actuator pairs which may be stabilized over a significant range of system parameters using the simplest possible control law. In addition, for those

Perturbation Variable	Normalized By
Flow	Time mean flow through compressor
Pressure	Time mean compressor pressure rise
Thermal input	Mean compressor work
Moving wall work input	Mean compressor work
Plenum bleed valve area	Area to fully close valve
Close-coupled valve area	Area to fully open or close
	(whichever is smaller)

Table 6.4: Normalization Factors

pairs with significant stabilization, the required gain gives a measure of the combined effectiveness of this choice of sensing and actuating locations. As was discussed, it is useful to eliminate those systems which could mathematically be stabilized but stand little chance of succeeding in an actual implementation. To this end, two constraints were imposed. First, the allowable magnitude of the normalized proportional gain was limited to be not more than twenty. For example, at the maximum allowable gain, a five percent change in compressor mass flow would yield a one hundred percent change in the allowable plenum bleed valve area; that is, the valve would be fully opened or closed. Second, the bandwidth of the feedback loop was limited by modeling a two-pole, low pass Butterworth filter in the feedback path. This filter can be given various physical interpretations such as probe dynamics, amplifier dynamics, actuator dynamics or unmodeled dynamics in the compression system itself. Whatever the interpretation, the insertion of the filter insures that the feedback path has finite bandwidth, a constraint which will always exist in practice. The study was carried out with the cutoff frequency of this filter maintained at ten times the Helmholtz frequency of the system formed by the plenum and compressor ducts and sensitivity

to this assumption will be examined subsequently.

The figure of merit used to assess the sensor/actuator pairs was to examine the stability boundaries in a compressor slope versus B parameter plane. Preliminary studies and consideration of the underlying system dynamics showed that these two parameters have a dominant effect on system stability. It is more relevant, for example, to quantify the amount of stabilization that can be achieved in terms of the compressor slope, which enters into the stability criterion in an explicit manner, rather than the change in mass flow at stall. Since the positive compressor slope typically increases as flow decreases, all else being equal, the greater the maximum stabilizable slope is, the greater the range extension will be. The relative extent of the stabilized region in this compressor slope B-parameter plane thus provides an appropriate and useful basis for comparison. The stability boundaries were computed by performing an incremental search over the three-dimensional (slope, B parameter gain) parameter space. For each fixed B, the value of gain which maximized the slope at instability (within the allowable range), as well as the corresponding slope, was found. The stability boundaries in the B parameter versus slope plane thus represent the maximum slope which could be stabilized using any normalized gain with a magnitude less than twenty.

6.3.2 Results of the Control Scheme Evaluations

The results of the calculations are summarized in Figure 6-1 which shows the stability boundaries for the twenty sensor/actuator pairs. The figure is broken into four plots, one for each sensor. Within each plot, the five curves indicate the different actuators.

The region below and to the left of any given line is the region in which stabilization can be achieved. In the upper left hand plot, for example, all the region to the left of the dash-dot line represents the range of compressor slope and B in which the combination of compressor mass flow sensor and close-coupled valve is capable of suppressing the instability.

Several general conclusions can be drawn from the results in Figure 6-1:

1. The overall trend is that control becomes more difficult as the compressor slope and B parameter increase, with the maximum stable slope decreasing with increasing B.

2. Only the actuators located in the compressor duct, which act upon the compressor duct momentum (injector and close-coupled control valve), are capable of stabilization at steep slopes over the full range of B.

3. Plenum heat addition gives little or no stability enhancement

4. In general, there is no best sensor independent of the actuator.

For reference, the B parameter that might be associated with large axial gas turbine engines is very roughly 0.5 (e.g., Mani [27]). For other engine geometries and industrial compressors with large downstream volumes, B parameters of 2 or greater might be encountered.

A more specific conclusion is given by the comparison of the results with the mass flow sensor to the other sensor locations. As B reaches a value of roughly unity, the ability of all the pairs to stabilize the system becomes quite small, except for the

close-coupled valve and the injector which use mass flow sensing. This points out clearly that not only is actuator position important, but sensor position is as well.

The conclusion about the effect of actuator position is one that is in general accord with intuitive ideas of system behavior, but that having to do with sensors is generally less familiar. It is therefore worthwhile to give some physical motivation for the impact of sensor position. The different dynamics brought about by the various sensors can be understood with reference to the non-dimensional characteristic equation for the unsteady system behavior with no feedback:

$$s^2 + \left(\frac{1}{Bm_{T_e}} - Bm_{C_e}\right) s + \left(1 - \frac{m_{C_e}}{m_{T_e}}\right) = 0 \tag{6.11}$$

For stability the coefficients of the second and third terms must be positive, so that

$$m_{C_e} < \frac{1}{B^2 m_{T_e}} \tag{6.12}$$

$$m_{C_e} < m_{T_e} \tag{6.13}$$

As described by Greitzer, [19], the mechanism of instability can either be static, corresponding to the inequality in Equation 6.13 being violated or dynamic, corresponding to the violation of that in Equation 6.12. Whichever of these events occurs the underlying cause is a positive slope of the compressor pressure rise characteristic. Therefore, let us examine how the destabilizing effect of positive slope is ameliorated when different sensing schemes are used. As a case of practical interest, we consider the close-coupled valve with two different sensors, one measuring compressor mass

flow and the other measuring the total pressure at the compressor inlet face.

In the first of these, the valve position and, hence, the valve pressure drop, is proportional to the sensed perturbations in compressor mass flow. The pressure perturbations across the compressor and across the valve are both proportional to the mass flow perturbations. Because the valve is just downstream of the compressor, the two act in series, creating an effective compressor slope which is the sum of the (positive) slope across the compressor and the (negative) slope across the valve. It is this combined characteristic which the system "sees".

Suppose the constant of proportionality between sensed mass flow and valve open area is K, and the rate of change of valve pressure drop per increment in open area is v_c. For a given mass flow perturbation, the effective slope of the compressor will change from m_{C_e}, with no feedback, to $(m_{C_e} - Kv_c)$ when feedback is applied. Sensing the compressor mass flow and feeding the signal back to the valve actuator thus works directly on the cause of the instability, the positive compressor slope. Insertion of the slope $(m_{C_e} - Kv_c)$ in Equation 6.11 in fact gives Equation 6.3, the previously derived closed-loop characteristic equation for this situation.

A different situation prevails for the inlet total pressure sensor. The inlet total pressure perturbation is related to the derivative of the inlet mass flow, i.e., the fluid acceleration in the compressor duct, through the unsteady Bernoulli Equation

$$p_{0_0} - p_{0_1} = \rho \int_0^1 \frac{\partial u}{\partial t}\, dx \tag{6.14}$$

Non-dimensionalizing and linearizing gives

$$-\widehat{\psi_1} = \frac{1}{B} d\phi/d\tau \tag{6.15}$$

where $\widehat{\psi_1}$ is the total pressure perturbation at the compressor face in non-dimensional form. If the valve area perturbation is proportional to the compressor inlet total pressure, the result is to create a pressure change across the valve proportional to the acceleration, which is the derivative of the state variable ϕ. In other words, the effect of feedback in this case is to alter the overall pressure difference from duct inlet to exit for a given fluid acceleration rate. As far as the system is concerned, this is seen as a change in the equivalent duct length, $\mathcal{L}$, of the compressor. That is, the longer the duct, the larger will be the instantaneous pressure change required to produce a given fluid acceleration. An increase in effective length of the duct does several things to the system, the most important being that it changes the effective value of the B-parameter, which scales as $1/\sqrt{\mathcal{L}}$. This can be seen in the resulting closed loop characteristic equation which is given by:

$$(1 + Kv_c)s^2 + \left(\frac{1}{Bm_{T_e}} - Bm_{C_e} + 2Kv_c\overline{\phi_c}B + \frac{Kv_c}{Bm_{T_e}}\right)s + \left((1 - \frac{m_{C_e}}{m_{T_e}} + \frac{2Kv_c\overline{\phi_c}}{m_{T_e}}\right) \tag{6.16}$$

in which the critical value of B for instability is increased by $\sqrt{1 + Kv_c}$, with $(1+Kv_c)$ being just the factor by which the effective length is increased. In the case of total pressure sensing, however, only the dynamic instability is influenced, because the increase in effective mass does nothing to alter the static stability. The instability

limit is thus still $m_{C_e} \geq m_{T_e}$.

Somewhat similar arguments can be made for other sensor/actuator pairs; the main point is that the use of different sensors for the feedback gives the system quite different dynamical behavior.

6.3.3 Effect of Control System Bandwidth

The preceding study of the sensor/actuator pairs was carried out with the bandwidth of the feedback loop limited by a two-pole Butterworth inserted in the feedback path. The cutoff frequency, ω_c, of this filter was held fixed at ten times the compression system Helmholtz frequency ω_h and we can also examine the influence of this parameter, in other words, of controller bandwidth, on the stabilization process. Figure 6-2 shows the changes in instability onset that occur with different controller bandwidths for the close-coupled control valve, with feedback on mass flow, and a B-parameter of 2.

In the figure, the horizontal axis is the controller gain, and the vertical axis is the slope of the compressor characteristic at instability. Curves are shown for values of ω_c/ω_h from 1.0 to 100, representing extremes of this ratio, and it is seen that large changes in the maximum slope that can be stabilized result from these changes in bandwidth of the controller.

Several trends are exhibited in Figure 6-2. First, for a controller bandwidth of $\omega_c/\omega_h = 1$, use of the control is actually destabilizing. The more gain the less steep the compressor slope that can be achieved. In this regime, the control system is adversely affected by the slow actuator dynamics. Second, as ω_c/ω_h becomes larger,

increasing the controller gain increases the compressor slope that can be attained. Third, for a given level of bandwidth, increasing gain increases stability only up to a point; beyond this point the stabilization decreases as gain increases. The maximum slope which can be stabilized, however, always increases with bandwidth.

The necessity to go to higher bandwidth at higher slope arises because, as the slope increases, the system dynamics become faster relative to the undamped natural frequency (Helmholtz frequency). The relevant time scale becomes the fluid acceleration time in the compressor duct and thus the actuator must be fast relative to this time scale rather than that set by the Helmholtz frequency. This point is an important one since it is difficult, in many cases, to engineer actuators with bandwidths many times that of the Helmholtz frequency. The analysis suggests that actuator bandwidth will be a prime determinant of practical system performance and that research and development on this topic is useful to pursue.

6.4 Comparison Based On Actuator Response To Disturbances

From the study of individual sensor/actuator pairing using a proportional control, the close-coupled valve and injector emerge as the most promising actuators. A further question to address, however, is whether the type of compensation (control law) or choice of sensors would affect this conclusion. In this section, linear, optimal

stochastic, control theory is used to provide a definite answer to this question[3].

6.4.1 Background

To motivate the approach taken, some basic aspects of linear dynamic system stabilization are first presented. For small disturbances, the compression system, actuators and disturbances are described by the linear differential equation set:

$$\dot{\mathbf{x}} = \mathbf{A}\mathbf{x} + \mathbf{b}u + \mathbf{L}\mathbf{w} \tag{6.17}$$

where $\mathbf{x}$ is a vector of system states, u is a scalar representing a particular actuated variable, $\mathbf{w}$ is a p-dimensional vector of external disturbances, and $\mathbf{A}$, $\mathbf{b}$, and $\mathbf{L}$ are constant matrices of appropriate dimensions. This is just Equation 6.9 modified to include the effect of external disturbances. It is known (see, for example, Kwakernaak and Sivan, [24]) that systems of this type can be stabilized for all conditions using the control law $u = -K\mathbf{x}$, where K is now a one-by-five constant gain matrix, provided only that the pair $\{A, B\}$ is controllable. Such a control law is known as full state feedback. For a system with n states, this would require n properly placed sensors. For the situation of interest here, over the range of parameters which have been analyzed, the requirement of controllability is met. Thus, with enough properly placed sensors, nominal stabilization of the idealized linear system is theoretically possible. (See also

[3]This problem was addressed by a different approach in Chapter 5 using the concept of degree of controllability. The degree of controllability explicitly accounts for the bounded actuation aspect of the problem but not the nature of the disturbances. In contrast, the stochastic approach explicitly accounts for the disturbances but can address the actuator bounds only in term of RMS (root mean square) activity rather than fixed bounds.

Chapter 5 which considers the case of a single sensor.)

6.4.2 Methodology

All actuators are not equally effective. All else being equal, an ineffective actuator will require more motion to maintain stability in the presence of disturbances than an effective one. In the analysis, therefore, the actuators are compared based upon their minimal required RMS (root mean square) response to a persistent broadband disturbance, while maintaining system stability. This comparison is independent of choice of sensor, because it is assumed that the state of the system is known at all times. Further, the comparison is based upon the minimal possible RMS amplitude, and hence there is no question as to whether a particular actuator would perform better if another control law were used. In this sense, the comparison is also independent of the control law.

Specific details of the computations performed are included in Appendix D and a more general treatment can be found in Kwakernaak and Sivan [24]. The central concept utilized is that, if the disturbance can be described as a stationary, Gaussian, white noise process, a particular gain matrix K can be found which will minimize the root mean square value of the actuated variable u. The gain matrix K and the RMS value of u will depend upon the matrix $\mathbf{L}$ which determines how the disturbance enters the system and upon the statistical properties of the disturbance.

For this analysis, the disturbances driving the system must be chosen. Three disturbances were studied: 1) a compressor with an unsteady pressure rise; 2) an unsteady heat release in the plenum chamber; and 3) an unsteady outflow through the

throttle. In order to compare disturbances which have effectively the same strength, in each case, the input disturbance amplitude (white noise intensity) was normalized to that required to produce a one percent RMS fluctuation in compressor mass flow at a fixed, stable operating point of $\phi_c = 0.20$. The results of this analysis are illustrated in Figure 6-3. In the figure, the maximum allowable slope at which the system can be stabilized is plotted as a function of B for five different actuators, based on the restriction that the RMS actuation is no greater than 25% of the full actuator range, for the most deleterious type of disturbance. The choice of this level of maximum RMS actuation is somewhat arbitrary, but it is taken to be one that can be achieved in practice. In addition, computations have been carried out at other levels, and the results show similar trends.

For all the actuators, the maximum allowable slope that can be attained decreases as the B- parameter increases. However, the effect of varying B on the maximum allowable slope varies markedly between different actuators. As with proportional control, those actuators which are most closely coupled to the compressor (injection and the close-coupled valve) are the most effective. The figure shows that, for B greater than unity, the maximum allowable compressor slope is quite limited. (For reference, the characteristic of the turbocharger used in the experiments, as described in Chapter 2, has a maximum slope of approximately six, i.e., $m_c = 6$). In addition, except for the close coupled valve, whose performance becomes independent of B, the maximum allowable slope decreases monotonically with B parameter. Heat addition, which might seem attractive because of ease of implementation through fuel injection, shows little potential for stabilization at values of B larger than unity.

Another result is that the behavior of the plenum bleed, the injector, and the moving wall are roughly comparable, although the injector has some advantage for larger values of B (greater than two, say). At these high values of B parameter, however, the close coupled valve has a clear advantage, over all of the other schemes examined, in stabilizing the system.

6.4.3 Effect of Disturbance Type

The influence of the disturbance type on the minimal required actuator activity is shown in Figure 6-4 for the close coupled valve, the actuator shown to be most effective in enhancing flow range for large values of B. The horizontal axis is the slope of the compressor characteristic, and the vertical axis is the normalized RMS actuation level. Three curves are plotted, showing the RMS level corresponding to three disturbances of equivalent strength but different type. The difference between the three curves indicates the impact of disturbance type on the ability to control the system. Compressor pressure rise disturbances, such as might arise from local unsteady flow in the impeller or diffuser, create a situation that is more difficult to control than disturbances due to combustor heat release or throttle mass flow fluctuation.

The implication of Figure 6-4 is that the nature of the disturbances driving the system is an important factor in setting the requirements for stabilization. There is little known at present about the detailed disturbance structure within turbomachinery and engines and characterization of these unsteady phenomena is thus a research item of considerable practical concern.

6.5 Summary

An evaluation of strategies for the control of compression system surge has been carried out as a first step towards developing rational design procedures for surge stabilization. A basic result is that the close-coupled actuators and sensors which measure and act upon the momentum of the fluid in the compressor duct are the most effective for geometries and compressor slopes of interest for gas turbine applications. Although this result was qualitatively anticipated based upon the system physics, the analysis has quantified the severity of these trends, showing them to be extremely important over the parameter range of interest. The following specific conclusions can be made:

- Proper choice of actuator and sensor is an important part of the overall design of a surge stabilization system.
- Mass flow measurement with either a close-coupled valve or an injector for actuation are the most promising approaches of those evaluated.
- Fuel modulation is not a promising candidate for practical ranges of system parameters.
- Characterization of compression system disturbance sources is important for determining the requirements for stabilizing control schemes.
- As either the compressor slope or the B parameter increase over the anticipated range of interest, control becomes substantially more difficult.

- Actuator bandwidth can be an important constraint in many practical implementations.

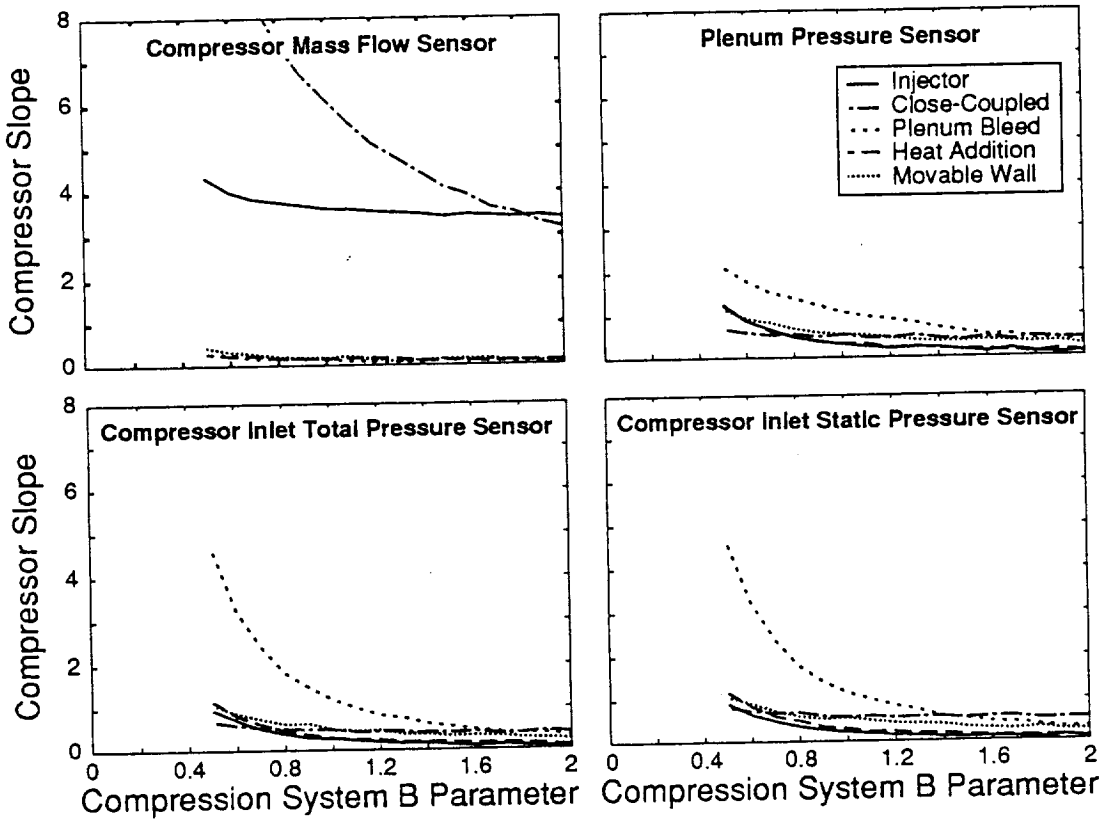

Figure 6-1: Influence of sensor and actuator selection on maximum stabilized slope for a bandwidth and gain limited system

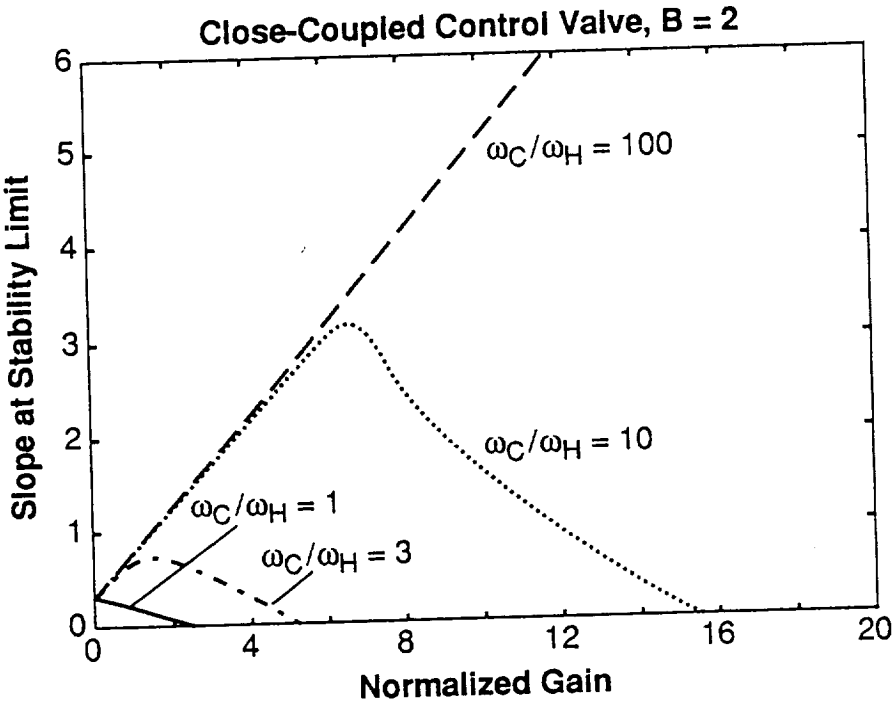

Figure 6-2: Influence of normalized control system bandwidth ($\frac{\omega_c}{\omega_h}$) on the feedback gain required and slope at instability onset;close-coupled control valve

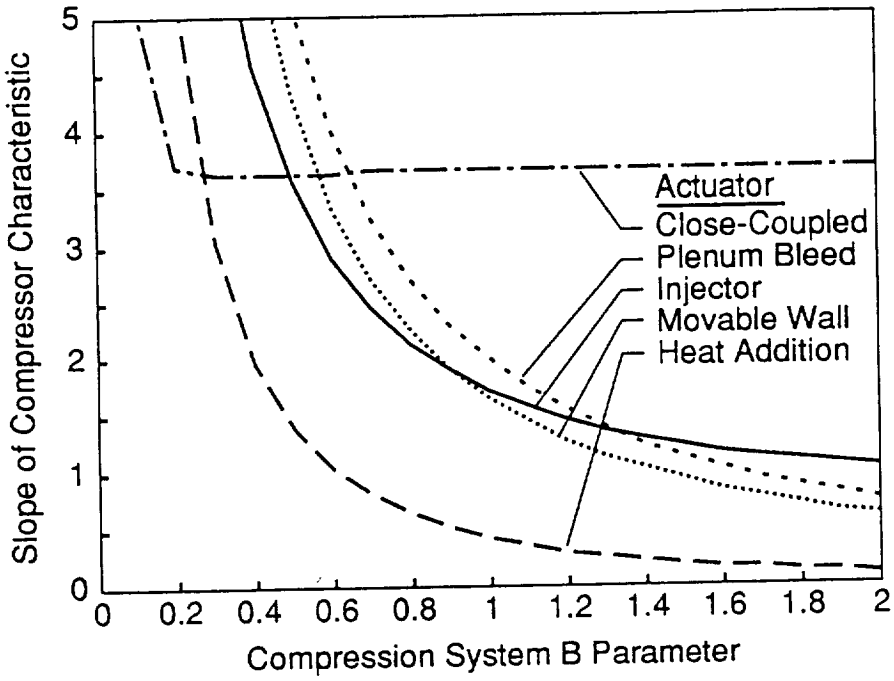

Figure 6-3: Maximum slope at which the RMS actuation will be no greater than 25% of the maximum actuator authority

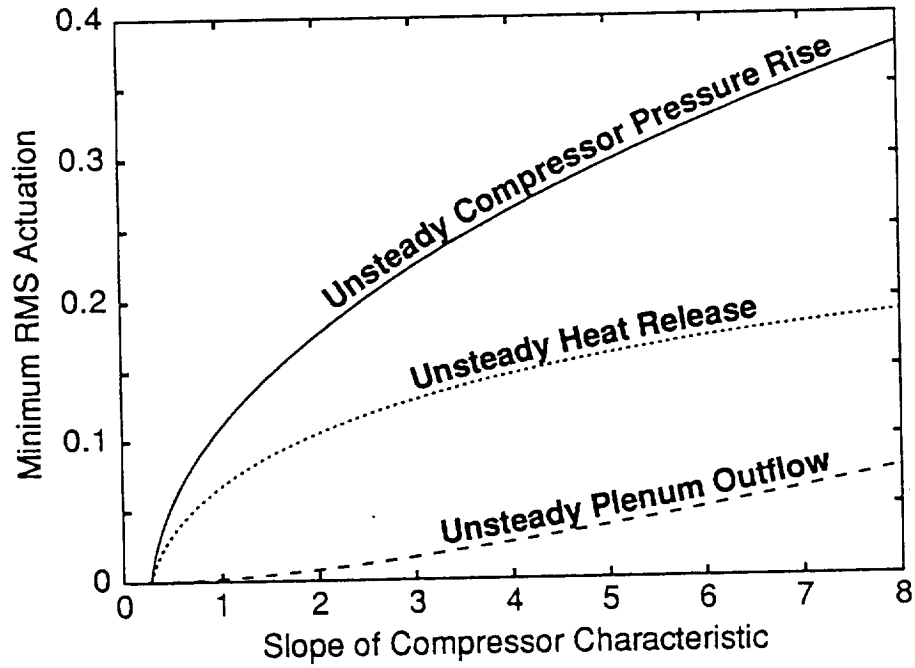

Figure 6-4: Influence of compression system disturbance type on actuator motion; close-coupled valve, $B = 2$

Chapter 7

Close-Coupled Control

The analysis of Chapter 6 indicates that close-coupled control schemes, i.e., measurements and actuation in close proximity to the compressor, appear to be the most promising generic strategy for this class of systems. Further investigation of this specific approach is therefore warranted. This chapter presents analytical and experimental results for a particular implementation in which a valve close-coupled to the compressor serves as the actuator and a hot wire anemometer in the compressor duct is used as the sensor.

The chapter is organized into two main sections. The first considers some theoretical aspects of close-coupled stabilization and shows that there are benefits to stabilizing the system using a feedback controlled valve as opposed to a simple flow restriction. In the second section, the results of close-coupled stabilization experiments are presented and compared with theory.

7.1 Close-coupled Control Theory

7.1.1 Introduction

As discussed in Chapter 6 the compression system will be linearly stable at any operating point where the slope of the compressor pressure-rise characteristic (pressure-rise as a function of flow) is negative. The basic mechanism for close-coupled stabilization using a close-coupled valve is conceptually straightforward, the valve in series with the compressor effectively forms an equivalent compressor whose pressure-rise characteristic is is negative at the desired operating point so that the overall system is stable. Stabilization can be accomplished using either a valve whose area is modulated in response to measured flow perturbations or with a fixed flow restriction, i.e., with or without feedback, respectively. These two approaches are illustrated schematically in Figure 7-1, which shows, for both cases, the compressor characteristic, valve characteristic, and combined characteristic which is negatively sloped at the operating point. In the case of the feedback controlled valve, a family of dashed curves is shown representing the valve pressure-drop characteristics corresponding to a range of fixed valve areas. The feedback control adjusts the instantaneous valve area according to the measured flow rate resulting in the solid curve which is identified in the figure as the valve characteristic with feedback.

7.1.2 Pressure-drop Penalty With and Without Feedback

As suggested by Figure 7-1, the pressure loss across the valve required for stabilization can be reduced using feedback and this possibility will now be investigated. Consider

the basic closed-loop characteristic equation for a compression system with a close-coupled valve actuator and compressor duct mass flow measurement (see Chapter 6):

$$s^2 + (1/(Bm_T) - B(m_C - m_{V_c}) - BK(s)v_c)s + (1 - (m_C - m_{V_c})/m_T + K(s)v_c/m_T) = 0 \tag{7.1}$$

In Equation 7.1, B is the Greitzer B parameter, $K(s)$ is the transfer function of the compensator (not necessarily the constant gain of Chapter 6), m_C is the slope of the compressor pressure rise characteristic, m_{V_c} and m_T are the slopes of the close-coupled valve and throttle pressure drop characteristics and v_c is the valve sensitivity (change in non-dimensional pressure drop per unit change in valve closure). With the exception of m_C all of these coefficients will always be positive.

Close-coupled Stabilization Without Feedback

For stability all the coefficients of the characteristic equation, Equation 7.1, must be positive. This could be accomplished with no feedback at all (i.e., $K(s) = 0$) if $m_{V_c} > m_C$ that is, if the slope of the pressure-drop versus flow characteristic of the close-coupled valve is steeper than the positively sloped pressure-rise versus flow characteristic of the compressor. However, such a stabilization mechanism has an associated cost because the slope of the valve pressure-drop characteristic is directly related to the pressure loss across the valve. For an incompressible flow:

$$\Psi_v = C(\alpha_c)\phi_v{}^2, \tag{7.2}$$

where $C(\alpha_c)$ is a fixed constant for any particular valve opening which depends upon the particular geometry and piping arrangement for the valve. The slope and pressure drop across the valve are thus related by:

$$m_{V_c} = 2\Psi_v/\phi_v \tag{7.3}$$

which is independent of the valve coefficient $C(\alpha_c)$ and cannot be modified by changing the valve design. The use of a close-coupled valve not augmented by feedback control therefore has associated with it an unavoidable pressure loss penalty given by:

$$\Psi_v \geq \phi_c m_C/2 \tag{7.4}$$

which is obtained from Equation 7.3 and the stability requirement, $m_{V_c} > m_C$.

Close-coupled Stabilization With Feedback

Now consider the situation when the valve area is modulated in response to the measured flow using a proportional feedback. In this case, from Equation 7.1, it is sufficient for stability that,

$$m_C - (m_{V_c} + Kv_c) > 0, \tag{7.5}$$

so that the valve slope, m_{V_c}, required for stabilization may be reduced by increasing the proportional gain, K. The pressure loss across the valve required for stabilization as given by Equation 7.3, is accordingly reduced. The use of feedback is thus seen

to reduce the required pressure drop required for stabilization. The sum, $m_{v_c} + Kv_c$ appearing in Equation 7.5 can be interpreted as the slope of the effective pressure drop characteristic of the feedback controlled valve. Thus, as depicted schematically in Figure 7-1, the effective pressure-drop characteristic of the feedback controlled valve can have a steep slope at the desired operating point with very little steady state pressure-drop.

Pressure Drop Penalty With Feedback

Ideally, the required steady state pressure drop across the control valve could be made arbitrarily small by sufficiently increasing the gain. For several reasons, in practice, some drop across the valve will be required. First, in order for the valve to be able to produce pressure perturbations which act to accelerate as well as decelerate the duct flow it must be able to both open and close slightly from its equilibrium operating point. This requires some amount of valve closure and corresponding steady state pressure loss. The actual amount required depends upon both the proportional gain and on the level of disturbances which must be counteracted, and is therefore application dependent.

The second factor which may necessitate some steady-state pressure-drop across the control valve is that there are inevitably additional dynamic elements in any real system. The effects of these dynamics are not accounted for in Equation 7.1, which indicates that any slope can be stabilized by making the gain sufficiently large. In reality, it is not possible to make the gain arbitrarily large without eventually experiencing instability. On the other hand, if the gain is too small the system

will also be unstable. As a result, there will generally be some maximum value of the equivalent compressor slope, $m_{C_e} = m_C - m_{V_c}$ which can be stabilized. This is discussed in Chapter 6 and such maximum values of equivalent slope are plotted in Figure 6-2 in which additional dynamics, represented by a low-pass filter, are included in the calculation. Let the maximum equivalent compressor slope which can be stabilized with the proportional control in the presence of the additional dynamics be denoted, $\tilde{m_{C_e}}$. If $m_C > \tilde{m_{C_e}}$ the system can still be stabilized but only by increasing m_{V_c} so that $m_C - m_{V_c} < \tilde{m_{C_e}}$ which in turn requires some steady-state pressure drop across the valve.

7.1.3 Optimal scheduling

As discussed above, at any given operating point, with or without feedback, there will be some minimum pressure-drop required for stabilization. If the compressor is to be stabilized over a range of flows it will, therefore, be desirable to schedule the mean valve opening with operating point so as to provide only the minimum pressure-drop required for stability. This will be referred to as the optimal scheduled valve area. Since the use of feedback reduces the valve pressure drop requirement, the optimal scheduled valve area will be different depending on whether or not feedback is used. In the following sections, numerical calculation of the optimal schedules will be considered both with and without feedback.

Optimal Schedule Without Feedback

We now obtain an expression for the minimal valve pressure drop required to stabilize the system with no feedback. With no feedback, the stability requirements are, from Equation 7.1:

$$\frac{1}{Bm_T} - Bm_{C_e} > 0 \tag{7.6}$$

$$1 - \frac{m_{C_e}}{m_T} > 0, \tag{7.7}$$

where, by definition, $m_{C_e} = m_C - m_{V_c}$. We assume that it is Equation 7.6 which is the more restrictive. Equation 7.6 can be rearranged to obtain the maximum stable value of m_{C_e} as,

$$m_{C_e} < \frac{1}{B^2 m_T} \tag{7.8}$$

For an incompressible flow through the throttle $m_T = 2\psi_p/\phi_t$, where ψ_p is the plenum pressure and ϕ_t is the flow through the throttle. At equilibrium $\psi_p = \Psi_c - \psi_v$, where Ψ_c, and ψ_v are the compressor exit pressure and valve pressure drop respectively and $\phi_c = \phi_t$. Making these substitutions Equation 7.8 can be written as:

$$m_{C_e} < \frac{\phi_c}{2B^2(\Psi_c - \psi_v)} \tag{7.9}$$

From Equation 7.9, the maximum stable slope with no pressure-drop across the valve is then given by

$$m_C < \frac{\phi_c}{2B^2\Psi_c}. \tag{7.10}$$

If the compressor slope is small enough to satisfy Equation 7.10 the optimal valve area is therefore fully open. For steeper compressor slope some loss across the valve is required. Assuming incompressible flow through the valve so that $m_{V_c} = 2\psi_v/\phi_c$, and using Equation 7.9 we find the stability that at the stability boundary, m_{V_c} satisfies the quadratic equation:

$$m_{V_c}{}^2 - (m_C + 2\Psi_c/phic)m_{V_c} + (2\Psi_c m_C/\phi_c - 1/B^2) = 0. \tag{7.11}$$

We are interested in cases where some pressure drop across the valve is required from stabilization, so from Equation 7.10, $2\Psi_c m_C/\phi_c - 1/B^2 > 0$. Using this fact it is relatively straightforward to show that Equation 7.11 has two real, positive roots. Since we are interested in the minimal stabilizing pressure drop, we choose the smaller of the two roots, which we will denote by $\tilde{m}_{V_c}$. The minimum pressure drop is then calculated using,

$$\psi_v = \tilde{m}_{V_c}\phi_c/2. \tag{7.12}$$

Using this value for the valve pressure drop, the required valve area can then be calculated, with the specific relationship to be used dependent upon the particular valve geometry.

Optimal Scheduling With Feedback

It will not generally be possible to obtain a closed form solution to determine optimal scheduling with feedback and so a numerical procedure must be implemented. The following approach was taken here to determine the minimal stabilizing pressure drop

and corresponding valve area at a given operating point.

1. Using a polynomial curve fit for the compressor characteristic, calculate the compressor pressure rise and compressor slope at the desired flow coefficient.

2. Enter a loop in which the valve pressure-drop is incremented starting with zero pressure drop. Inside this loop the following steps are taken:

   (a) The plenum pressure and resulting slope of the throttle characteristic are determined.

   (b) The linear system, A,b,c matrices describing the compression system dynamics are calculated.

   (c) The compression system model is augmented with a linear system model for the actuator dynamics.

   (d) The resulting system is tested to determine if there is any stabilizing gain. The algorithm described by [28] was implemented as a Matlab routine for this purpose.

   (e) If there is no stabilizing gain the valve pressure drop is incremented and the loop is repeated.

7.1.4 An Illustrative Example

The preceding theory will now be illustrated with an example in which the optimal scheduled valve areas are calculated with and without feedback using the compressor characteristic for the Holset Model H1D turbocharger described in Chapter 2. The

positively sloped portion of the characteristic was experimentally measured by using a close-coupled valve without feedback to stabilize the system.

For the example, a system B parameter of 2 was used and the actuator dynamics were represented by a second order, low-pass Butterworth filter, as in Chapter 6. The -3dB cutoff frequency of this filter was set to ten times the Helmholtz frequency of the compression system. The compressor tip Mach Number was 0.76. The flow through the close-coupled valve was assumed to be incompressible and the total pressure loss through the valve, which dumped directly into the plenum, was taken as 1.98 times the dynamic pressure based upon the minimal valve area. This value was based upon empirical data obtained for the valve used in the experimental facility.

Optimal Scheduled Characteristics

The resulting optimal scheduled performance with and without feedback for this illustrative example are shown in Figure 7-2. The figure shows net pressure-rise for the compressor/valve combination as a function of flow coefficient for three cases: 1) Following the optimal valve area schedule without feedback; 2) following the optimal valve area schedule with feedback; and 3) with the valve fully open (compressor alone).

The vertical distance from the compressor alone characteristic to either of the optimal characteristics represents the minimal required valve pressure drop for stabilization. The figure shows the basic benefit of using feedback; the requisite pressure drop is decreased and the resulting delivery pressure of the stabilized system is therefore higher. For this particular case it can be seen that, with feedback, essentially zero pressure-drop across the valve is required for flow coefficients from approximately

0.135 (the natural surge point) down to 0.08. In this range the compressor slope is less than the maximum stabilizable slope and all the stabilization is accomplished using feedback. (Some additional pressure drop would be required depending on the disturbance level as discussed in Section 7.1.2.) At lower flow coefficients the compressor slope increases and some pressure-drop must be taken across the feedback controlled valve in order to stabilize the system. The corresponding optimal valve area and gain as a function of flow for the feedback controlled valve are shown in Figure 7-3 and Figure 7-4 respectively. These figures show that the optimal valve area and gain are highly nonlinear functions of flow, and thus a purely linear control scheme cannot be used if the optimal performance is to be obtained. The system implementation could, however, be split into a linear and nonlinear portion. A linear proportional control would act on a high pass filtered flow measurement signal (ac coupled) which provide an indication of the rapid flow perturbations, and a nonlinear control would act on a low-pass measurement of the flow to slowly adjust valve area and gain to follow the optimal schedules shown in Figure 7-3 and 7-4. It is noted that a large part of the nonlinearity in the optimal gain is due to the particular valve geometry used here in which the valve area varied linearly with valve angular position. This valve geometry results in a valve whose per unit change in pressure drop, per unit change in angular position, varies significantly with the nominal valve area. As a result, the proportional gain of the controller must vary to maintain a constant overall loop gain. By properly tailoring the valve geometry it may be possible to maintain a constant gain, thereby simplifying the implementation.

Effect of Flow Rate

It is interesting to examine the effect of changes in mean flow rate on the optimal scheduled performance. To do this, the optimal scheduled performance was recalculated using a new compressor characteristic obtained by shifting the previous compressor characteristic so that corresponding points would occur at a higher flow. That is, the new compressor characteristic, $\Psi_c'(\phi_c)$ is given by:

$$\Psi_c'(\phi_c) = \Psi_c(\phi_c - \Delta\phi_c), \tag{7.13}$$

where Ψ_c is the original compressor characteristic and $\Delta\phi_c$ is the shift. The optimal characteristics for the original characteristic and the shifted characteristic are compared in Figure 7-5, for $\Delta\phi_c = 0.15$. Comparing the requisite valve pressure drop with and without feedback for the low and high flow cases, it can be seen that, all else being equal, the benefits of using feedback are greater for a compressor whose characteristic has steep positive slope at higher flow coefficients. This can be understood by considering that for the same compressor slope, the pressure drop required to stabilize the system without feedback increases directly with flow coefficient, as shown by Equation 7.4, while over a substantial range of flows a negligible amount of pressure drop is required for the feedback controlled valve.

7.2 Close-coupled Stabilization Experiments

7.2.1 Description of Tests

A discrete time (digital) proportional control was implemented which commanded the close-coupled valve area to be directly proportional to the mass flow at the compressor duct inlet (mass flow was derived from a constant temperature anemometer sensor). The control implementation is described in Chapter 2. The system was tested over a range of values of proportional gain in order to determine the optimal value to minimize the control valve pressure losses. The tests were conducted holding the tip Mach number, M_T (or equivalently corrected speed) constant. A value of $M_T = 0.76$ was used for all tests.

The same basic testing procedure was used for each gain setting. The operating point was first set by adjusting the area of the throttle valve located at the plenum exit. throttle The open area of the close-coupled valve was then gradually adjusted in order to stabilize the compressor with the minimum amount of pressure loss across the close coupled valve. After each small change in close-coupled valve area the turbine supply pressure would be adjusted to keep the compressor speed constant. Once the maximum stable valve opening was established, the time mean operating point data would be measured. The plenum exit throttle would then be closed slightly and the process would be repeated. This procedure was continued (that is operating points with gradually decreasing flow were measured) until the system could no longer be stabilized for any close-coupled valve area. With feedback, the system can not always be stabilized simply by reducing the area of the close-coupled valve. As the valve

is closed beyond a certain point, a high frequency instability develops, and when it is opened too much the system also goes unstable. At the limiting flow there is no longer any range between these two settings, that is any further closure or opening of the valve results in instability.

7.2.2 Experimental Results

The results of the close-coupled experiments are shown in Figure 7-6 which plots the total to static pressure rise characteristic of the compressor in combination with the close coupled valve for a range of gain settings. Data points with the same gain are connected by straight lines. As described in the test procedure, each data point represents the maximum stable output pressure which could be obtained for a given gain and flow coefficient. For reference, the total to total characteristic of the compressor alone is also plotted in Figure 7-6. We are primarily interested in the optimum scheduled performance with and without feedback (see Section 7.1.2) as indicated in Figure 7-6 by the solid curves which have been fared in to form upper and lower bounds respectively for the experimental data. The figure shows that, as expected from the theory, the pressure-drop across the close-coupled valve required for stabilization can be decreased by using feedback, thus providing higher output pressure over the stabilized range of flows.

7.2.3 Comparison with Theory

It is of interest to compare the experimental results directly with theory. In order to make this comparison, an analytical model representing the actuator dynamics for the experiment is required. For these purposes, we include all the dynamics from the analog input to the computer to the actual position of the valve in one overall transfer function representing the actuator dynamics. The frequency response of this transfer function was measured with an HP3582A spectrum analyzer using a broadband drive signal. A fifth order, (five pole, four zero) transfer function was then fit to this data. This was found to be the lowest order model which could adequately represent the measured response. Both the experimentally measured frequency response and the response of the transfer function used to fit this data are shown in Figure 7-7, which shows that the actuator system has a natural frequency, as indicated by the peak in the magnitude characteristic, at approximately ten times the Helmholtz frequency. Using this model for the actuator dynamics and the model for the compression system, the theoretical optimal scheduled performance could be determined with and without feedback as described in Section 7.1.2. The compression system model was based upon the known geometry of the system and a polynomial fit to the measured steady state compressor characteristic. The quasi-steady compressor model (see 3 was used here.

The resulting theoretical optimal scheduled performance and experimental data are shown in Figure 7-8. The curves indicating the theoretical optimal scheduled performance with and without feedback should bound the envelope of the experimen-

tal data. This is the case, indicating good agreement with theory, from the natural surge point at $\phi_c = 0.135$ down to roughly $\phi_c = 0.085$. Below this flow theory and experiment deviate both with and without feedback.

The fact that the experimental data departs from the theory even without feedback indicates that the discrepancy cannot be solely due to inaccurate modeling of the actuator or feedback system and we therefore turn attention to the open loop compression system model. It is thought that this discrepancy arises primarily as a result of unsteady compressible (organ pipe) behavior in the compressor duct, and in particular, the 0.3(m) section of duct between the compressor exit and the close-coupled valve. The model assumes that the flow in the compressor duct is one dimensional, and incompressible so that the compressor along with its upstream and downstream ducts may be represented using a lumped element element model. For this assumption to be valid, the acoustic time scale, that is the amount of time required for an acoustic wave to propagate down the length of the duct, should be small with respect to the growth rate of the instability. We will call the ratio of these two time scales, the reduced frequency; for model validity the reduced frequency should be much less than unity. The reduced frequency was calculated as a function of flow coefficient for both the inlet duct, (bellmouth inlet to compressor face) and exit duct (compressor exit flange to close-coupled valve) and the results are plotted in Figure 7-9. For both ducts the reduced frequency increases as the flow rate decreases. This is to be expected because at lower flows, the positive slope of the compressor characteristic becomes steeper and we would expect that the growth rate of the instability would increase and with it the reduced frequency. The reduced frequencies for the upstream duct are

higher because the upstream duct is longer. There is a prominent knee in both the curves (discontinuity in the slope), at approximately $\phi_c = 0.85$, which corresponds to the flow at which the theory and experiment begin to deviate, and the reduced frequencies increase rapidly below this flow coefficient. The knee occurs as a result of a change in the nature of the instability which transitions from an undamped sinusoid (complex conjugate poles in the right half complex plane) to a pure exponential growth (real poles in the right half plane) at $\phi_c = 0.085$. as shown in Figure 7-10 in which the real and imaginary part of the open loop compression system poles are plotted as a function of flow coefficient. The basis of the close-coupled theory is that there is no mass storage between the compressor and the close-coupled valve so that the characteristics of these components can be added together. Thus it is the validity of the lumped assumption for the exit duct which is of primary concern, which in turn requires that the reduced frequency be much less than unity. For flow coefficients greater than 0.085, where agreement with theory was good, the figure shows that the reduced frequency based upon the downstream duct is less than 0.1., below this flow the reduced frequency increases rapidly as the system instability transitions to pure a pure exponential growth. It thus appears likely that the deviation between theory and experiment at lower flow coefficients is in large part due to unsteady compressible effects in the downstream duct.

Because the flow sensor was located at the bellmouth inlet, while the close coupled valve was located downstream of the compressor, the effects of mass storage in the inlet duct also become quite important when the feedback control is used. Thus the fact that the reduced frequency of the upstream duct which approaches unity

at $\phi_c = 0.085$ suggest that the performance of the system with feedback would be improved by collocating the actuator and sensor immediately at the compressor exit.

7.3 Summary

An analytical and experimental investigation has been made into the use of a particular stabilization scheme in which measurements of compressor mass flow are fedback to adjust the area of a valve close-coupled to the compressor exit. The results are summarized as follows:

- It has been shown that theoretically a compression system can be stabilized using a close-coupled valve either with or without feedback. The pressure-drop across the control valve required for stabilization can be reduced, however, by using feedback, thus providing higher delivery pressure over the stabilized range.

- Ideally, with feedback, no pressure-drop is required across the close-coupled valve. Practically, some pressure-drop is required due to finite disturbances, and limitations on controller gain, and bandwidth.

- A feedback controlled close-coupled valve has been implemented on a radially bladed, centrifugal compressor and it has been experimentally demonstrated that system can be stabilized using less pressure-drop with feedback over a wide range of flows.

- Good agreement with theory was found when the theoretical growth rate of instability was consistent with the lumped parameter modeling assumptions for

compressor duct.

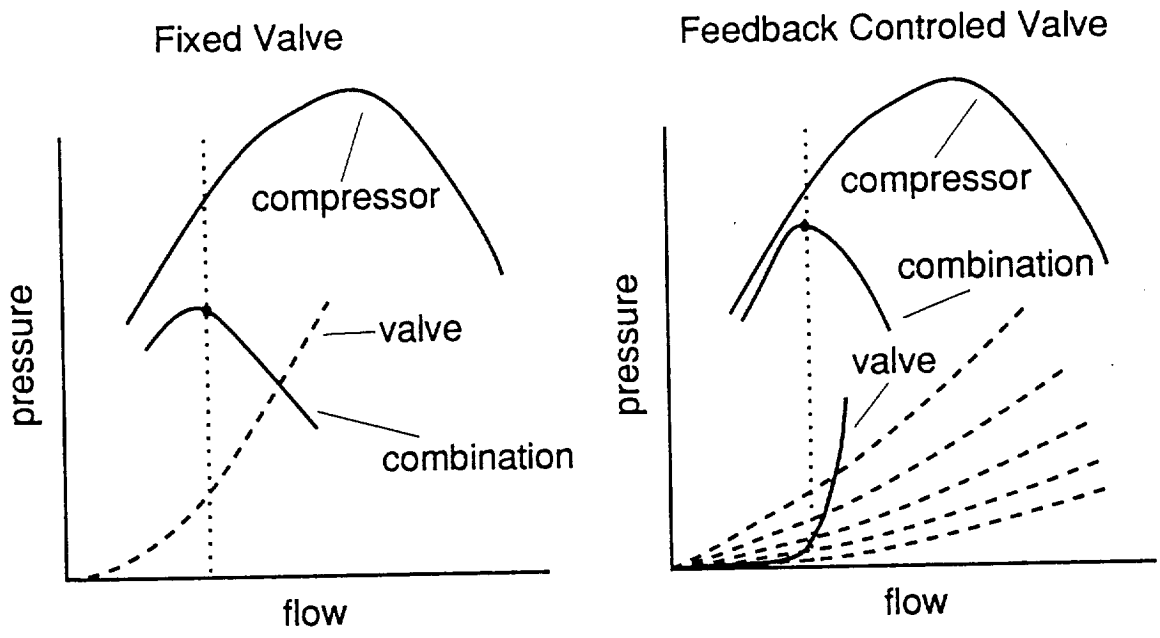

Figure 7-1: Close-coupled stabilization with fixed valve and with feedback controlled valve (schematic)

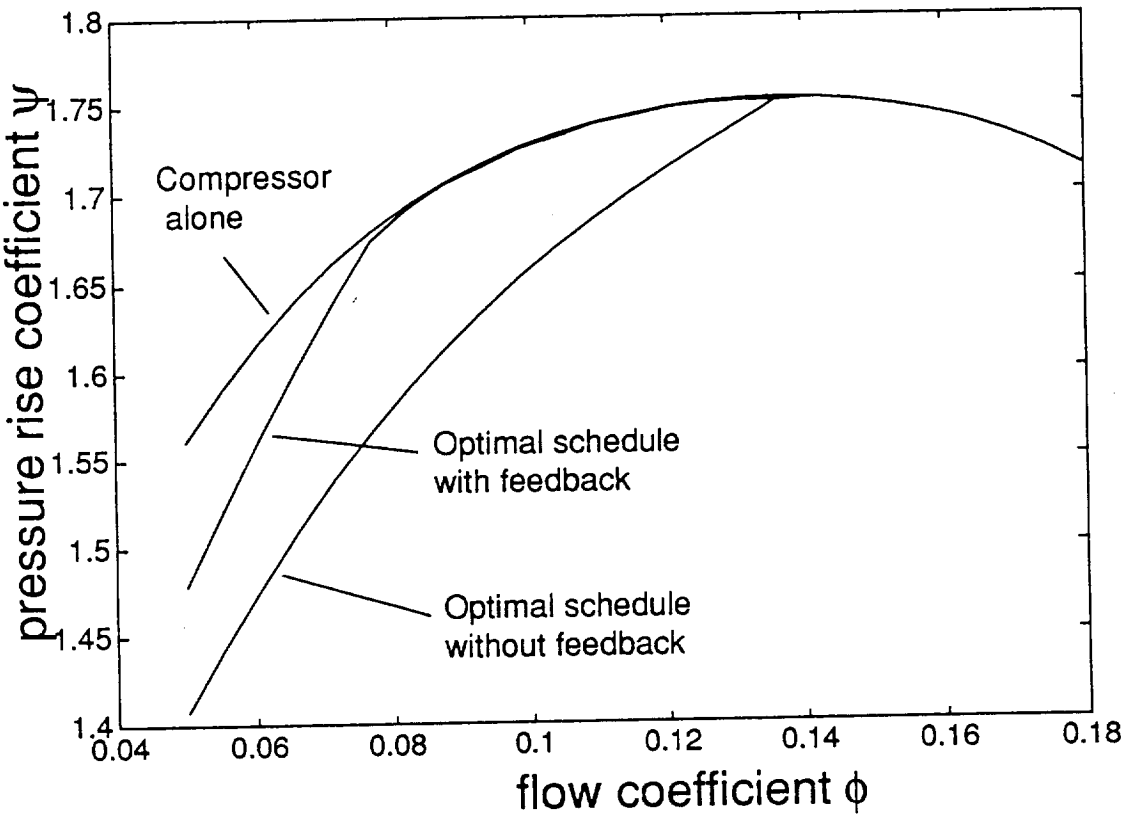

Figure 7-2: Optimal scheduled performance with and without feedback for illustrative example

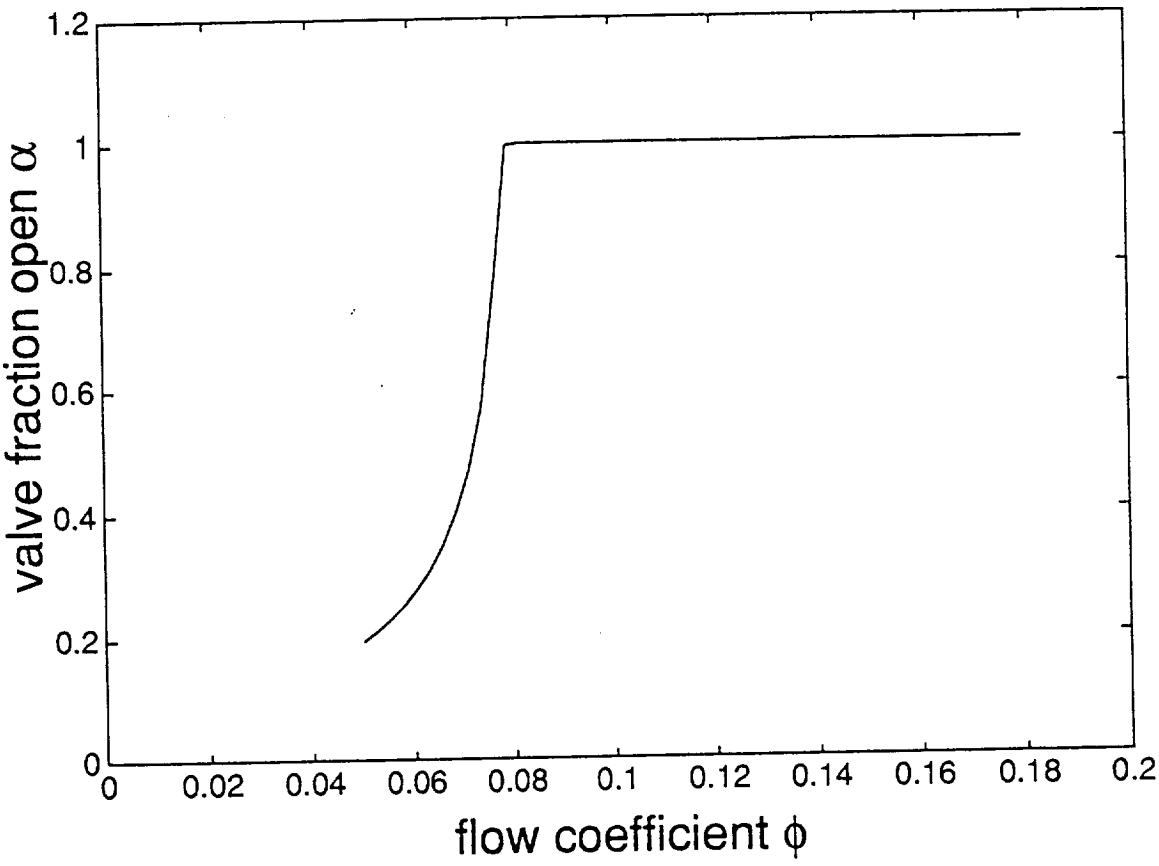

Figure 7-3: Optimal scheduled valve area as a function of flow for illustrative example

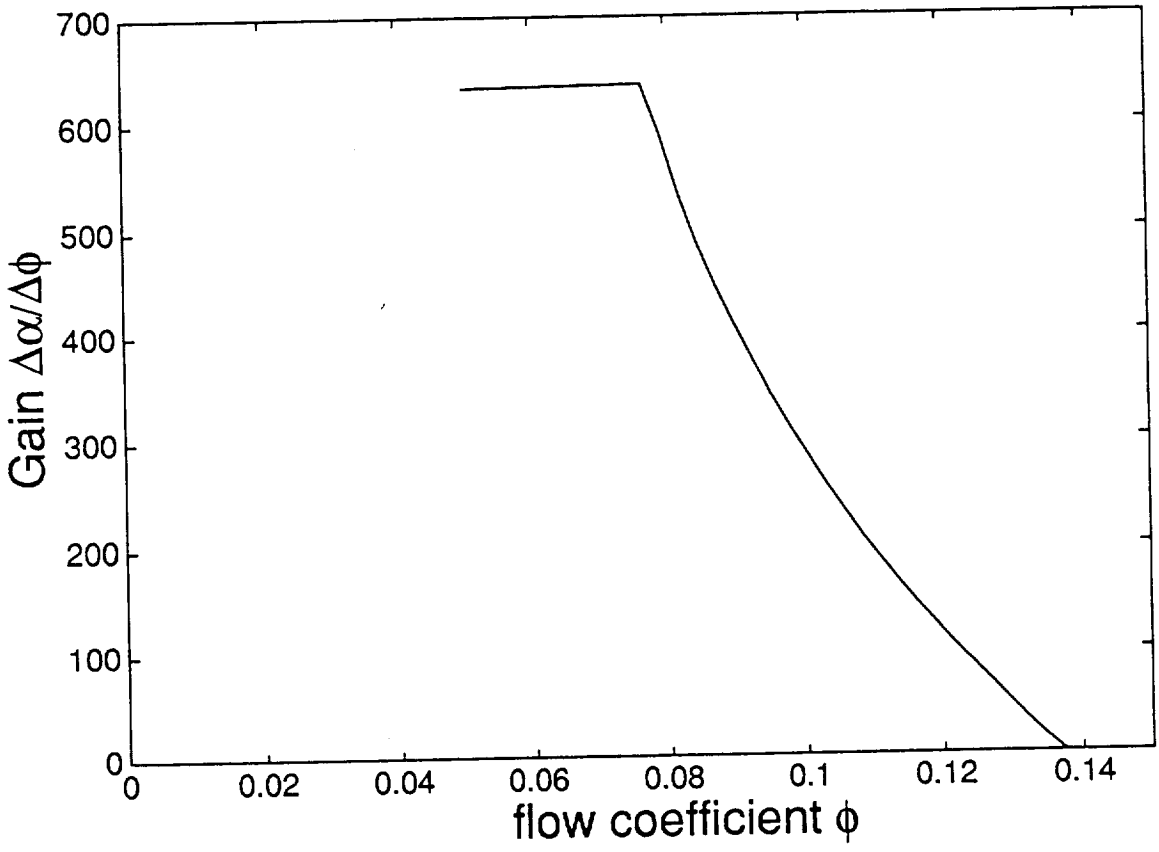

Figure 7-4: Optimal scheduled proportional gain as a function of flow for illustrative example

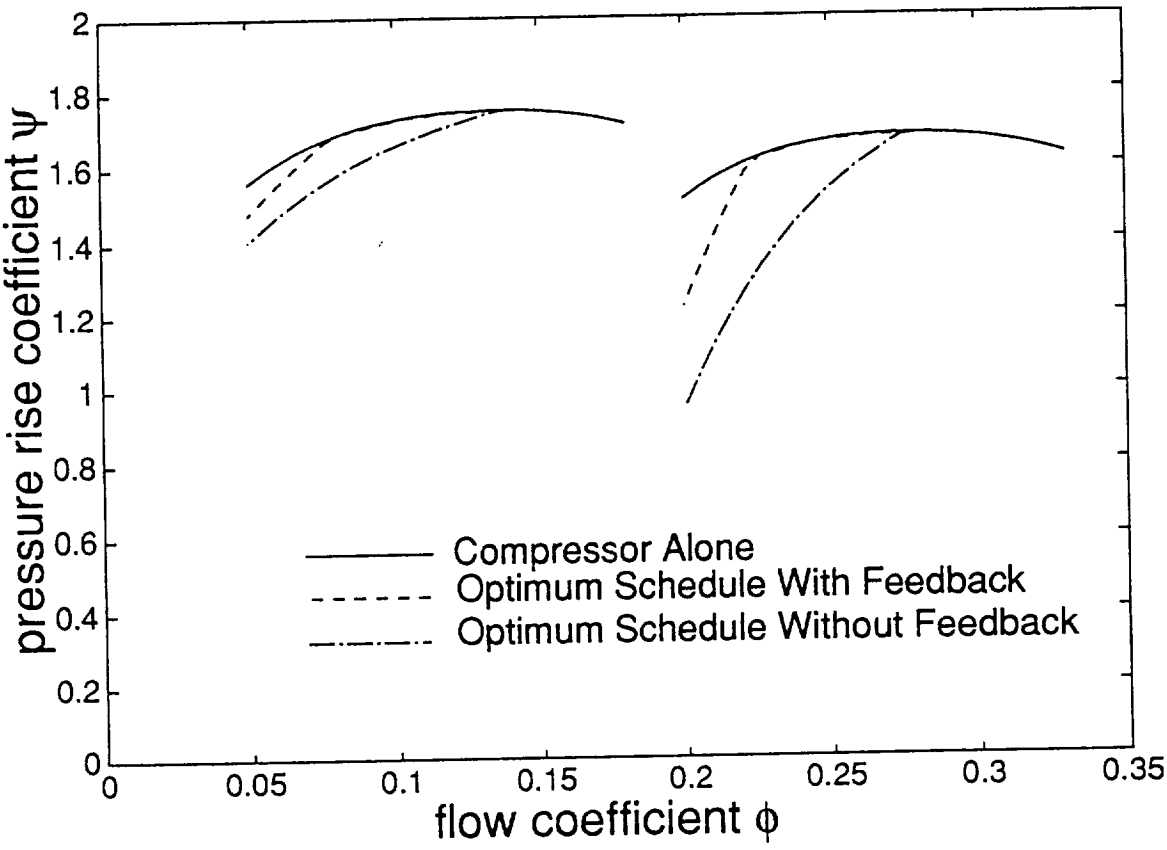

Figure 7-5: Effect of flow rate on optimal scheduled performance similar compressor characteristics

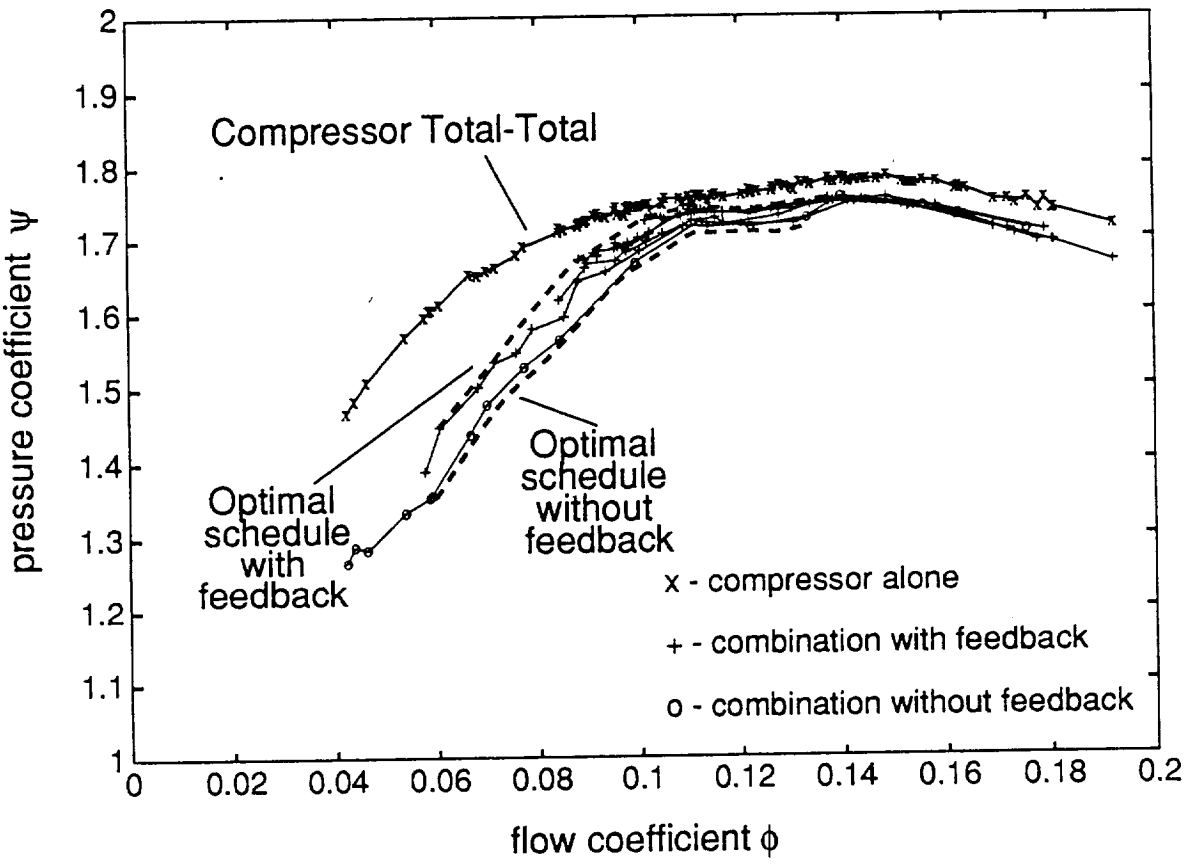

Figure 7-6: Close-coupled stabilization experimental results

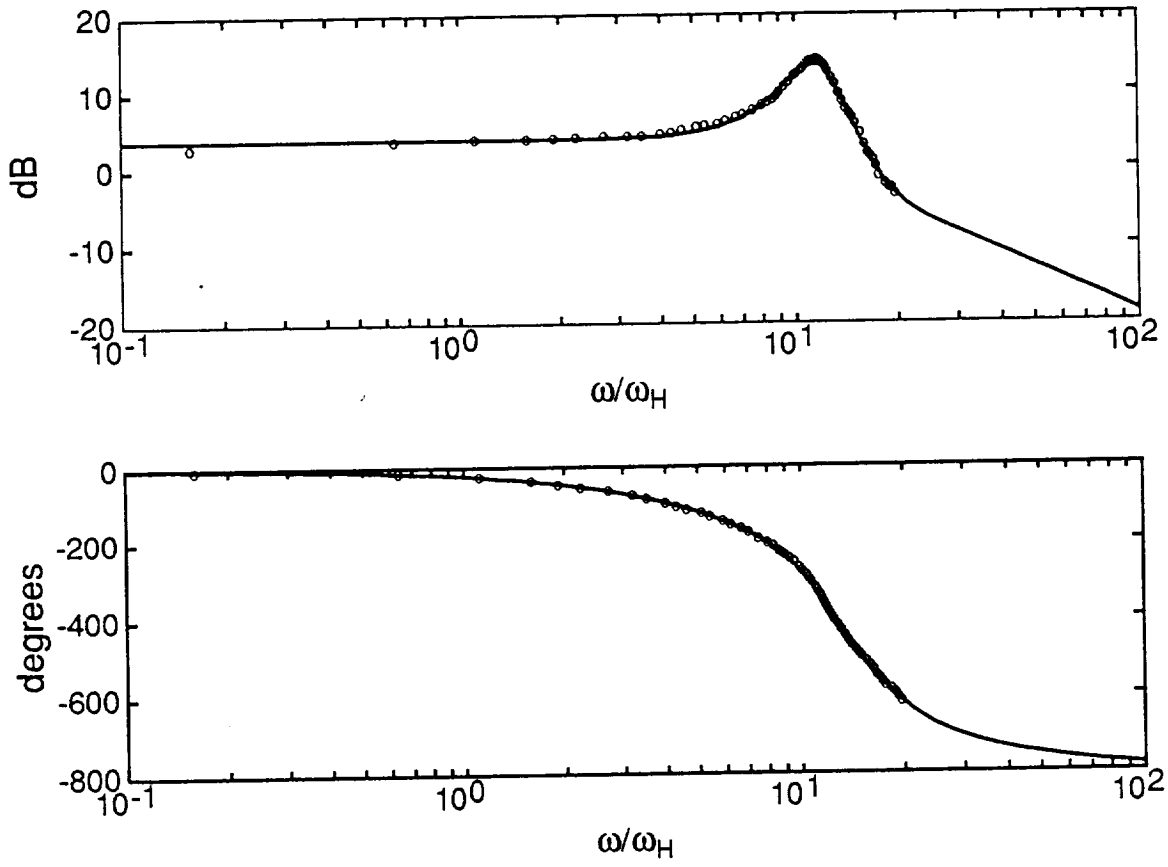

Figure 7-7: Bode plot of experimentally measured transfer function representing actuator dynamics showing fit to fifth order model

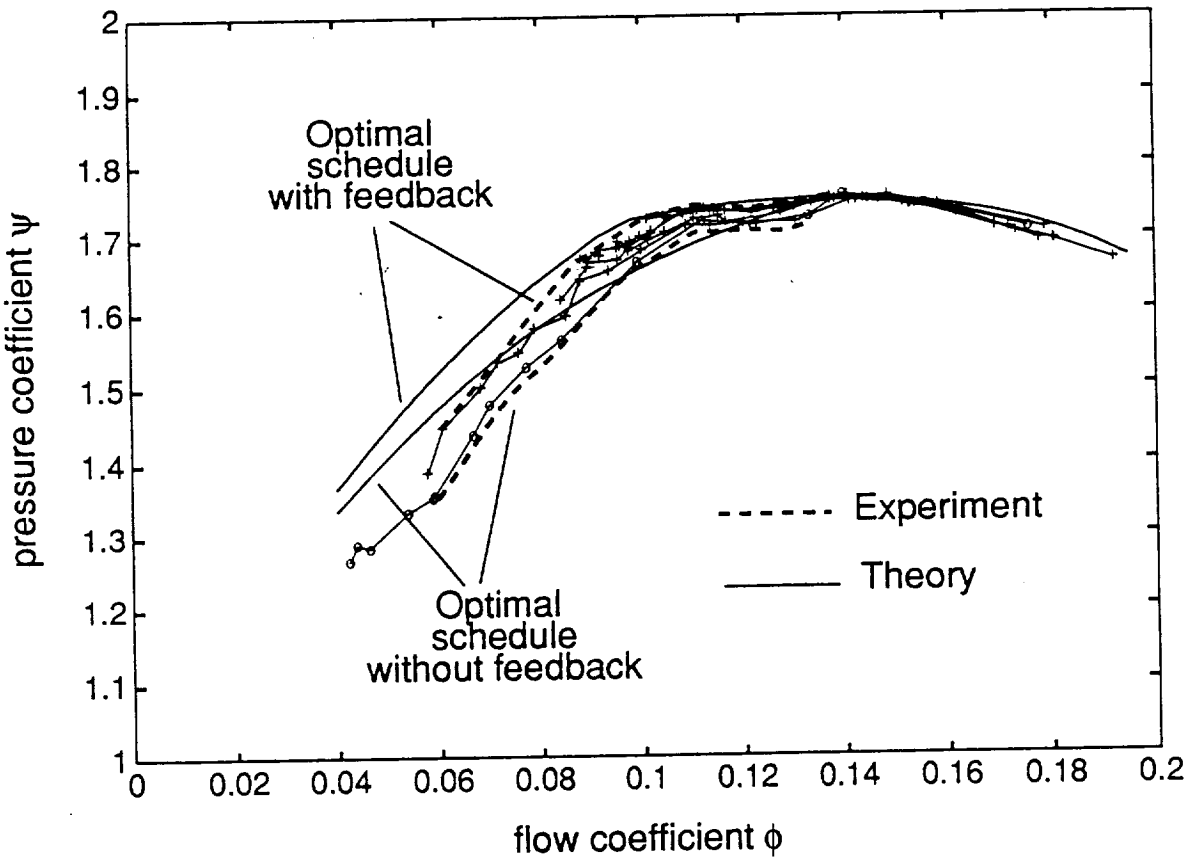

Figure 7-8: Comparison of close-coupled experimental results with theory

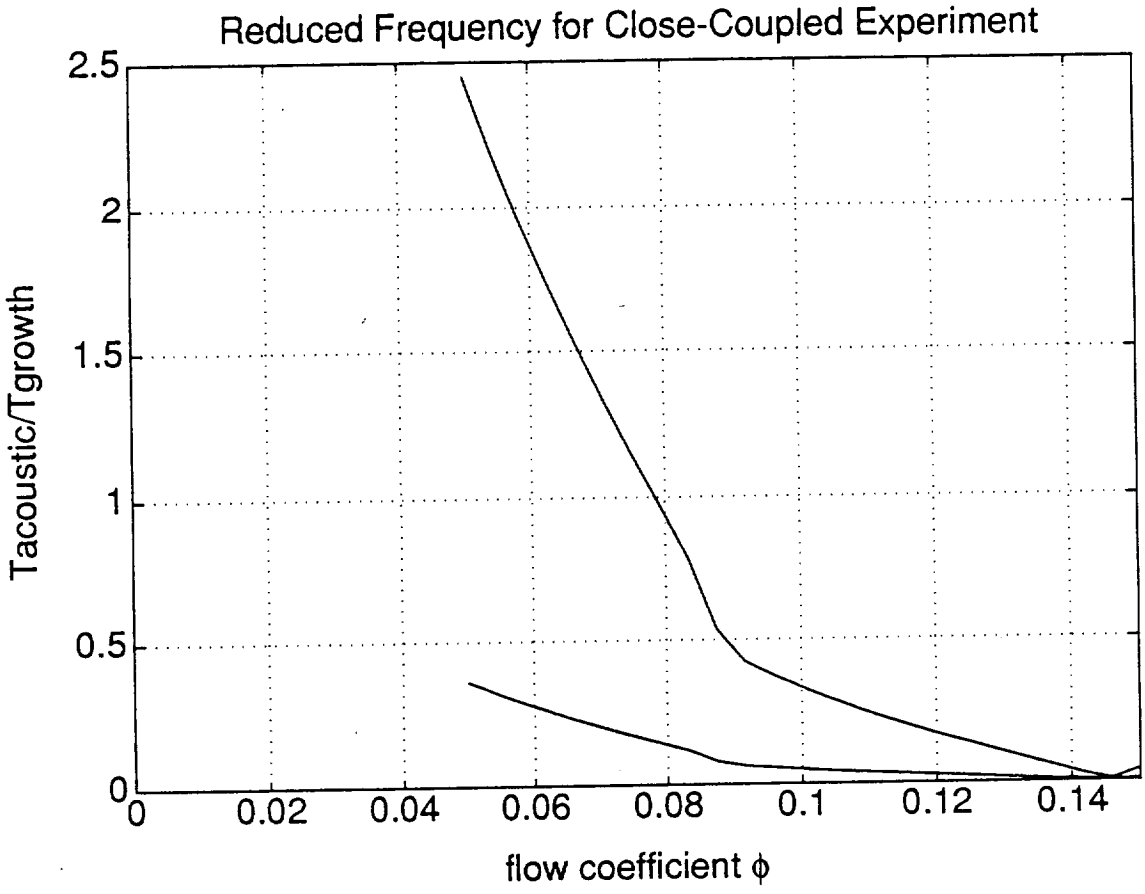

Figure 7-9: Reduced frequency as a function of flow rate for ducts in experimental apparatus

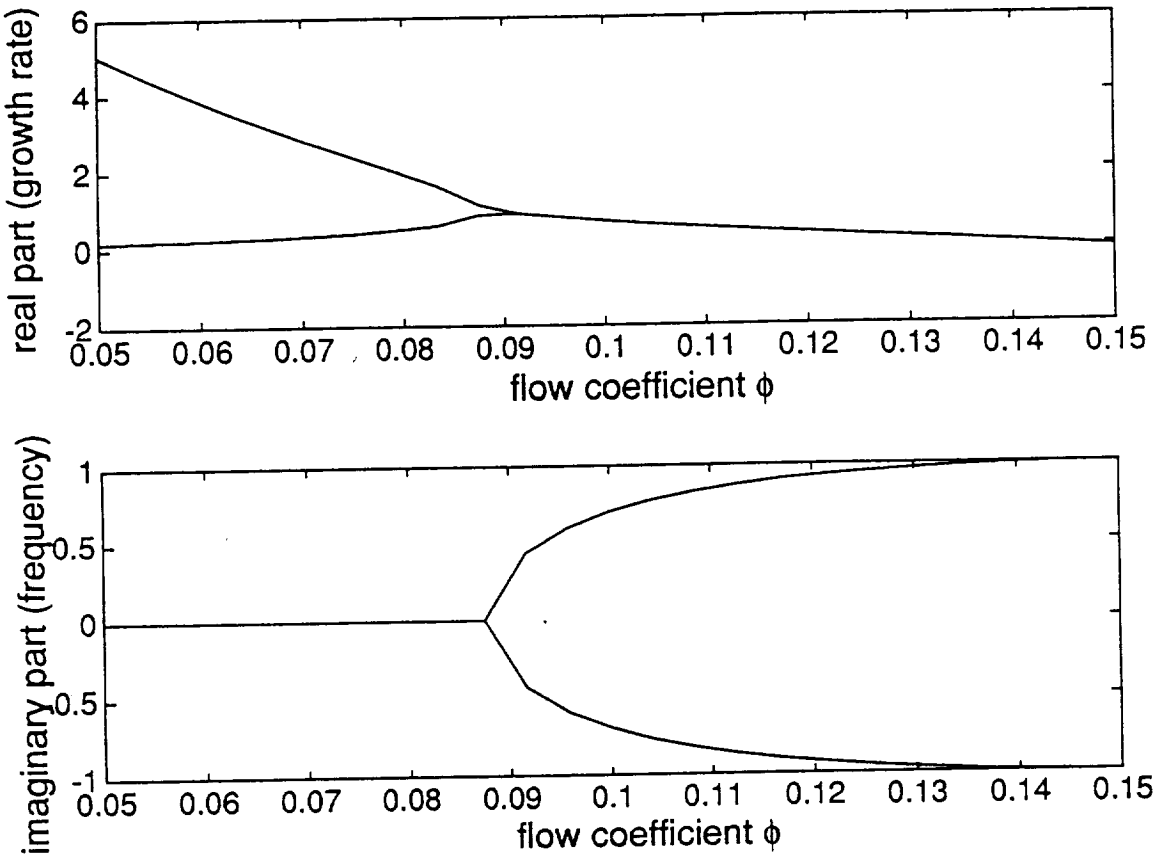

Figure 7-10: Open loop compression system pole location as a function of flow coefficient

Chapter 8

Summary and Conclusions

An in depth study of the use of feedback stabilization to prevent surge in compression systems has been carried out. While previous compressor stabilization studies have focused on particular implementations and experimental proof of concept, the work reported here has been directed towards obtaining a fundamental understanding of the problem. In this chapter, the approach taken is first briefly summarized and then specific conclusions are provided.

8.1 Summary

The sinusoidal frequency response of a radial bladed centrifugal compressor was experimentally measured over a wide range of equilibrium operating points. The resulting transfer functions were analyzed and used to validate a simple, lumped element dynamic model of the compressor. This model includes the dynamic effects of fluid inertia but assumes that the pressure rise and flow through the compressor are alge-

braically related by the steady-state characteristic of the compressor. This is referred to as the quasi-steady assumption.

Improvements in the model obtained by relaxing the quasi-steady assumption were also examined. In particular it was assumed that flow development process can be accounted for by a simple first order time lag between the instantaneous and steady-state pressure losses occurring in the flow passages.

Much indirect support for the use of these types of simple component models for the compressor has previously been provided by the adequacy of overall compression system dynamic models which incorporated them. However, there has been very little unambiguous data and comparison with theory previously reported. The experimental results which have now been obtained show that in fact such simple models provide a good representation of the compressor; the element which is fundamentally responsible for the overall compression system instability.

A second aspect of compression system modeling addressed in this thesis has been the development of overall system dynamic models which included a variety actuators and sensors of practical interest which had not been previously modeled. Development of these models in a form readily suitable for the analysis and design of control systems was of immediate utility in this thesis work for evaluating alternative control strategies and will also be beneficial to future researchers.

The concept of stabilizing a compression system to prevent surge is a new one and its ultimate practicality remains to be determined. As an important first step towards providing this assessment, some fundamental limitations to compression system stabilization were identified and methods were developed for quantifying their severity.

This problem was approached by determining the relevant and useful control theory and then appropriately adapting and applying it to obtain results for this class of systems. This is thought to represent the first such examination of the fundamental limitation to feedback stabilization of compression systems.

The study of fundamental limits to stabilization showed that the severity of such limitations, over the expected range of applications, could be greatly mitigated by proper actuator and sensor selection. The importance of proper actuator and sensor selection for this problem was further emphasized by the results of performing a first time, quantitative, side by side, comparison to assess the relative merits of a variety of potentially attractive actuation and sensing options.

The overall sensor actuator evaluation study and consideration of the basic system dynamics indicated that close-coupled sensing and actuation has the best potential for being an effective, generic, approach to compression system stabilization. A detailed analysis and experimental investigation into this approach was, therefore, carried out. Basic design trade-offs were identified and quantified parametrically and the underlying mechanism for close-coupled stabilization was presented.

A complete digital control and data acquisition system was designed and implemented on a representative compression system, in order to experimentally evaluate the close-coupled control concept. An I-80386 microprocessor based system, capable of implementing a linear, fourth order discrete time control algorithm at a 1KHz sampling rate, was developed for this purpose.

Using this system, experiments were conducted demonstrating the use of a close-coupled feedback controlled valve to extend the stable operating range of the com-

pression system.

8.2 Conclusions

On the basis of the analysis and experiments presented in this thesis the following specific conclusions have been reached:

- Experimental measurements show that the centrifugal compressor which was tested has a clearly defined sinusoidal transfer function which relates the response of the flow through the compressor to a differential pressure fluctuation applied across the compressor duct (ie., an admittance).
  - Comparison of model predictions with the experimentally determined frequency response shows that for control and design analysis purposes the compressor can be assumed to be operating quasi-steadily, with all dynamic effects due to the fluid inertia in the compressor flow passages.
  - The experimentally identified parameter values associated with the quasi-steady model are physically reasonable, indicating that both the model structure and assumed physics are consistent.
  - A simple unsteady loss model (the instantaneous pressure losses occurring in the compressor are related to the steady state losses by a first order lag) is useful for explaining observed departures from quasi-steady behavior which occur as the reduced frequency (based on flow through time) becomes non-negligible. In particular, the model provides a physically plau-

sible means of accounting for the apparent increase in equivalent length (a purely geometric parameter) with decrease in flow coefficient observed in a prior study [1].

- The experimental data shows that, as reduced frequencies approach unity, there is a substantial dependence of the real part of the compressor impedance (inverse admittance) with frequency. In particular, for a compressor operating on a positively sloped portion of its characteristic (a condition where open loop instability can occur) the real part goes from being negative to positive as the frequency increases. With the sign conventions assumed here, this shows that the system goes from being active at low frequencies to passive at high frequencies.

- The observed high frequency passivity, which is not predicted by the quasi-steady theory, is consistent with but not entirely accounted for by the simple unsteady loss model.

- The fact that the compressor becomes passive at high frequency indicates that, above some frequency, it would no longer act as a destabilizing element. Thus, this finding has the important implication that the quasi-steady model may be conservative in predicting control system bandwidth requirements.

- There are many actuator/sensor pairs available for which the basic compression system model is controllable and observable and the ability to nominally stabilize the system is generally not problematic. As a consequence, studies

which attempt to evaluate actuator sensor selection based upon their ability to nominally stabilize the system will provide little discrimination between the alternatives and are not recommended.

- For many applications of interest, bounded actuation and the performance penalties required in order to robustly stabilize the system against unavoidable high frequency modeling errors can be expected to severely restrict the ability to stabilize the system.

- The limitations imposed by bounded actuation and high frequency modeling errors are much more severe for some actuator/sensor combinations than others, so that proper choice of actuators and sensors will be essential for many applications.

- The non-dimensional slope, m_C, of the compressor characteristic and the value of non-dimensional B parameter have been shown to be key parameters dictating the fundamental difficulty of the stabilization problem and the range of options available. The compressor slope determines if the compressor is active or passive. If it is active (positively sloped), its ability to supply the unsteady power required to sustain an instability scales with the magnitude of the slope. The B parameter determines the amount of coupling between the compressor and the downstream components. Thus, as values of either of these parameters increase stabilization becomes more difficult.

- For many potential applications, where B and compressor slope can reasonably be expected to be relatively large, ($B > 1$, $m_c > 2$) only close-coupled control strategies which measure and act directly on the fluid in the compressor duct will be viable.

- Characterizing both the source and nature of the process disturbances acting on compression systems is important in determining the physical hardware requirements and expected range of stabilization of practical compression system stabilization schemes.

- The ability to stabilize a compression system using a servo controlled valve close-coupled to the compressor exit, with proportional feedback of compressor mass flow, has been experimentally demonstrated. The experiments verified theoretical predictions that the use of a high bandwidth feedback to modulate the valve allows the system to be stabilized with less steady-state pressure loss across the valve than would be required with a fixed valve (or one which is only slowly varied with operating point).

8.3 Suggestions for Future Research

There are a number of interesting questions and problems which were beyond the scope of this current research but should be be considered. These suggested areas of research are organized into two groups: those related to the specific problem of compression system stabilization and those which are more general problems in control theory.

8.3.1 Stabilization of Compression Systems

- With the results and findings reported here providing a starting point, a basic systems engineering study to determine the potential risks and benefits associated with the stabilization of compression systems for particular application areas would now be quite useful. The results of such a study could help both in assessing the extent to which this technology should be pursued and to target the applications where it has the greatest potential benefit.

- Either in conjunction with such a systems engineering study or alone, a demonstration of feedback stabilization on an actual jet engine, industrial process compressor or gas turbine would answer many questions as to the practical applicability of this technology.

- The work presented in this thesis strongly indicates that the availability of actuators with sufficiently high bandwidth and control authority for practical applications may be a potentially limiting factor. Development of such high performance actuators, either in conjunction with a particular application or as an independent effort is highly recommended.

- A study to characterize both the source and nature of disturbances acting on typical compression systems, which has been shown here to be an important design factor, would provide extremely useful data for any of the studies recommended above.

8.3.2 Control Theory

The investigation of this particular control application has pointed out the following areas where it would appear beneficial to develop some general theoretical results.

- There appears to be a great need for the development of control design and analysis techniques which are specifically suited to the problem of stabilizing open loop unstable systems. It appears that the majority of the controls literature is oriented towards improving the performance of stable systems and either ignores or only indirectly addresses some of the difficulties inherent in stabilizing open loop unstable systems.

  Two problems which would be of particular interest to address are: 1) How to design a stabilizing control within the limitations of fixed hardware constraints. and 2) The related problem, given the objective of stabilizing a particular plant, what are the minimum hardware requirements in terms of experimentally verifiable performance specifications.

- As discussed, actuator/sensor selection and evaluation problem has been investigated by a number of authors. An interesting aspect of this problem which is recommended for future investigation is the one encountered in this thesis where the basic plant is not a fundamentally fixed entity with a pre-defined actuator sensor set to select amongst but instead, can be modified by the addition of arbitrary sensors and actuators. Under these conditions, can a physically realizable choice of actuator and sensor which is in some sense optimal be directly synthesized? The problem is further complicated by the fact that addition of

certain actuators actually changes the plants dimension (ie., number of states in its state space description). For example adding an injector in the inlet duct of the compressor requires an additional state because the flow in the ducts upstream and downstream of the injector no longer need be the same.

Appendix A

Modeling the Injector

The injector is comprised of a short section of duct in which additional mass flow is injected coaxially as shown in Figure A-1. All flow stations referred to in the following analysis are as shown in Figure A-1.

A.1 Assumptions

The following assumptions are made:

1. The densities of all fluid streams have a common density, ρ, which remains constant with time.

2. Wall shear stress is negligible.

3. The flow from plane-1 to plane-4 is inviscid and irrotational.

4. The static pressure across plane-4, p_4, is spatially uniform.

5. The static pressure, p_2, and velocity, u_2 across plane-2 are spatially uniform.

6. There is no loss in total pressure between plane-3 and plane-4.

7. At plane-4 the flow velocity has two distinct velocities: the jet velocity, u_j, at the exit of the injector tube, and u_m for the coaxial main flow surrounding the jet.

8. The injector behaves quasi-steadily ie, we can consider the injector to follow its steady-state performance characteristics.

Let p_{0_i} denote the total pressure at plane i. Define,

$$\begin{aligned} \Delta p_{0_1} &= p_{0_1} - p_{0_3} \\ \Delta p_{0_2} &= p_{0_2} - p_{0_3}. \end{aligned}$$

The ejector will be inserted between two sections of duct each having fluid inertia, thus, the upstream and downstream flow rates, $\dot{m}_1$ and $\dot{m}_2$ will be state variables whose value are known at all time. We, therefore, want to express Δp_{0_1} and Δp_{0_2} as functions of $\dot{m}_1$, $\dot{m}_2$, fluid properties, and the injector geometry.

We first obtain the desired expression for Δp_{0_2} as follows. At steady state, a momentum balance from plane-4 to plane-2 neglecting wall shear and assuming fully mixed conditions at plane-2 gives:

$$p_4 A + \dot{m}_3 u_j + \dot{m}_1 u_m = p_2 A + \dot{m}_2 u_2, \tag{A.1}$$

where A is the cross sectional area of the duct.

Using the assumptions of uniform static pressure at plane-4 and no total pressure losses from plane-3 to plane-4

$$p_4 = p_{0_3} - 1/2\rho u_j^2, \tag{A.2}$$

and by definition:

$$p_2 = p_{0_2} - 1/2\rho u_2^2. \tag{A.3}$$

Making these substitutions gives:

$$\Delta p_{0_2} = -1/2\rho u_j^2 + \dot{m}_3 u_j/A + \dot{m}_1 u_m/A + 1/2\rho u_2^2 - \dot{m}_2 u_2/A. \tag{A.4}$$

Conservation of mass (continuity) gives:

$$\begin{aligned} \dot{m}_3 &= \dot{m}_2 - \dot{m}_1 \\ u_j &= \frac{\dot{m}_2 - \dot{m}_1}{\rho A_j} \\ u_m &= \frac{\dot{m}_1}{\rho(A - A_j)} \\ u_2 &= \frac{\dot{m}_2}{\rho A}, \end{aligned}$$

where, A_j is the cross sectional area of the jet at plane-4.

Substituting into Equation A.4 gives:

$$\Delta p_{0_2} = \frac{1}{\rho A^2}\left(-\frac{1}{2}\frac{(\dot{m}_2 - \dot{m}_1)^2}{(A_j/A)^2} + \frac{(\dot{m}_2 - \dot{m}_1)^2}{(A_j/A)} + \frac{{\dot{m}_1}^2}{(1 - (A_j/A))} - \frac{1}{2}{\dot{m}_2}^2\right) \tag{A.5}$$

We now obtain the desired expression for Δp_{0_1} as follows. With the assumptions made, we can apply Bernoulli's equation from plane-1 to plane-4 to obtain:

$$p_4 = p_{0_1} - 1/2\rho u_m^2. \tag{A.6}$$

Using Equation A.2, and continuity gives, after some manipulation, the desired expression:

$$\Delta p_{0_1} = -\frac{1}{2\rho A^2}\left(-\frac{(\dot{m}_2 - \dot{m}_1)^2}{(A_j/A)^2} + \frac{{\dot{m}_1}^2}{(1 - 2(A_j/A) + (A_j/A)^2)}\right) \tag{A.7}$$

Equation A.7 and Equation A.5 are then made non-dimensional by normalizing pressure with respect to $1/2\rho {u_T}^2$, and mass flow with respect to $\rho u_T A_c$, where, u_T is the compressor tip speed, and A_c is the annular inlet area of the compressor. Defining, $\beta = A_j/A$, $A^* = A/A_c$, $\phi_i = \dot{m}_i/\rho u_T A_c$, $\Psi_{i_u} = \Delta p_{0_1}/(1/2\rho {u_T}^2)$, and, $\Psi_{i_d} = \Delta p_{0_2}/(1/2\rho {u_T}^2)$ the desired non-dimensional expressions are obtained:

$$\Psi_{i_u} = \frac{1}{(A^*)^2}\left(-\frac{(\phi_2 - \phi_1)^2}{\beta^2} + \frac{{\phi_1}^2}{(1-\beta)^2}\right), \tag{A.8}$$

and

$$\Psi_{i_d} = \frac{2}{(A^*)^2}\left(-\frac{(\phi_2 - \phi_1)^2}{2\beta^2} + \frac{(\phi_2 - \phi_1)^2}{\beta} + \frac{{\phi_1}^2}{(1-\beta)} - \frac{{\phi_2}^2}{2}\right) \tag{A.9}$$

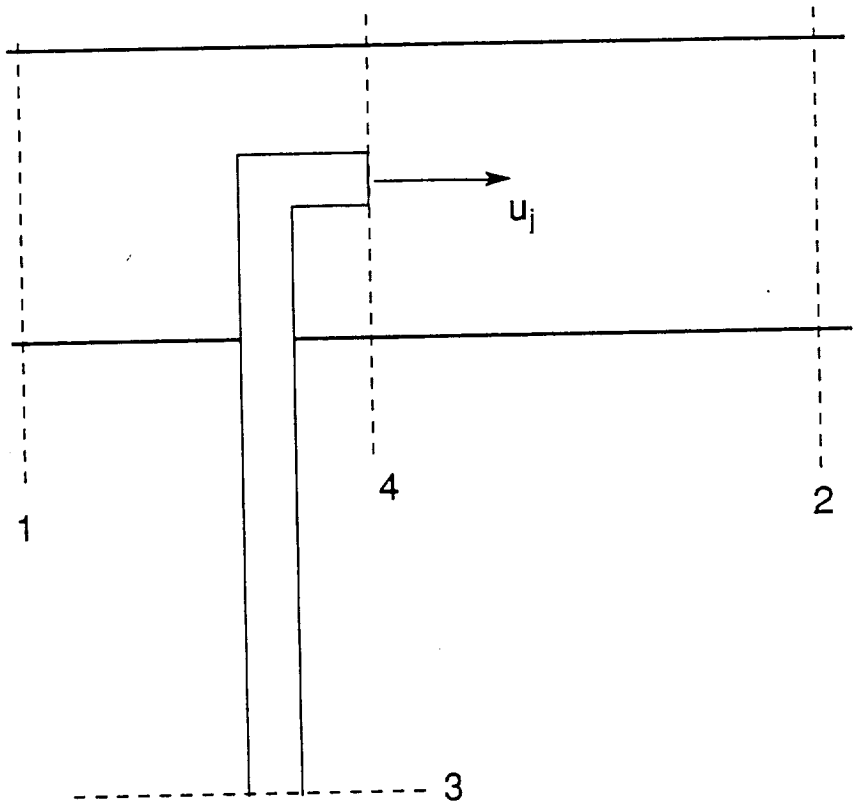

Figure A-1: Injector showing flow stations for analysis

Appendix B

Degree of Controllability

This appendix provides further details on the degree of controllability for discrete time systems. The development and terminology closely follows that for the continuous time case presented by Schmitendorf [42].

B.1 Recovery Region

Consider the linear, shift-invariant, discrete time system described by:

$$\mathbf{x}_{n+1} = \mathbf{A}\mathbf{x}_n + \mathbf{b}u_n \tag{B.1}$$

with the scalar control bounded by the constraint:

$$|u_i| \leq 1 \; i = 0, 1, 2, 3, \ldots \tag{B.2}$$

It will be useful to define the set Ω as the set of all control inputs satisfying Equation B.2, that is,

$$\Omega = \{u_i : |u_i| \leq 1 \; i = 0, 1, 2, 3, \ldots\} \tag{B.3}$$

Define $\mathcal{R}(N)$, the recovery region at step N as the set of all initial states, $\mathbf{x}_0$ which can be driven to the origin in N steps without violating the constraint B.2. An expression which can be used to generate the recovery region can be obtained as follows. Choose any control sequence, $u_0, u_1, \ldots, u_N$ which satisfies Equation B.2, and let $\mathbf{x}_0$ be the as yet unknown initial system state. The system, Equation B.1 then evolves as:

$$\begin{aligned}
\mathbf{x}_1 &= \mathbf{A}\mathbf{x}_0 + \mathbf{b}u_0 \\
\mathbf{x}_2 &= \mathbf{A}^2\mathbf{x}_0 + \mathbf{A}\mathbf{b}u_0 + \mathbf{b}u_1 \\
\mathbf{x}_3 &= \mathbf{A}^3\mathbf{x}_0 + \mathbf{A}^2\mathbf{b}u_0 + \mathbf{A}\mathbf{b}u_1 + \mathbf{b}u_2 \\
&\vdots \\
\mathbf{x}_N &= \mathbf{A}^N\mathbf{x}_0 + \mathbf{A}^{N-1}\mathbf{b}u_0 + \mathbf{A}^{N-2}\mathbf{b}u_1 + \cdots + \mathbf{b}u_{N-1}
\end{aligned}$$

So if $\mathbf{x}_N = 0$ we have:

$$0 = \mathbf{A}^N\mathbf{x}_0 + \mathbf{A}^{N-1}\mathbf{b}u_0 + \mathbf{A}^{N-2}\mathbf{b}u_1 + \cdots + \mathbf{b}u_{N-1} \tag{B.4}$$

If $\mathbf{A}$ is invertible (For the case of interest here, where the system Equation B.1 is obtained by discretizing a continuous time system , $\mathbf{A}$ is a matrix exponential and therefore always invertible.) then we can solve Equation B.4 for the initial state,

giving

$$\mathbf{x}_0 = -\left(\mathbf{A}^{-1}\mathbf{b}u_0 + \mathbf{A}^{-2}\mathbf{b}u_1 + \cdots + \mathbf{A}^{-N}\mathbf{b}u_{N-1}\right) \tag{B.5}$$

So that,

$$\mathcal{R}(N) = \left\{\mathbf{x}_0 : \mathbf{x}_0 = -\left(\mathbf{A}^{-1}\mathbf{b}u_0 + \mathbf{A}^{-2}\mathbf{b}u_1 + \cdots + \mathbf{A}^{-N}\mathbf{b}u_{N-1}\right), |u_i| < 1\right\} \tag{B.6}$$

B.2 Attainable Set

The attainable set at step N, , is defined as the set of all states which can be reached from an initial state, $\mathbf{x}_0$, in N steps, with the control bounded by the constraint, Equation B.2. Following a development similar to that just given for the recovery region, we have:

$$\alpha_N(\mathbf{x}_0) = \left\{x : x = \mathbf{A}^N\mathbf{x}_0 + \sum_{i=1}^{N}\mathbf{A}^{N-i}\mathbf{b}u_{i-1}, |u_i| \leq 1\right\}. \tag{B.7}$$

We will make use of the fact that the attainable set is a closed, bounded, convex set [26]. For the subsequent development, we will also utilize the fact that 0 is an element of $\alpha_N(\mathbf{x}_0)$, that is the system can be driven to the origin in N steps from the initial condition $\mathbf{x}$, if and only if the following condition holds.

$$\min_{\|\mathbf{z}\|=1}\left\{\mathbf{x}_0'\mathbf{z} + \max_{u_i\in\Omega}\left\{\sum_{i=1}^{N}u_{i-1}\mathbf{b}'(\mathbf{A}')^{-i}\mathbf{z}\right\}\right\} \geq 0. \tag{B.8}$$

This is shown as follows. Define the support function on the attainable set by:

$$h(\mathbf{x}) = \sup_{\lambda \in \alpha_N(\mathbf{x}_0)} \langle \lambda, \mathbf{x} \rangle, \tag{B.9}$$

for all $\mathbf{x} \in R^n$ for which the supremum is finite.

Since the attainable set is convex, closed and bounded, it may be shown utilizing the separating hyperplane theorem (See [25, Theorem 4.12]) that 0 is an element of $\alpha_N(\mathbf{x}_0)$ if and only if $h(\mathbf{x}) \geq 0$ for all $\mathbf{x}$.

Using the definition of the attainable set then gives the following necessary and sufficient condition for 0 to be in the attainable set:

$$0 \leq \sup_{u_i \in \Omega} \left\{ \lambda' \mathbf{A}^N \mathbf{x}_0 + \sum_{i=1}^{N} \lambda' \mathbf{A}^{N-i} \mathbf{b} u_{i-1} \right\} \tag{B.10}$$

Defining

$$\mathbf{z} = \frac{(\mathbf{A}')^N \lambda}{\|(\mathbf{A}')^N \lambda\|} \tag{B.11}$$

and substituting into Equation B.10 then gives the desired result.

B.3 Degree of Controllability

Define the degree of controllability at step N, $\varrho(N)$, as the largest ball centered at the origin[1] which is contained in $\mathcal{R}(N)$.

We now find an expression for the degree of controllability. From Equation B.8,

[1]The ball of radius r centered at the origin, denoted, $B_r(0)$, is the set of points given by $B_r(0) = \{x \in R^n : \|x\| \leq 0\}$.

0 is an element of $\alpha_n(\mathbf{x}_0)$ for every, $\mathbf{x}_0$ in a ball of radius r centered at the origin, if and only if:

$$\inf_{\mathbf{x}_0 \in B_r(0)} \{ \min_{\|\mathbf{z}\|=1} \{\mathbf{x}_0'\mathbf{z} + \max_{u_i \in \Omega} \{\sum_{i=1}^{N} u_{i-1}\mathbf{b}'(\mathbf{A}')^{-i}\mathbf{z}\}\} \geq 0. \tag{B.12}$$

Noting that,

$$\inf\{\mathbf{x}_0'\mathbf{z} : \mathbf{x}_0 \in B_r(0)\} = -r\|\mathbf{z}\| \tag{B.13}$$

$$= -r \tag{B.14}$$

we have from Equation B.12,

$$\min_{\|\mathbf{z}\|=1} \left\{ \max_{u_i \in \Omega} \left\{ \sum_{i=1}^{N} u_{i-1}\mathbf{b}'(\mathbf{A}')^{-i}\mathbf{z} \right\} \geq r \right\}, \tag{B.15}$$

as a necessary and sufficient condition, for $0 \in \alpha_N(\mathbf{x}_0)$ for every $\mathbf{x}_0 \in B_r(0)$. Since, by definition, the degree of controllability is the largest value of r for which this condition holds we have the result:

$$\min_{\|\mathbf{z}\|=1} \left\{ \max_{u_i \in \Omega} \left\{ \sum_{i=1}^{N} u_{i-1}\mathbf{b}'(\mathbf{A}')^{-i}\mathbf{z} \right\} \right\} = \varrho(N). \tag{B.16}$$

This expression can be further simplified to obtain:

$$\min_{\|\mathbf{z}\|=1} \left\{ \sum_{i=1}^{N} |\mathbf{b}'(\mathbf{A}')^{-i}\mathbf{z}| \right\} = \varrho(N). \tag{B.17}$$

To obtain a numerical value for the degree of controllability, we must in general

use a numerical method to find the minimum indicated in Equation B.12. For the computations presented in Chapter 5, a system having two state variables was studied. This requires a minimization of Equation B.17 around the unit circle. The search can be parameterized by a single variable over the closed interval, $[0, 2\pi]$, and the MATLAB routine "fmin" was used for this purpose.

Appendix C

Frequency Domain Limitations

This appendix provides a derivation for the lower bound on the Complementary Sensitivity function given by Equation 5.22.

From Freudenberg and Looze, [15, Equation 2.17], for a system with no right half plane zeros or time delays we have:

$$0 = \int_{-\infty}^{\infty} \log |T(j\omega)| d\theta_p(\omega) \tag{C.1}$$

Define the peak complementary sensitivity as:

$$\|T(j\omega)\|_\infty = \sup_\omega |T(j\omega)|. \tag{C.2}$$

Define $\Omega = \{\omega : -\omega_c \leq \omega \leq \omega_c\}$, and let Ω^C denote the complement of Ω.

Suppose that for some $\varepsilon > 1$, $|T(j\omega)| \leq 1/\varepsilon$ for all $\omega \in \Omega^C$. Let $\beta = 1/\varepsilon$. From

Equation C.1 we have:

$$
\begin{aligned}
0 &= \int_{\Omega} \log|T(j\omega)| d\theta_p(\omega) + \int_{\Omega^C} \log|T(j\omega)| d\theta_p(\omega) && \text{(C.3)} \\
&\leq \log(\|T(j\omega)\|_\infty)\theta_p(\Omega) + \log(\beta)\theta_p(\Omega^C && \text{(C.4)} \\
&= \log \|T(j\omega)\|_\infty^{\theta_p(\Omega)} + \log \beta^{\theta_p(\Omega^C)} && \text{(C.5)} \\
&= \log\left(\|T(j\omega)\|_\infty^{\theta_p(\Omega)} \beta^{\theta_p(\Omega^C)}\right). && \text{(C.6)}
\end{aligned}
$$

Exponentiating both sides of Equation C.6 and rearranging provides the desired expression:

$$
\|T(j\omega)\|_\infty \geq \varepsilon_m^{\left(\frac{(\pi-\theta_p)}{\theta_p}\right)} . \qquad \text{(C.7)}
$$

The derivation for the case with time delays and/or right half plane zeros is similar.

Appendix D

Minimal RMS Actuator Activity

Consider the linear time invariant system:

$$\dot{\mathbf{x}} = \mathbf{A}\mathbf{x} + \mathbf{b}u + \mathbf{L}w, \tag{D.1}$$

where $\mathbf{x}$ is a vector of system states, u is the scalar control input signal, w is a scalar external disturbance signal, and $\mathbf{A}$, $\mathbf{b}$, and $\mathbf{L}$ are constant matrices of appropriate dimensions. Assume that the system is open loop unstable, ie, $\mathbf{A}$ has eigenvalues in the closed right half complex plane. Suppose that u is given by the linear feedback control law:

$$u = K\mathbf{x} \tag{D.2}$$

where K is a real valued, constant matrix of appropriate dimension. Let us also assume that the closed loop system with feedback is stable, ie, the eigenvalues of $\mathbf{A} - \mathbf{b}K$ are all in the open left half complex plane.

A measure of actuator effectiveness is given by the the minimum possible RMS

(root mean square) closed loop response of u to a Gaussian white noise disturbance $w(t)$ with intensity V.

To calculate this value we proceed as follows. Find the gain matrix, K, which minimizes the performance criteria

$$J_1 = \int_0^\infty \left(\mathbf{x}(t)'\mathbf{R}_1\mathbf{x}(t) + \rho u^2\right) dt, \tag{D.3}$$

It is known (See [24, pages 260-264]that this same set of gains will minimize:

$$J_2 = \lim_{t\to\infty} E\{\mathbf{x}(t)'\mathbf{R}_1\mathbf{x}(t) + \rho u^2\}, \tag{D.4}$$

where E denotes the expectation operator. We are interested here in the asymptotic limit as $\rho \to \infty$. This limit will provide the solution with minimal RMS actuator motion and is known as the solution to the "expensive control problem."

To find the required gains, we first utilize the results of [24, Theorem 3.11] which tells us the optimal closed loop pole locations. We then use a standard pole placement technique to find the the required gain matrix. In particular it is noted that the closed loop and open loop pole locations are identical for any open loop poles in the left half complex plane. Any unstable open loop poles are reflected about the $j\omega$-axis into the left half of the complex plane to obtain the corresponding closed loop pole locations.

Once the optimal gain, K, is known, we can solve for the RMS actuator activity using:

$$\sqrt{\lim_{t\to\infty} E\{u(t)^2\}} = \sqrt{KQK'}, \tag{D.5}$$

where, Q is the solution of the Lyapunov equation:

$$0 = (\mathbf{A} - \mathbf{b}K)Q + Q(\mathbf{A} - \mathbf{b}K)' + V. \tag{D.6}$$

(See for example [24, Equation 3-377 and 3-338]

Appendix E

Lyapunov Analysis of Close-coupled Control

E.1 Introduction

The analysis presented in the body of this thesis has been primarily based upon linear system theory. Although much valuable information and insight can and has been derived from the linear analysis, there are important questions for which it cannot provide answers. A nonlinear analysis will be presented here to consider two such questions:

1. What is the extent of the allowable region of initial conditions from which subsequent system behavior will be acceptable?

2. Assuming that disturbances acting on the system are in some sense bounded, how large a bound can be tolerated while maintaining acceptable system be-

havior?

The nonlinear, Lyapunov based analysis, to be presented here[1], shows that the answers to these questions depends to a great extent upon the overall shape of the compressor's pressure-flow characteristic. This contrasts with the case of the linear stability analysis for which only the slope of the compressor characteristic is important. The fact that the overall shape of the compressor characteristic is important, suggest that a close-coupled resistance in series with the compressor could be used to modify the overall effective compressor characteristic to achieve more desirable system behavior. If a servo controlled valve is used for this purpose, rather than a fixed flow restriction, considerable freedom for shaping the characteristic can be obtained. The purpose of this appendix is to present some basic theory which can be employed to exploit this design freedom to best advantage.

E.2 Dynamic System Model

E.2.1 Basic Model

The basic physical configuration to be considered consists of a compressor feeding a plenum volume which then discharges through a load resistance. This is shown schematically in Figure E-1 which also shows typical non-dimensional pressure-flow characteristics for the compressor and load along with the assumed sign conventions. As indicated in Figure E-1 , the typical non-dimensional pressure-flow characteristic,

[1]The material included in this appendix was originally presented by the author in a similar form at the 1991 American Control Conference [45]. (For a closely related analysis also see Wyatt, [51] and Simon [44])

Ψ_c, of the compressor is non-monotonic. With the assumed sign conventions, it decreases monotonically in the second quadrant, has a single local minimum at a flow rate, ϕ_{c1}, and a single local maximum at a higher flow rate, ϕ_{c2}, in the first quadrant and then decreases monotonically into the fourth quadrant. The flow through the load, given by the load characteristic, Φ_t, monotonically increases with increasing plenum pressure, ψ_p, and passes only through the first and third quadrants. In the remainder of this appendix, sufficiently smooth, continuous characteristics having these general shapes will be assumed. The following assumptions are also made:

1. The flow in the compressor duct is one dimensional, incompressible and inertia dominated (inviscid).

2. An algebraic relationship exists between the compressor pressure rise and flow rate through the compressor at all times (sometimes called the *quasi-steady compressor assumption).*

3. The pressure in the plenum is uniform and the compression process in the plenum is isentropic.

Application of the principles of conservation of momentum in the compressor duct and conservation of mass in the plenum then allows the system dynamics to be represented by a coupled set of nonlinear ordinary differential equations Following Greitzer [17], and choosing as state variables the non-dimensional flow rate through the compressor duct, ϕ_c, and the non-dimensional pressure in the plenum, ψ_p, leads to the governing

set of state equations:

$$\begin{aligned} \dot{\phi}_c &= B(\Psi_c - \psi_p) \\ \dot{\psi}_p &= \frac{1}{B}(\phi_c - \Phi_t) \end{aligned} \tag{E.1}$$

Where ϕ_c, is the non-dimensional mass flow rate or flow coefficient, ψ_p, is the non-dimensional plenum pressure or pressure coefficient and the parameter, B, is a non-dimensional ratio of plenum capacitance to compressor duct inertance, as described in [17].

E.2.2 Model with Control

As will be shown, the stability of the basic compression system can be substantially modified by the introduction of a servo actuated, close-coupled control valve at the exit of the compressor. The term *close-coupled* here implies that there is no significant mass storage (fluid capacitance) between the valve and the compressor. The setup is shown schematically in Figure E-2. As indicated in this figure, the pressure drop through the valve is adjusted (by changing the valve area) as a function of the flow rate through the compressor to produce the desired functional relationship Ψ_v . With the introduction of the control action, Ψ_v, the state equations become:

$$\begin{aligned} \dot{\phi}_c &= B(\Psi_c - \psi_p - \Psi_v) \\ \dot{\psi}_p &= \frac{1}{B}(\phi_c - \Phi_t) \end{aligned} \tag{E.2}$$

In this form, the state equations explicitly exhibit the effect of the control action, which is to induce an acceleration of the fluid in the compressor duct. It is, however, convenient in the following analysis, to combine the compressor pressure rise, Ψ_c, and the control valve pressure drop Ψ_v, into a single function $\Psi_e(\phi)$, defined as:

$$\Psi_e(\phi) = \Psi_c - \Psi_v \tag{E.3}$$

The function, $\Psi_e(\phi)$, is interpreted as an equivalent compressor characteristic for the series combination of the compressor and control valve. This is shown graphically in Figure E-3. The state equations with control, Equation E.2, can then be rewritten using the equivalent compressor characteristic as:

$$\begin{aligned} \dot{\phi}_c &= B(\Psi_e(\phi) - \psi_p) \\ \dot{\psi}_p &= \frac{1}{B}(\phi_c - \Phi_t) \end{aligned} \tag{E.4}$$

A pair of values, (ϕ_{c0}, ψ_{p0}), which makes the time rate of change of the state vector, (the left hand side of Equation E.4) identically zero will be called an *equilibrium operating point.* In general, there may be more than one such point in the state space.

Finally, it will be useful to transform the state equations into a new local coordinate system in which the origin is located at an equilibrium operating point, (ϕ_{c0}, ψ_{p0}),

whose stability is being investigated. This is done by defining the transformations:

$$\hat{\phi} = \phi_c - \phi_{c0} \tag{E.5}$$

$$\hat{\psi} = \psi_p - \psi_{p0} \tag{E.6}$$

$$\hat{\Psi}_e(\hat{\phi}) = \Psi_e(\hat{\phi} + \phi_{c0}) - \Psi_e(\phi_{c0}) \tag{E.7}$$

$$\hat{\Phi}(\hat{\psi}) = \Phi(\hat{\psi} + \psi_{p0}) - \Phi(\psi_{p0}) \tag{E.8}$$

The resulting transformed state equations are:

$$\begin{aligned} \frac{d\hat{\phi}}{dt} &= B(\hat{\Psi}_e(\hat{\phi}) - \hat{\psi}) \\ \frac{d\hat{\psi}}{dt} &= \frac{1}{B}(\hat{\phi} - \hat{\Phi}(\hat{\psi})) \end{aligned} \tag{E.9}$$

The state equations in this local coordinate system will be used in the remainder of this appendix. The state variables in this local coordinate system will be called the unsteady flow and unsteady pressure. The values of these unsteady state variables measure deviations of the state from equilibrium, which are not assumed to be infinitesimally small.

E.3 Lyapunov Analysis

E.3.1 Unsteady Energy and the Lyapunov Formalism

A real, scalar, non-negative value, which will be called the *unsteady energy*, is assigned to each point in the state space by the Lyapunov function:

$$V(\hat{\phi},\hat{\psi}) = \frac{1}{2}(\frac{1}{B}\hat{\phi}^2 + B\hat{\psi}^2) \tag{E.10}$$

It is noted that this function is identically zero only at the origin (in the local coordinate system) and increases with increasing distance from the origin. Its graph is a bowl shaped surface whose level sets are ellipses enclosing the equilibrium point. The shape of these ellipses of constant $V(\hat{\phi},\hat{\psi})$ varies with the value of the B parameter, however, the axes of the ellipses are always aligned with the pressure-flow axes in the state plane.

The rate of change of $V(\hat{\phi},\hat{\psi})$ along trajectories (the material derivative of $V(\hat{\phi},\hat{\psi})$) is found by application of the chain rule to be:

$$\dot{V}(\hat{\phi},\hat{\psi}) = \hat{\phi}\hat{\Psi}_e(\hat{\phi}) - \hat{\Phi}(\hat{\psi})\hat{\psi} \tag{E.11}$$

which shows the remarkable fact that the time rate of change of unsteady energy along trajectories depends only upon the shape of the characteristics of the two resistive elements, namely, the equivalent compressor and the load. The inertial and capacitive elements (through the B parameter), therefore, only determine the amount of

unsteady energy, $V(\hat{\phi},\hat{\psi})$, at any particular operating point but not the rate at which it changes. The two terms on the right hand side of Equation E.11 are each products of unsteady pressure and unsteady flow and are thus power-like. These products are interpreted as unsteady power flows, the first term representing the unsteady power production of the equivalent compressor (compressor and control valve in series) and the second term represents the unsteady power dissipation of the load. The unsteady energy of the system,$V(\hat{\phi},\hat{\psi})$ is increasing, that is, $\dot{V}(\hat{\phi},\hat{\psi})$ is positive, at any state where more unsteady power is produced by the equivalent compressor than can be dissipated by the load. Similarly, the unsteady energy is decreasing, that is, $\dot{V}(\hat{\phi},\hat{\psi})$ is negative, whenever more unsteady power is dissipated in the load than is produced by the compressor.

Because the compressor pressure rise does not, in general, decrease monotonically with increasing flow, the algebraic sign of the unsteady power produced by the compressor can vary with flow rate as shown in Figure E-4. Thus, for a typical equilibrium operating point, the compressor will produce unsteady power over some ranges of flow, thereby tending to make the sign of $\dot{V}(\hat{\phi},\hat{\psi})$ positive while, over other ranges, it dissipates unsteady power, thereby tending to make the sign of $\dot{V}(\hat{\phi},\hat{\psi})$ negative. This contrasts with the case of the load resistance whose flow rate is assumed to increase monotonically with increasing pressure drop. The load, therefore, always dissipates unsteady power and so it always tends to make the sign of $\dot{V}(\hat{\phi},\hat{\psi})$ negative. This is also shown in Figure E-4.

E.3.2 Basins of Attraction and Ultimate Boundedness

Ideally, the system state would return rapidly to equilibrium, without excessive excursions along the way, from any initial point in the state space. As will be seen, this desirable property, which is called *Global Asymptotic Stability*, (for a precise definition see, for example, [41]) can be attained using the close-coupled control but only by incurring steady state losses across the control valve. If the required amount of loss is considered excessive, then some weaker form of stability must be accepted. In this case, all initial states will not return to the equilibrium point. The set of points that do return are called the *basin of attraction.* It will now be shown that the ellipsoidal level sets of unsteady energy, $V(\hat{\phi},\hat{\psi})$, can be used to bound a subset of the overall basin of attraction as well as to bound the maximum state excursion which the state will attain as it approaches equilibrium.

Suppose there is some open set, R_1, of points including the equilibrium point for which $\dot{V}(\hat{\phi},\hat{\psi}) \leq 0$ with equality holding only at the equilibrium point. Then, for a sufficiently small value of the unsteady energy, call it V_1, the ellipse of constant $V(\hat{\phi},\hat{\psi})$, given by $V(\hat{\phi},\hat{\psi}) = V_1$ will be entirely contained in the region R_1 . Since $\dot{V}(\hat{\phi},\hat{\psi})$ is negative for all points inside of this ellipse (except for the origin where it is zero), the value of $V(\hat{\phi},\hat{\psi})$ can only decrease along the trajectories of any point which originate in the interior of the ellipse $V(\hat{\phi},\hat{\psi}) = V_1$. Thus, any point originating inside of this ellipsoidal region can never leave it, and must eventually reach the equilibrium point as the value of $V(\hat{\phi},\hat{\psi})$ decreases inexorably to zero. This ellipse of constant $V(\hat{\phi},\hat{\psi})$, therefore, provides both a conservative estimate of the basin of

attraction and as a bound on the maximum state excursion which will be experienced along any trajectory originating in its interior. This estimate is termed conservative, because there may be some initial states outside of this boundary which nevertheless return to equilibrium. It is noted that if there are no points in the state space for which $\dot{V}(\hat{\phi},\hat{\psi})$ is positive then the bounding ellipse may be made arbitrarily large, that is, the basin of attraction will be the entire state space, which implies that the equilibrium point is globally asymptotically stable.

It is also useful to be able to obtain some bounds on the transient excursions as well as the ultimate asymptotic behavior along trajectories which originate outside of the previously estimated basin of attraction. It will now be shown that level sets of the unsteady energy, $V(\hat{\phi},\hat{\psi})$, can also be used for this purpose.

Suppose that a bounded set, R_2, can be found which contains all the points in the state space for which $\dot{V}(\hat{\phi},\hat{\psi})$ is positive. Then, for a sufficiently large value, V_2, of the unsteady energy, the entire region, R_2 can be contained in the interior of an ellipse defined by $V(\hat{\phi},\hat{\psi}) = V_2$. For brevity, this bounding ellipse will be called V_2. By the above construction, $\dot{V}(\hat{\phi},\hat{\psi})$ will be strictly negative outside of V_2 . The initial unsteady energy, call it V_3, along any trajectory originating outside of this ellipse must therefore be decreasing and so the trajectory can never again leave the interior of the region bounded by the ellipse $V(\hat{\phi},\hat{\psi}) = V_3$ determined by the initial unsteady energy. Furthermore, the unsteady energy will continue to decrease until the state enters the interior of the ellipse V_2 . Once inside of the boundary, V_2, the trajectory can never again leave. To see this, note that for the system's state to leave the region bounded by V_2 its unsteady energy would have to exceed the value V_2 but,

since outside of the region bounded by the ellipse V_2 the unsteady energy is strictly decreasing, this would be impossible. A similar argument shows the impossibility of the trajectory ever leaving the region bounded by the ellipse $V = V_3$ set by the initial unsteady energy. Thus it can be concluded that:

1. Any trajectory originating outside of the ellipse V_2 will eventually be inside it. This is *ultimate boundedness* (See, for example, [41]).

2. The maximum excursion along any trajectory originating outside of the ellipse V_2 is bounded by the ellipse $V(\hat{\phi}, \hat{\psi}) = V_3$ determined by the initial unsteady energy, V_3.

3. Once inside of the region bounded by the ellipse V_2 the state can never again leave this region.

4. Trajectories originating inside of the region bounded by the ellipse V_2 can also never leave this region

The bounds developed in this section are illustrated schematically in Figure E-5. In this figure, there is a single isolated region in state space where $\dot{V}(\hat{\phi}, \hat{\psi})$ is positive. In this region, the compressor is producing more unsteady power than can be dissipated by the load.

E.3.3 Effect of B parameter

As previously noted, the value of the B parameter does not affect the rate at which unsteady power is produced at a given location in state space. It does however, change

the shape of the level sets of $V(\hat{\phi}, \hat{\psi})$ and, thereby, changes the previously described ellipsoidal bounds on the transient excursion and estimates of the basin of attraction.

The effect of the value of the B parameter on the shape of the ellipsoidal level sets of constant $V(\hat{\phi}, \hat{\psi})$ can be determined by inspection of Equation E.10. Three distinct regimes can be identified corresponding to "large", "intermediate" and "small" values of the B parameter as follows:

Large B For $B > 1$ the major axis of the ellipsoidal level sets lies along the unsteady flow axis.

Intermediate B For $B = 1$ the level sets are circular.

Small B For $B < 1$ the major axis of the ellipsoidal level sets lies along the unsteady pressure axis.

Thus, as shown schematically in Figure E-6, for the same equilibrium operating point and resistive element characteristics, the bounds on the possible system behavior may vary markedly with changes in the value of B, even though the regions of unsteady power production remain the same. In particular, it is noted that as the B parameter increases, the estimated bound on the basin of attraction shrinks, indicating that the acceptable region of initial conditions will become increasing difficult to maintain as B becomes excessively large.

E.4 Regions of Positive $\dot{V}(\hat{\phi}, \hat{\psi})$

In order to find the bounds developed in the previous section, it is necessary to first determine the regions in state space where there is a net production of unsteady power, that is, where $\dot{V}(\hat{\phi}, \hat{\psi})$ is positive. Further, in order to make this theory useful, it must be determined how the control action of the close coupled valve can be used to modify the location and extent of these regions of unsteady power production. This will be the subject of this section.

E.4.1 General Features

In general, for the compressor and load characteristics which are assumed here, regions of unsteady energy production will be be bounded, open sets, containing portions of the unsteady flow axis. In fact, $\dot{V}(\hat{\phi}, \hat{\psi})$ will be maximal along the unsteady flow axis.

These facts will now be justified. First of all, it was assumed at the outset that the compressor characteristic was continuous and, for sufficiently large positive or negative values of the flow through the compressor, $\hat{\phi}$, the characteristic falls in the second and fourth quadrant respectively. That is, for sufficiently large magnitudes of $\hat{\phi}$, the compressor dissipates unsteady power. Thus, from the sum expressed by Equation E.11, it can be seen that regions of positive $\dot{V}(\hat{\phi}, \hat{\psi})$ can only exist over a finite interval of unsteady flow values. Further, from the continuity of the compressor characteristic, it can be seen that that the unsteady power produced by the compressor is bounded. On the other hand, because of the assumed monotonicity and quadrant constraints on the load characteristic, the unsteady power dissipated by the load in-

creases without bound as the magnitude of the unsteady plenum pressure increases (in either a positive or negative sense). Therefore, for sufficiently large magnitudes of unsteady pressure, the bounded unsteady power production of the compressor will be dominated by the dissipation of the load resulting in a net negative value of $\dot{V}(\hat{\phi},\hat{\psi})$. Thus, it can be concluded that the possible regions of positive $\dot{V}(\hat{\phi},\hat{\psi})$ are bounded. Since any nonzero value of the unsteady plenum pressure, $\hat{\psi}$, will cause dissipation by the load, the maximum value of $\dot{V}(\hat{\phi},\hat{\psi})$ must occur along the unsteady flow axis (that is the set of point in the state space where $\hat{\psi} = 0$). It can, therefore, be concluded that any regions of positive $\dot{V}(\hat{\phi},\hat{\psi})$ must include portions of the unsteady flow axis and it will be maximal there.

E.5 Effect of Bounded Disturbances

In this section, the effect of persistent disturbances on the compression system will be considered. Up to this point, the compression system has been treated as if there were no persistent disturbances driving it; only the effect of initial conditions has been considered. An actual system will certainly be disturbed by local (sub-model scale) flow instabilities in the compressor and load flow as well as by external disturbances at the inlet and exit of the system. For acceptable operation, the compression system must be able to remain reasonably close to equilibrium in the face of these persistent disturbances. In this section, it will be assumed that such disturbance are bounded in magnitude, which is thought to be a reasonable physical assumption. No further assumption regarding the statistical nature or time structure of these disturbances will

be made. They could range from constant biases, reflecting some uncertainty in the compressor characteristic, to rapidly fluctuating forces due to turbulence in the flow through the compressor. Such a disturbance model is called *an unknown but bounded model* (see [43]). (Actually, to be completely rigorous, some additional restrictions probably must be made on the allowable class of disturbance functions in order to assure that the solutions to the differential equation representing the modeled system are well defined. It will be assumed here that the class of nonpathological functions, (ones for which the formulation used here is valid) is large enough to motivate the effort of studying them. The exact technical restrictions which are required can be investigated at some future time as deemed necessary.) It will now be shown that the previously defined unsteady energy, $V(\hat{\phi},\hat{\psi})$, can be used to obtain useful bounds on the excursions from equilibrium which result from these bounded disturbances.

E.5.1 Analytical Formulation

Consider the effect of a bounded pressure disturbance, $\hat{\Psi}_d(t)$, tending to accelerate the flow in the compressor duct and a bounded flow disturbance, $\hat{\Phi}_d(t)$, modeling unsteady plenum outflow. The previously derived state equations in the local (unsteady) coordinate system, Equation E.9, become with the addition of these disturbance terms:

$$\begin{aligned} \frac{d\hat{\phi}}{dt} &= B(\hat{\Psi}_c(\hat{\phi}) - \hat{\psi} + \hat{\Psi}_d(t)) \\ \frac{d\hat{\psi}}{dt} &= \frac{1}{B}(\hat{\phi} - \hat{\Phi}(\hat{\psi}) - \hat{\Phi}_d(t)) \end{aligned} \tag{E.12}$$

The set of equations E.12 will be referred to as the *disturbed state equations.* Using the unsteady energy, $V(\hat{\phi},\hat{\psi})$, as previously defined by Equation E.10, the chain rule is used compute the material derivative as in Section E.3.1. However, this expression is evaluated using the disturbed state equations E.12 to obtain the formula:

$$\dot{V}(\hat{\phi},\hat{\psi}) = \hat{\phi}\hat{\Psi}_e(\hat{\phi}) - \hat{\Phi}(\hat{\psi})\hat{\psi} + \hat{\phi}\hat{\Psi}_d(t) - \hat{\Phi}_d(t)\hat{\psi} \tag{E.13}$$

Comparison of Equation E.13 with the previously derived expression given for $\dot{V}(\hat{\phi},\hat{\psi})$, Equation E.11, shows that the first two terms on the right hand side of both equations are identical. The additional two terms on the right hand side of Equation E.13 are unsteady power flows from the disturbances. They can be seen to have the effect of causing fluctuations in the overall unsteady energy balance. Thus, the regions in state space where $\dot{V}(\hat{\phi},\hat{\psi})$ is positive, now vary with time. Because the disturbances are bounded, the possible regions in the state space where $\dot{V}(\hat{\phi},\hat{\psi})$ can be positive also remain bounded. The boundaries of these regions however fluctuate with time. In particular, points in a neighborhood of the origin, where in the undisturbed case $\dot{V}(\hat{\phi},\hat{\psi})$ was non-positive but close to zero, may now occasionally become positive. Because the algebraic sign of the disturbances may be either positive or negative, the disturbances may be either dissipating or producing unsteady power. As illustrated in Figure E-7, the envelope of these fluctuations gives a *best case* and *worst case* bound on the regions in state space where $\dot{V}(\hat{\phi},\hat{\psi})$ may be positive, where the best case is the smallest possible region of positive $\dot{V}(\hat{\phi},\hat{\psi})$ and the worst case is the largest possible region. For a conservative design the larger (worst case) region must be used.

Although the magnitude of the disturbances is bounded, the unsteady power products involving them are not. It, therefore, might not be clear at this point that these regions of positive $\dot{V}(\hat{\phi},\hat{\psi})$ remain bounded. To clarify this point, the unsteady power balance, Equation E.13 is rearranged to obtain:

$$\dot{V}(\hat{\phi},\hat{\psi}) = \hat{\phi}[\hat{\Psi}_e(\hat{\phi}) + \hat{\Psi}_d(t)] - \hat{\psi}[\hat{\Phi}(\hat{\psi}) + \hat{\Phi}_d(t)] \tag{E.14}$$

It was assumed at the outset that $|\hat{\Psi}_e(\hat{\phi})|$ increases without bound as $|\hat{\phi}| \rightarrow \infty$. However, the disturbance term, $\hat{\Psi}_d(t)$ is bounded. Thus, for sufficiently large absolute values of $\hat{\Psi}_e(\hat{\phi})$ the sum, $\hat{\Psi}_e(\hat{\phi}) + \hat{\Psi}_d(t)$, will have the same algebraic sign as $\hat{\Psi}_e(\hat{\phi})$. A similar argument shows that for sufficiently large absolute values of $\hat{\psi}$, the sum $\hat{\Phi}(\hat{\psi}) + \hat{\Phi}_d(t)$, will have the same algebraic sign as $\hat{\Phi}(\hat{\psi})$. This implies that, for sufficiently large distances from equilibrium, the overall sum, Equation E.14 representing $\dot{V}(\hat{\phi},\hat{\psi})$ for the disturbed system, will have the same algebraic sign as that of the undisturbed system given by Equation E.11. In particular, if beyond some distance from equilibrium the value of $\dot{V}(\hat{\phi},\hat{\psi})$ for the undisturbed system is negative, then the same will hold for the disturbed system. Thus, the boundedness of the regions of positive $\dot{V}(\hat{\phi},\hat{\psi})$ for the undisturbed case,which was established earlier in Section E.4.1, implies the boundedness of these regions for the disturbed case.

From Equation E.14, the disturbances can be seen as having the effect of putting a bounded range of uncertainty on the compressor and load characteristics. This interpretation is illustrated in Figure E-8 which shows the nominal characteristics along with the envelope of the bounded disturbances. These upper and lower bounds

will be denoted by $\overline{\hat{\Psi}}_c(\hat{\phi})$ and $\underline{\hat{\Psi}}_c(\hat{\phi})$ respectively where these terms are defined by:

$$\begin{aligned} \overline{\hat{\Psi}}_c(\hat{\phi}) &= \sup_{t\geq 0}(\hat{\Psi}(\hat{\phi}) + \hat{\Psi}_d(t)) \\ \underline{\hat{\Psi}}_c(\hat{\phi}) &= \inf_{t\geq 0}(\hat{\Psi}(\hat{\phi}) + \hat{\Psi}_d(t)) \end{aligned} \tag{E.15}$$

As indicated in this figure, this envelope on the characteristics, may cross into a quadrant of unsteady power production, while the nominal characteristic is dissipating unsteady power. This shows graphically that the possible regions of unsteady power productions will become larger as a result of the disturbances.

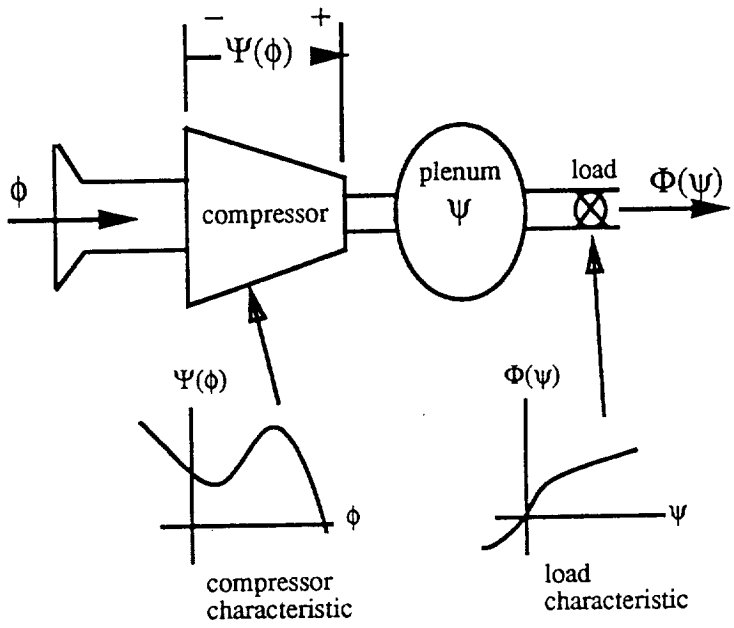

Figure E-1: Basic Compression System Configuration

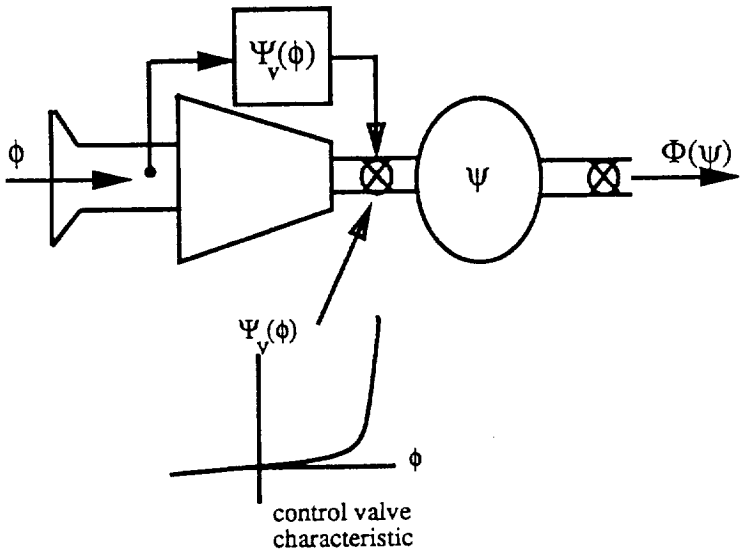

Figure E-2: System with Close-Coupled Control Valve

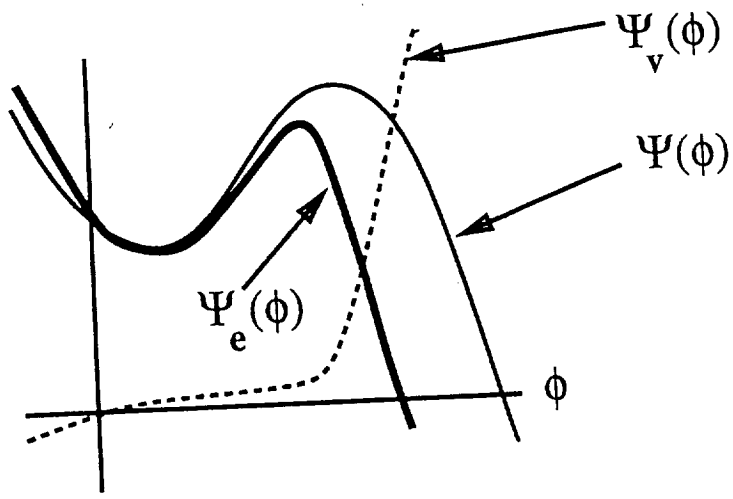

Figure E-3: Equivalent Compressor Characteristic

Compressor:
active with
with respect to
operating point

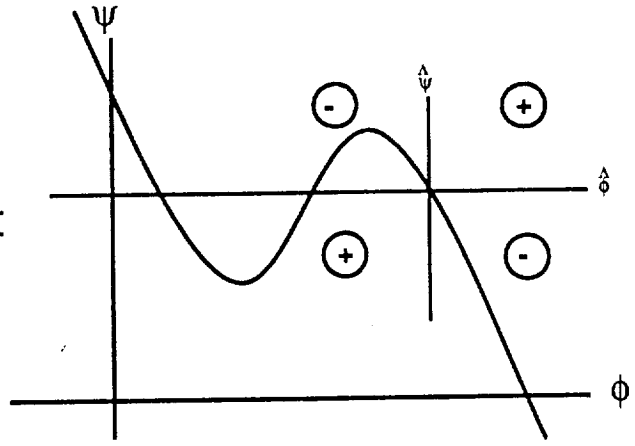

Load:
passive with
respect to
operating point

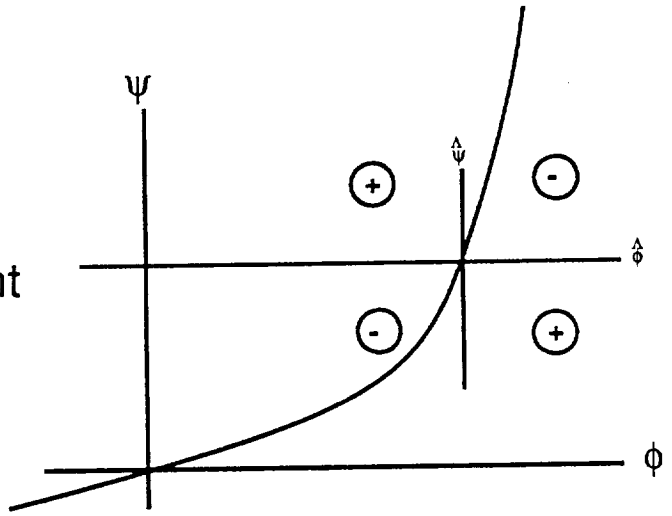

Figure E-4: Activity and Passivity with respect to Operating Point

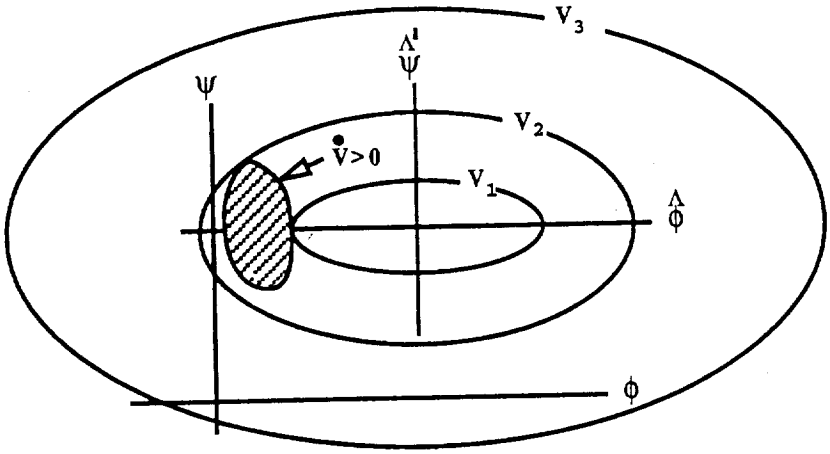

Figure E-5: Constant Unsteady Energy - Ellipsoidal Bounds

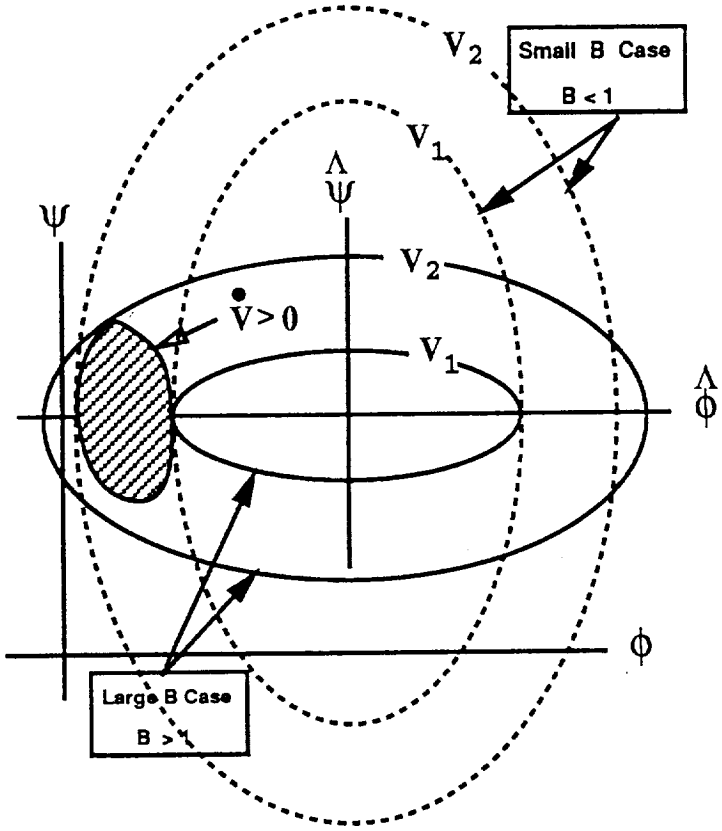

Figure E-6: Effect of B Parameter on Ellipsoidal Bounds

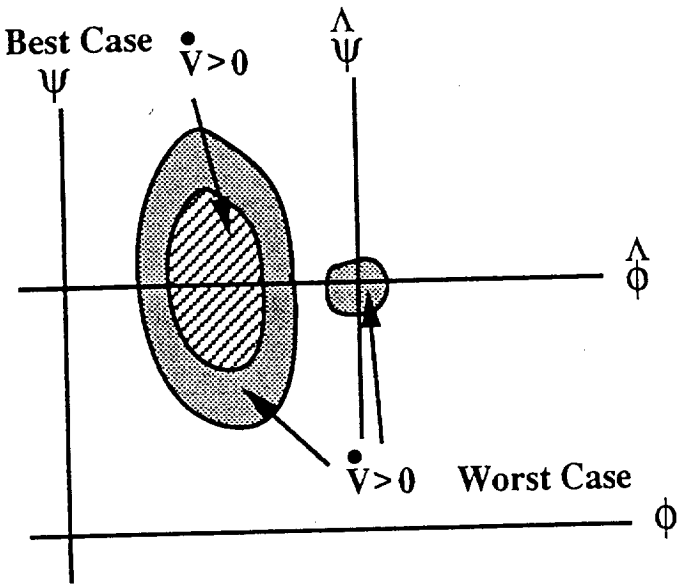

Figure E-7: Effect of Bounded Disturbance on Region of Unsteady Power Production

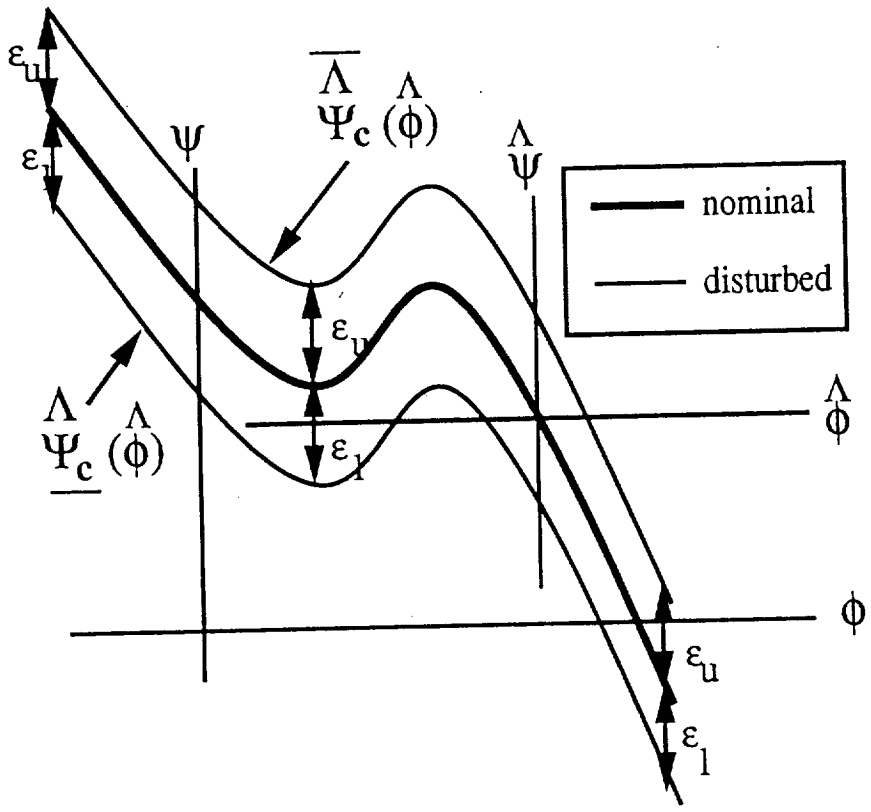

Figure E-8: Envelope of Bounded Disturbance on Compressor Characteristic

Bibliography

[1] A.N. Abdel-Hamid. "Dynamic Response of a Centrifugal Blower to Periodic Flow Fluctuations". ASME Paper 85-GT-195,1985.

[2] R.S. Benson and A. Whitfield. "An Experimental Investigation of the Non-Steady Flow Characteristic of a Centrifugal Compressor". *Proceedings of the Institution of Mechanical Engineers*, 180(27):641–672, 1965. part 1.

[3] H.W. Bode. *Network Analysis and Feedback Amplifier Design.* Van Nostrand, 1945.

[4] A.G Bodine. "Sonic Control of Dynamic Compressor Instability". In *Symposium on Stall, Surge and System Response*, ASME Gas Turbine Power Division, March 1960.

[5] J. Bons. *Instabilities and Unsteady Flow in Centrifugal Pumps.* Master's thesis, Department of Aeronautics and Astronautics, Massachusetts Institute of Technology, 1990.

[6] Gwo-Tung Chen. *Active Control of Turbomachinery Instability - Initial Calculations and Results.* Master's thesis, Department of Aeronautics and Astronau-

[14] D.A Fink, N.A. Cumpsty, and E.M Greitzer. "Surge Dynamics in a Free-Spool Centrifugal Compressor System". *Journal of Turbomachinery*, 114:321–332, April 1992.

[15] J.S. Freudenberg and D.P. Looze. "Right Half Plane Poles and Zeros and Design Tradeoffs in Feedback Systems". *IEEE Transactions on Automatic Control*, AC-30:555–565, 1985.

[16] F.R. Goldschmied and D.N. Wormley. "Frequency Response of Blower/Duct/Plenum Fluid Systems". *Journal of Hydronautics*, 11:18–27, January 1977.

[17] E. M. Greitzer. "Surge and Rotating Stall in Axial Flow Compressors Part I: Theoretical System Model". *Journal of Engineering for Power*, 98:190–198, April 1976.

[18] E. M. Greitzer. "Surge and Rotating Stall in Axial Flow Compressors Part II: Experimental Results and Comparison With Theory". *Journal of Engineering for Power*, 98:199–217, April 1976.

[19] E. M. Greitzer. "The Stability of Pumping Systems - The 1980 Freeman Scholar Lecture". *Journal of Fluids Engineering*, 103:193–242, June 1981.

[20] D.L. Gysling, J. Dugundji, E.M. Greitzer, and A.H. Epstein. "Dynamic Control of Centrifugal Compressor Surge Using Tailored Structures". *Journal of Turbomachinery*, 113(4):710–722, 1991.

[21] K.E. Hansen, P. Jorgensen, and P.S. Larsen. "Experimental and Theoretical Study of Surge in a Small Centrifugal Compressor". *Journal of Fluids Engineering*, 103:391–395, September 1981.

[22] V.V. Kazakevich. *Self Excited Oscillations in Compressors.* Mashinostrogenie, Moscow, 1974. in Russian.

[23] W.J. Kearton. *Turbo-blowers and Compressors.* Sir Isaac Pitman and Sons Ltd., 1931.

[24] H. Kwakernaak and R. Sivan. *Linear Optimal Control.* John Wiley and Sons, 1972.

[25] S.R. Lay. *Convex Sets and Their Application. Pure and Applied Mathematics,* John Wiley and Sons, 1982.

[26] J.N. Lin. "Determination of Reachable Set for a Linear Discrete Time System". *IEEE Transactions on Automatic Control*, AC-15:339–342, June 1970.

[27] R. Mani. AIAA Short Course on Air Breathing Propulsion, Cleveland, OH, June 20, 1982.

[28] E. Maslen and M. Townsend. "Stability Limits of Linear Feedback Control Systems". *Journal of Dynamic Systems Measurement and Control*, 111:138–141, June 1989.

[29] R.S. Mazzawy. "Surge Induced Structural Loads in Gas Turbines". *ASME Journal of Engineering for Power*, 102:162–168, January 1980.

[30] D.H. McQueen. "On the Dynamics of Compressor Surge". *Journal of Mechanical Engineering Science*, 18(5), 1976.

[31] P.C. Muller and H.I. Weber. "Analysis and Optimization of Certain Qualities of Controllability and Observability for Linear Dynamical Systems". *Automatica*, 8(3):237–246, 1972.

[32] E.A. Nisenfeld. *Centrifugal Compressors: Principles of Operation and Control.* Instrument Society of America Monograph Series, 1982.

[33] G.A. Norris and R.E. Skelton. "Selection of Dynamic Sensors and Actuators in the Control of Linear Systems". *Journal of Dynamic Systems Measurement and Control*, 111:389–397, 1989.

[34] K. Ogata. *Modern Control Engineering.* Prentice Hall, 1970.

[35] H. Ohashi. *Analytical and Experimental Study of Dynamic Characteristics of Turbopumps.* Technical Report NASA TN D-4298, NASA, April 1968.

[36] S.M. Oliva and C.N Nett. "A General Nonlinear Dynamical Analysis of a Second Order One Dimensional Theoretical Compression System Model". In *American Controls Conference, Boston MA*, 1991.

[37] A.V. Oppenheim and R.W Schafer. *Discrete Time Signal Processing.* Prentice Hall, 1989.

[38] J. Paulon. "Theoretical and Experimental Determination of the Transfer Function of a Compressor". ASME Paper 84-GT-283, 1984.

[39] J.E Pinsley. *Active Control of Centrifugal Compressor Surge.* Master's thesis, Department of Aeronautics and Astronautics, Massachusetts Institute of Technology, 1988.

[40] J.E. Pinsley, G.R. Guenette, A.H. Epstein, and E.M. Greitzer. "Active Stabilization of Centrifugal Compressor Surge". *Journal of Turbomachinery*, 113:723–732, 1991.

[41] J. La Salle and S. Lefschetz. *Stability by Lyapunov Direct Method.* Volume 4 of *Mathematics in Science and Engineering*, Academic Press Incorporated, 3 edition, 1961.

[42] W.E. Schmitendorf. "An Exact Expression for Computing the Degree of Controllability". *Journal of Guidance*, 7(4):502–504, 1984.

[43] F.C. Schweppe. *Uncertain Dynamic Systems.* Prentice Hall, 1973.

[44] J.S. Simon. *Modeling and Stability Analysis of Axial Flow Fans Operating in Parallel.* Master's thesis, Department of Mechanical Engineering, Massachusetts Institute of Technology, 1985.

[45] J.S. Simon and L. Valavani. "A Lyapunov Based Nonlinear Control Scheme for Stabilizing a Basic Compression System Using a Close-Coupled Control Valve". In *Proceedings of the 1991 American Control Conference*, American Control Council, 1991.

[46] J.S. Simon, L. Valavani, A.H. Epstein, and E.M. Greitzer. "Evaluation of Approaches to Active Compressor Surge Stabilization". ASME Paper 92-GT-182 (To be published in the ASME Journal of Turbomachinery),1992.

[47] N. Staroselsky and L Ladin. "Improved Surge Control for Centrifugal Compressors". *Chemical Engineering*, 175–184, ?? ??

[48] E.S Taylor. The Centrifugal Compressor. In W.R Hawthorne, editor, *Part J in Aerodynamics of Compressors*, Princeton University Press, Princeton,NJ, 1964.

[49] A. Tondl. "On the Dynamics of Compressor Surge". *International Journal of Nonlinear Mechanics*, 14:259–266, 1979.

[50] M. Vidyasagar. *Control System Synthesis a Factorization Approach.* MIT Press, 1987.

[51] J. L. Wyatt. *"Lectures on Nonlinear Circuit Theory".* VLSI Memo 84-158, Department of Electrical Engineering and Computer Science Massachusetts Institute of Technology, 1984.

[52] J.L. Wyatt, L. O. Chua, J.W. Gannett, I.C. Goknar, and D.N. Green. "Energy Concepts in the State-Space Theory of Nonlinear n-Ports: Part I - Passivity". *IEEE Transactions on Circuits and Systems*, CAS-28(1):48–61, January 1981.

[53] Y.Takahashi, M.J. Rabins, and D.M. Auslander. *Control and Dynamic Systems.* Addison-Wesley Publishing Company, 1972.